BALLOON-BORNE THREE-METER TELESCOPE FOR FAR-INFRARED AND SUBMILLIMETER ASTRONOMY

Grant NAGW-509

Final Report
For the period 1 September 1983 through 31 March 1988

Principal Investigator
Giovanni G. Fazio

June 1988

Prepared for
National Aeronautics and Space Administration
Washington, DC 20546

Smithsonian Institution
Astrophysical Observatory
Cambridge, Massachusetts 02138

The Smithsonian Astrophysical Observatory
is a member of the
Harvard-Smithsonian Center for Astrophysics

The NASA Technical Officer for this grant is Dr. Frederic C. Gillett, Code EZ-7, National Aeronautics and Space Administration, Washington, D.C. 20546

BALLOON-BORNE THREE-METER TELESCOPE FOR FAR-INFRARED AND SUBMILLIMETER ASTRONOMY

Grant NAGW-509

Final Report

For the period 1 September 1983 through 31 March 1988

Principal Investigator

Dr. Giovanni G. Fazio

Co-Investigators

Dr. William F. Hoffmann
Steward Observatory
University of Arizona

Dr. Doyal A. Harper
Yerkes Observatory
University of Chicago

June 1988

Smithsonian Institution
Astrophysical Observatory
Cambridge, Massachusetts 02138

The Smithsonian Astrophysical Observatory
is a member of the
Harvard-Smithsonian Center for Astrophysics

The NASA Technical Officer for this grant is Dr. Frederic C. Gillett, Code EZ-7, National Aeronautics and Space Administration, Washington, D.C. 20546

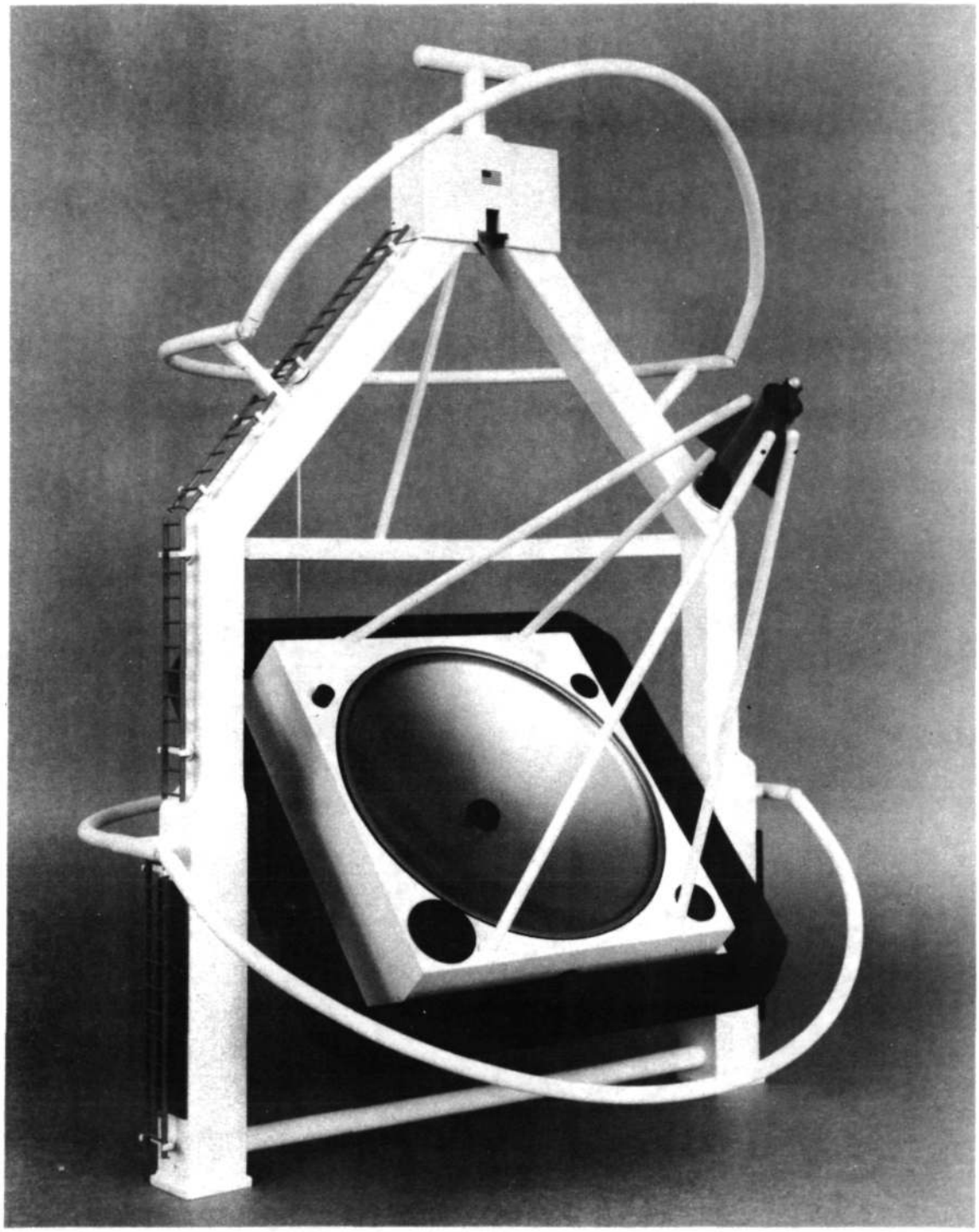

Model of Proposed Balloon-Borne Two-Meter Telescope for Far-Infrared and Submillimeter Astronomy

Abstract

This final report presents the scientific objectives, engineering analysis and design, results of technology development, and focal-plane instrumentation for a two-meter balloon-borne telescope for far-infrared and submillimeter astronomy. Next to observing from space, balloon-borne platforms offer the best opportunity to escape the absorption and emissivity of the earth's atmosphere, permitting high photometric sensitivity and spectroscopy of atomic and molecular lines normally blocked by the earth's atmosphere. Quite apart from duplicating the capabilities of an airborne telescope, a balloon-borne telescope permits study of several astrophysically important atomic and molecular lines that will otherwise have to await study from such proposed facilities as ISO, SIRTF, and, in many cases LDR. However, even when observable by ISO or SIRTF, the larger aperture of a two-meter balloon-borne telescope will mean that these lines can be studied with a spatial resolution 2 to 3 times greater than from these spacecraft. For photometry, the two-meter balloon telescope would be able to simultaneously provide better angular resolution at far infrared wavelengths, larger reference-beam spacings, and larger scanned areas than is practical with airborne or ground-based measurements. Thus the balloon telescope will fill a crucial niche between facilities like SOFIA and 10-meter class ground-based telescopes which can provide good data on smaller structures and IRAS sky-maps which provide excellent data on structures larger than a few arcminutes at wavelengths less than 120 microns. It is impossible to completely understand the the complex relationships between molecular clouds, ambient stars and low-mass protostars without thorough coverage of this range of spatial scalelengths. The balloon telescope can also play a crucial role in extragalactic astronomy by its ability to image large areas at a variety of scale-sizes, wavelengths, and angular and spectral resolutions. It will be particularly valuable for examining the nearest galaxies, which are inconveniently large for airborne and ground-based instruments but which offer the best opportunities for examining the detailed structure of spiral arms, nuclear regions, bars, and individual star-forming complexes.

This is the Final Report under Grant NAGW-509 for a "Balloon-Borne Three-Meter Telescope for Far-Infrared and Submillimeter Astronomy". Work under this grant initially focused on the development of a preliminary design for a three-meter telescope and gondola. That work was essentially complete in August 1985 and reported on in Semiannual Report #4, (dated October 1985). Subsequently, additional engineering work simplified the design of the telescope gimbal system and downsized the telescope and gondola to a two meter primary. Our goals were to reduce the costs, to meet the weight constraints for launch at the National Scientific Balloon Facility in Palestine Texas and to provide easy transportability for rapid recovery and for operations from remote launch sites. Under related NASA Grant 01-NGR-03-002371 to the University of Arizona, several light weight mirror panels were tested and techniques developed for overcoating and polishing these mirrors in a continuing development effort. Semiannual Report #5 describes the simplified gimbal system. This report describes

the unique scientific objectives a two-meter telescope could attain, the downsized two-meter telescope, and the gondola and initial instruments. It reports recent advances in lightweight mirror technology and presents a preliminary plan for carrying out the project.

CONTENTS

		Page
Abstract		iii
1.0	INTRODUCTION	1
1.1	Unique Capabilities of Balloon-Borne Observations	1
1.2	Program Summary - Development of the Two-Meter Design	3
1.3	The Two-Meter Balloon-Borne Infrared and Submillimeter Telescope	4
1.4	Relationship of Three-Meter/Two-Meter Telescope to the Large Deployable Reflector (LDR)	5
2.0	SCIENTIFIC OBJECTIVES	6
2.1	Introduction	6
2.2	Submillimeter Spectroscopy	10
2.2.1	Introduction	10
2.2.2	Far-Infrared and Submillimeter Lines	10
2.2.3	Models of Atmospheric Transmission	15
2.2.4	Unique Balloon Altitude Science Programs	17
2.3	Photometry	29
2.3.1	Star Formation and the Interstellar Medium	29
2.3.2	Galactic Structure	30
2.4	Cometary Science with a Two-Meter Balloon-Borne Telescope	31
2.5	Scientific Performance	32
3.0	GONDOLA DESIGN	34
3.1	Telescope Design	34
3.1.1	Telescope Requirements	34
3.1.2	Description of the Cassegrain Telescope	37
3.1.3	Optics Design Trade-Offs	41
3.1.4	Telescope Mechanical Design	44
3.1.5	Telescope Thermal Design	46
3.1.6	Chopping Technique	47
3.2	Support Structure Design	48
3.2.1	Mechanical Concept	48
3.2.2	Launch, Landing, and Recovery Considerations	50
3.3	Pointing System	52
3.3.1	Pointing Requirements	52
3.3.2	Operating Modes	52
3.3.3	Gimbal Design	53
3.3.4	Azimuth Servo	55
3.3.5	Elevation and Cross-Elevation Servos	56
3.3.6	Aspect System	60

CONTENTS (Cont.)

		Page
3.3.7	Estimate of Total Pointing Performance	61
3.4	Electrical Systems Design	62
3.4.1	Command and Telemetry System	62
3.4.2	Gondola Electronics System	64
3.4.3	Gondola Power Requirements	64
3.4.4	Electronics Packaging	64
4.0	MIRROR DEVELOPMENT PROGRAM	66
4.1	Approach and Scope	66
4.2	Conclusions from Mirror Development Program	68
4.2.1	The Dornier Mirrors	68
4.2.2	The Hexcel/JPL Mirrors	68
4.2.3	The Pyrex Face Sheet Composite Mirror	68
4.2.4	The United Technology Graphite/Glass Mirrors	72
4.2.5	Foamed Aluminum Core Mirror	72
4.2.6	Optical Polishing Composite Facesheets	72
4.2.7	Silicon Monoxide Over Coating and Polishing	72
5.0	EXPERIMENT ACCOMMODATIONS	74
5.1	Focal Plane	74
5.2	Photometric Infrared Camera	74
5.2.1	Instrument Description	74
5.2.2	Limits to Sensitivity	75
5.3	Heterodyne Submillimeter Receiver	75
6.0	GROUND SUPPORT EQUIPMENT REQUIREMENTS	82
6.1	Optical GSE	82
6.2	Mechanical GSE	83
6.3	Electrical GSE	83
7.0	NSBF DESIGN DRIVERS AND PAYLOAD SUPPORT REQUIREMENTS	86
7.1	Payload Support Requirements	86
7.1.1	Staging	86
7.1.2	Command and Telemetry Trailer	86
7.2	Launch Requirements	88
7.3	Ascent and Float Environment	90
7.4	Termination, Landing and Recovery	91
8.0	IMPLEMENTATION PHASE SUMMARY DEVELOPMENT PLAN	91
8.1	Introduction	91
8.2	Statement of Work	92
8.3	Schedule	93
8.4	Implementation Phase Budgetary Cost Estimate	95
8.4.1	Introduction	95
8.4.2	Program Plan	95
8.4.3	Cost Estimate Assumptions	102
9.0	COMPARISON OF THREE-METER AND TWO-METER GONDOLA CONCEPTS	102
References		104

FIGURES

		Page
FIGURE 1.1-1	Atmospheric transmission	2
2.1-1	Typical Sizes of Objects to be Studied by the Two-Meter Balloon-Borne Telescope	9
2.2-1	Atmospheric transmission at 14 and 32 km in the vicinity of the [OI]63.184μm line	22
2.2-2	Atmospheric transmission at 14 and 32 km in the vicinity of the [OI]145.526μm line	23
2.2-3	Atmospheric transmission at 14 and 32 km in the vicinity of the [N II]121.889μm line	24
2.2-4	Atmospheric transmission at 14 and 32 km in the vicinity of the ground-state transition of para-H_2O	25
2.2-5	Atmospheric transmission at 14 and 32 km in the vicinity of the O_2 487 GHz line	26
2.2-6	Atmospheric transmission at 14 and 32 km in the vicinity of the [SI] 56.322μm line	27
2.2-7	Total cooling per H_2 molecule as a function of H_2 density	28
2.5-1	Broadband Sensitivity at 100μm vs. the Diffraction-Limited Beam Size.	33
3.1-1	Optical Design of Two-Meter Balloon Telescope	36
3.1-2	Image Blur vs. Field Position and Chopper Angle	38
3.2-1	Three Views of Gondola	49
3.3-1	Gimbal Assembly	54
3.3-2	Fine-Pointing Control System Response to a Sinusoidal Command Signal	58
3.3-3	Telescope Point Response to a $5x10^{-3}$ Nms Torque Pulse	59
3.4-1	On-Board Command and Telemetry System for the Balloon-Borne Three-Meter Infrared Telescope	63
3.4-2	Gondola Electronics Systems	65
4.2-1	Dornier Quad 25 As Replicated Surface Figure Error Contour Level 2μm	69
4.2-2	Quad 25 Peak-to-Valley Change in Figure over 82°C Temp. Change	70
4.2-3	Hexcel 4 Comparison of JPL Model	71
4.2-4	Silicon Monoxide CFRP Mirror Coating Chamber	73
5.3-1	Comparison of actual receiver performances in terms of number of noise photons at the input.	77
5.3-2	Bowtie and Bowtie-Array SIS Junctions	79
5.3-3	Laboratory SIS results at 345 GHz.	80
5.3-4	Block Diagram of Proposed Heterodyne Submillimeter Receiver	81
6.3-1	Gondola Electrical Ground Support Equipment	85
7.1-1	Gondola Supported Within the NSBF High Bay Experiment Staging Building.	87
7.2-1	Gondola Suspended fr m Launch Vehicle	89
8.3-1	Program Schedule	94

TABLES

			Page
TABLE	2.2-1	Important Submillimeter Transitions - Atomic Ions . .	11
	2.2-2	Important Submillimeter Transitions - Neutrals . . .	11
	2.2-3	Important Submillimeter Transitions - Hydrides . . .	12
	2.2-4	Important Submillimeter Transitions - Heavy Molecules	13
	2.2-5	Parameters Used in Three-Layer Atmospheric Approximation	16
	2.2-6	V_{LSR}'s of Selected Galactic HII Regions and Planetary Nebulae	18
	2.2-7	V_{LSR}'s of Nearby, Gas-Rich Star Forming Galaxies . .	19
	2.2-8	Some Important Transitions Observable from a Balloon, but not an Airplane, ...	20
	2.2-9	Some Important Transitions Observable from a Balloon, but not an Airplane, ...	21
	3.1-1	Telescope and Gondola Specifications	35
	3.1-2	Telescope Optics Design and Performance	40
	3.1-3	Telescope Optics Alignment Tolerances	41
	3.1-4	Two-Meter Telescope Subassembly Weight Summary . . .	45
	3.2-1	Gondola Weight Summary	51
	3.2-2	Gondola and Telescope Products and Moments of Inertia	52
	3.3-1	System Error Performance for Two Star Tracker Configurations	62
	3.4-1	Estimated Power Requirements	66
	8.4-1	Total Cost Estimate	96
	8.4-2	Equipment, Services and Subcontract Cost Summary . .	97
	8.4-3	Engineering Cost Estimate	99
	8.4-4	Heterodyne Submillimeter Receiver Estimated Costs . .	100
	8.4-5	Two-Meter Balloon-Borne Telescope - Cost Summary . .	101
	9-1	Comparison of Two-Meter and Three-Meter Gondola Specifications	103

1.0 INTRODUCTION

1.1 Unique Capabilities of Balloon-Borne Observations

At far-infrared and submillimeter wavelengths, the dominant observational obstacle is atmospheric opacity due mainly to lines of H_2O, O_3, and O_2; the lower the altitude, the greater is the pressure broadening of these lines, and the more severe is the overall atmospheric attenuation. In spite of this general problem, a couple of low (10-20%) transmission "windows" at 350 and 450μm and a few somewhat higher (50-80%) transmission "windows" between 700μm and 1mm permit glimpses into the submillimeter from mountaintop altitudes (see Figure 1.1-1). Higher altitude airborne platforms allow for significantly improved access to the entire range of far-infrared and submillimeter wavelengths, although even at an altitude of 12km interference from atmospheric features can prevent observations of many important atomic and molecular species from galactic and extragalactic sources. Next to observing from space, balloon-borne platforms offer the best opportunity to escape the effects of the earth's atmosphere. It will be shown below that quite apart from duplicating the capabilities of an airborne telescope, a balloon-borne telescope permits study of several astrophysically important species that will otherwise have to await study from such proposed facilities as ISO, SIRTF, and, in many cases, LDR. However, even when observable to ISO or SIRTF, the larger aperture of a two-meter balloon-borne telescope will mean that these lines can be studied with a spatial resolution 2 to 3 times greater than from these spacecraft.

For photometry, the background radiation for a balloon-borne telescope is primarily from the telescope mirror and not the sky, since at these altitudes the atmospheric emissivity is less than 1%. Also at balloon altitudes the ambient temperature of the mirror is lower, typically 230 K. Hence, if the mirror emissivity can be made <10% the photometric sensitivity can be considerably improved over observations from an airborne platform. The balloon platform also offers a more stable environment in terms of fluctuations in the background radiation. As a result, the balloon-borne telescope can simultaneously provide at far-infrared and submillimeter wavelengths better angular resolution, larger reference-beam spacings, and larger scanned areas than is practical with airborne or ground-based measurements.

In terms of combined photometric and spectroscopic capabilities a two-meter balloon-borne telescope can fill a crucial niche between facilities such as SOFIA and a 10-meter class ground-based telescope and space telescopes such as IRAS, ISO, and SIRTF.

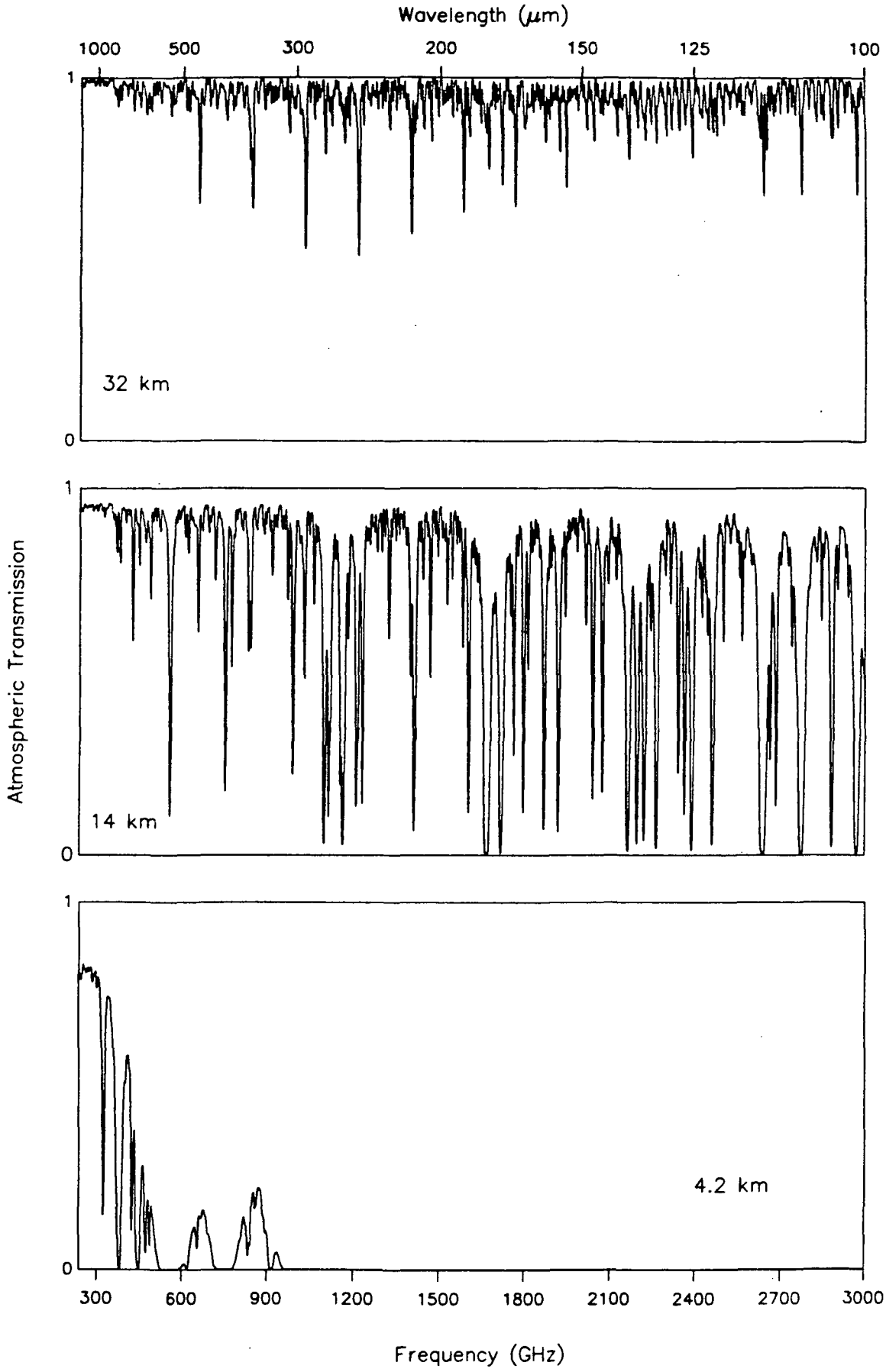

Figure 1.1-1. Atmospheric transmission at mountaintop (4.2km), airplane (14km), and balloon (32 km) altitudes for 1mm, 7.0μm and 0.32μm of precipitable water vapor, respectively, along a 45° elevation line-of-sight.

1.2 Program Summary - Development of the Two-Meter Design

The primary focus of this grant has been the definition of a balloon-borne three-meter telescope for infrared and submillimeter astronomy and the identification of the wide ranging scientific program this exciting new facility could support.

This work was essentially completed in August 1985 and reported on in Semiannual Report #4 under this grant (NAGW-509) released in October 1985 and subsequently re-released as an independent study report: "Balloon-Borne Three-Meter Telescope for Far-Infrared and Submillimeter Astronomy Preliminary Design Report" also dated October 1985 (the "yellow cover report"). References in this report to "the PDR" are to either of these documents.

In releasing these reports, we felt we had carried the design process as far as we could under the funding constraints of the grant and were prepared to move into a four-year program to complete the engineering design of the gondola, and to build, test and fly it. Had we been able to proceed, we would be today in the final stages of assembly and test of the gondola and looking forward to field operations next year.

Unfortunately, NASA funding constraints precluded beginning the hardware program at once and our attention was directed towards the exploration of potential international collaborative efforts to develop the gondola. Although no collaborations resulted from these initiatives, the discussions led us to conclude that many of the scientific objectives of the original program could be met with a two-meter telescope and futhermore, that the newly burgeoning field of sub-millimeter astronomy could make even more effective use of such a facility than we originally believed.

Accordingly, the small balance of funds remaining after the completion of the three-meter telescope report was directed towards rescoping the design of the telescope downward to accommodate a primary mirror two meters in diameter. The result of this "mini study" has been the conceptual design of the two-meter telescope described in this report. The new design is smaller, lighter, easier to transport and far less costly than the three-meter design. Furthermore, it could fly from Palestine Texas, the most convenient and efficient launch site, under the new, more stringent, flight rules.

Additional development and evaluation of lightweight mirror technology and telescope design has been carried out under NASA Grant 01-NGR-03-002371, Dr. William F. Hoffmann, University of Arizona, Principal Investigator. Dr. Hoffmann is also a Co-Investigator on this grant.

Contributors to this report include Giovanni Fazio, George Nystrom, William Hoffmann, Doyle Harper, Robert Martin, Paul Ho, Gary Melnick, John Black, Christopher Walker, and Richard S. Taylor. It was compiled and edited by Richard S. Taylor.

1.3 The Two-Meter Balloon-Borne Infrared and Submillimeter Telescope

As shown in the photograph of the gondola model in the frontispiece, the telescope is of Cassegrain design. It uses a two-meter primary with a focal ratio of 1.0 and a 20 cm secondary. The telescope is mounted at or near its center of gravity in a yoke frame which provides both telescope support and three axis pointing.

Coarse azimuthal pointing is achieved by driving the yoke against the balloon attachment bearing in the yoke. Fine azimuthal pointing utilizes the telescopes limited range ($\pm 3^{\circ}$) cross-elevation bearings. Coarse and fine elevation pointing are achieved with the single elevation bearing set.

Active closed loop pointing systems control motion in all three axis with a stability approximately 1 arcsecond rms. A three axis gyro, updated by a focal plane star tracker, is the fine pointing co-ordinate reference.

For launch and landing, the telescope is held vertically by means of a capture lock just below the balloon attachment bearing.

The total weight of the two-meter gondola is 1,731 kg (3,809 lbs.) including all NSBF required equipment. The overall height is 5.8 meter (19 feet). The overall diameter is 2.4 meters (8 feet), or just less than the maximum limits for normal highway loads, making hauling, shipping and recovery operations possible without disassembly of the gondola structure. We believe that careful design can bring the weight of the gondola below the 3500 lb. Palestine Texas launch limit.

The two-meter design baselines the CFRP aluminum honey comb-core primary mirror because of its very low weight availability and demonstrated performances. In addition, we are continuing to evaluate other lightweight mirror approaches. Section 4.0 summarizes the status of the University of Arizona mirror development program.

The two-meter mirror size also opened up the possibility of seriously re-considering focal plane guiding because of the superior optical finish we expect to be able to achieve on the smaller mirror. Focal plane guiding removes a series of structural instability terms from the pointing system stability equations. We have baselined focal plane guiding, using either the infrared imaging photometer experiment or a separate optical imaging camera and expect to be able to achieve sub-arcsecond rms pointing stability (Section 3.3).

Additional work has also been done on the development of experiment concepts. We report on the design of a new submillimeter spectrometer for the gondola (Section 5.3) and on the status of the infrared imaging photometer experiment which is nearing completion at the University of Chicago (Section 5.2).

Gondola costs reported in Section 8, although based on the ground-up, bolt by bolt estimate developed for the three-meter design, have some uncertainty due to the repeated application of inflation factors and post-facto adjustments to the rate of exchange of the DM. We estimate the total

price of this design to be $6,830K without instruments. Approximate costs for the submillimeter spectrometer are $1,071K and the IR Photometer are $475K, bringing the total program cost to $8,377K including the first flight. Alternative design approaches and the use of more modern technology may allow us to reduce this cost somewhat. The primary costs drivers are the lightweight mirror, the lightweight telescope structure and the pointing system. Lightweight mirror technology has developed significantly since the original quotations were obtained from Dornier and MAN and considerable savings may now be possible in that area. One verbal quote we received recently from ERG, Inc., Oakland, CA, indicates that a suitable 2M mirror might be made for as little as $250K rather than the $500K estimated by MAN. A local Boston firm, Nuclear Metals Inc., is also developing a sintered casting process for large lightweight mirrors which may allow similar savings. Similarly, a new evaluation of the telescope structure design may allow cost savings in that area. It may also be possible to take a sequential approach to the development of the pointing system allowing refinement of the design and achievement of the final specifications over the first few flights.

1.4 Relationship of Three-Meter/Two-Meter Telescope to the Large Deployable Reflector (LDR)

There are three areas where the balloon-borne telescope can contribute to LDR development: motivating and focusing light weight submillimeter and far infrared mirrors and structures; providing a test bed for submillimeter heterodyne receivers for space; and increasing the body of scientific observations needed to effectively plan LDR scientific programs. In each of these areas, the balloon-borne telescope has a unique potential contribution.

Already, the balloon mirror development program has identified carbon fiber reinforced plastic (CFRP sandwich panel mirrors) as a promising approach for the LDR mirror. Our collaborative development program with Dornier System has provided characterization of the thermal distortion of state-of-the-art CFRP mirrors in the temperature region of LDR and has resulted in a factor of 25 improvement in test mirror thermal distortion. This work is continuing in a collaboration with JPL and Hexcel Corporation. We are currently experimenting with overcoating and polishing CFRP mirrors to provide visible wavelength imaging capability, of importance to both the balloon telescope and LDR for alignment and pointing.

A major issue the LDR for photometric observations is whether the sensitivity will be limited by the fundamental shot noise in the background photon flux, which is on the order of a millionth of the background flux, or whether it will be limited by variations in the background flux due to varying thermal loads on the telescope. Also of importance for both telescope is the stability of the point spread function of the telescope for "super resolution" imaging analysis and for detecting faint companions and structures near bright sources.

Since the background for the balloon telescope, like LDR, is primarily from the telescope, not the sky, and since both telescopes have a similar

radiation environment, experience in understanding and dealing with these problems with the balloon telescope will be directly relevant to LDR. In addition, it will be possible to test particular reimaging and beam switching techniques for LDR on the balloon telescope. As an example, the secondary chopper approach to sky chopping, which has dominated over other approaches of infrared astronomy, has achieved this position through experience. No other technique has worked as well in practice. Beam switching will be essential for photometric observations with LDR. It would be desirable to demonstrate any innovative techniques with astronomical observations before committing the LDR design.

The second area is as a test bed for LDR instruments, in particular newly developed submillimeter heterodyne receivers. Only very limited observations are possible from the ground because of the poor submillimeter atmospheric windows. In addition, these instruments are complex and warrant gaining experience with remote operation in a space-like environment. Balloon-borne systems have provided a test bed for instruments developed for space UV, X-ray, gamma ray, and cosmic background astronomy. One reason cited for the lack of success of submillimeter proposals in the recent Explorer competition was limited experience with the required heterodyne receivers. The balloon-borne telescope offers a motivation and text bed for such development.

The third area concerns the body of scientific knowledge available to effectively plan LDR scientific programs. In this area, the balloon- borne telescope has a special capability for carrying out exploratory observations of important astrophysical lines which cannot be observed from the ground or from aircraft altitudes because of strong, broad atmospheric absorptions lines at the same wavelengths. Two such examples are observation of the ground state transitions of ortho and para water and low level transitions of molecular oxygen. Even at balloon altitudes, the atmospheric absorption prevents observation of these lines in galactic sources. However, for extragalactic objects with radial velocities of 300 km/sec or more, the lines are Doppler shifted sufficiently out of the narrow atmospheric absorption lines at balloon altitudes to be potentially observable. This is discussed in more detail in Section 2.0.

2.0 SCIENTIFIC OBJECTIVES

2.1 Introduction

Far-infrared and submillimeter observations are essential for attacking a number of very fundamental astronomical questions:

(1) Structure and evolution of galaxies and the nature of energy sources in active galactic nuclei.

(2) Understanding the large scale structure of our galaxy.

(3) Star formation and evolution processes in molecular clouds.

(4) Properties of the interstellar medium.

(5) Properties of the sun and solar system objects.

Specific balloon-borne far-infrared and submillimeter astronomical observations that can contribute to the solution of these scientific problems include:

(1) High resolution far-infrared and submillimeter spectroscopy of galactic, extragalactic, and solar system objects.

(2) Large area surveys of the galactic plane in spectral lines, e.g., OI (146 microns), C II (157 microns), etc.

(3) High angular resolution large area mapping of star formation regions, galaxies, etc., at submillimeter wavelengths.

Until LDR is flown, no presently planned infrared satellite experiment can perform these observations. The potential for balloon-borne infrared astronomy is great, and to date it has not been determined what its limitations are.

The balloon-borne telescope permits observations of several ionic, atomic, and molecular transitions from galactic sources that are inaccessible from airborne telescopes and offers particularly impressive advantages for the study of these lines in other galaxies.

Far-infrared atomic fine-structure lines, unlike their optical counterparts, are essentially unaffected by reddening or self-absorption. Far-infrared fine-structure lines are also very insensitive to electron temperature. Thus, they can provide very direct information on electron density, relative ionic and atomic abundances, cloud masses, and spectral types of ionizing stars. In addition, lines like those from O I at 63 μm and 146 μm and C II at 157 μm, which are major coolants for neutral gas at temperatures of 100-1,000°K, provide essential data on the heating of interface regions between ionic and molecular clouds and on shock heating of the interstellar medium. N II lines at 122 μm and 204 μm can be combined with the N III line at 57 μm to study electron density, nitrogen abundances, and ionization structure in H II regions.

Molecular lines at far-infrared and submillimeter wavelengths are important for two reasons. First, they represent dominant coolants and important diagnostic indicators for gas with temperatures of a few hundred degrees. Observations of emission from many different levels of CO, for example, can yield accurate estimates of molecular hydrogen density, temperature, and total CO column density in warm, shocked gas in active star formation regions. Second, far-infrared observations may allow detection of molecular species not accessible at other wavelengths (e.g., many of the most abundant hydrides). This could provide important clues to both abundances and chemical processes in the clouds. Other important molecules include OH, CH, and NH_3.

Perhaps the greatest contribution of a balloon-borne telescope would be to significantly expand the ability to observe important molecular coolants, such as H_2O and O_2, in extragalactic sources. These molecules compete with CO as the most important coolants of the denser portions of

molecular clouds.

In Figure 2.1-1 the typical sizes of objects this Two-Meter Balloon-Borne Telescope will study are indicated, as well as the distances at which they are likely to lie. Three diagonal lines indicate angular resolutions of 30 arcseconds, about the best achievable at 100μm wavelength with one-meter-class telescopes, such as the Kuiper Airborne Observatory (KAO), other balloon-borne telescopes, and the Space Infrared Telescope Facility (SIRTF); 12 arcseconds, the resolution achievable with the Two-Meter Balloon-Borne Telescope; and 1 arcsecond, the resolution achievable with the LDR. From the figure it can be seen that the two-meter telescope will allow us to resolve and study in detail such objects as collapsing proto-stellar condensations in our own galaxy, clusters of protostars in the Magellanic Clouds, giant molecular clouds in nearby galaxies, and spiral arms in distant galaxies.

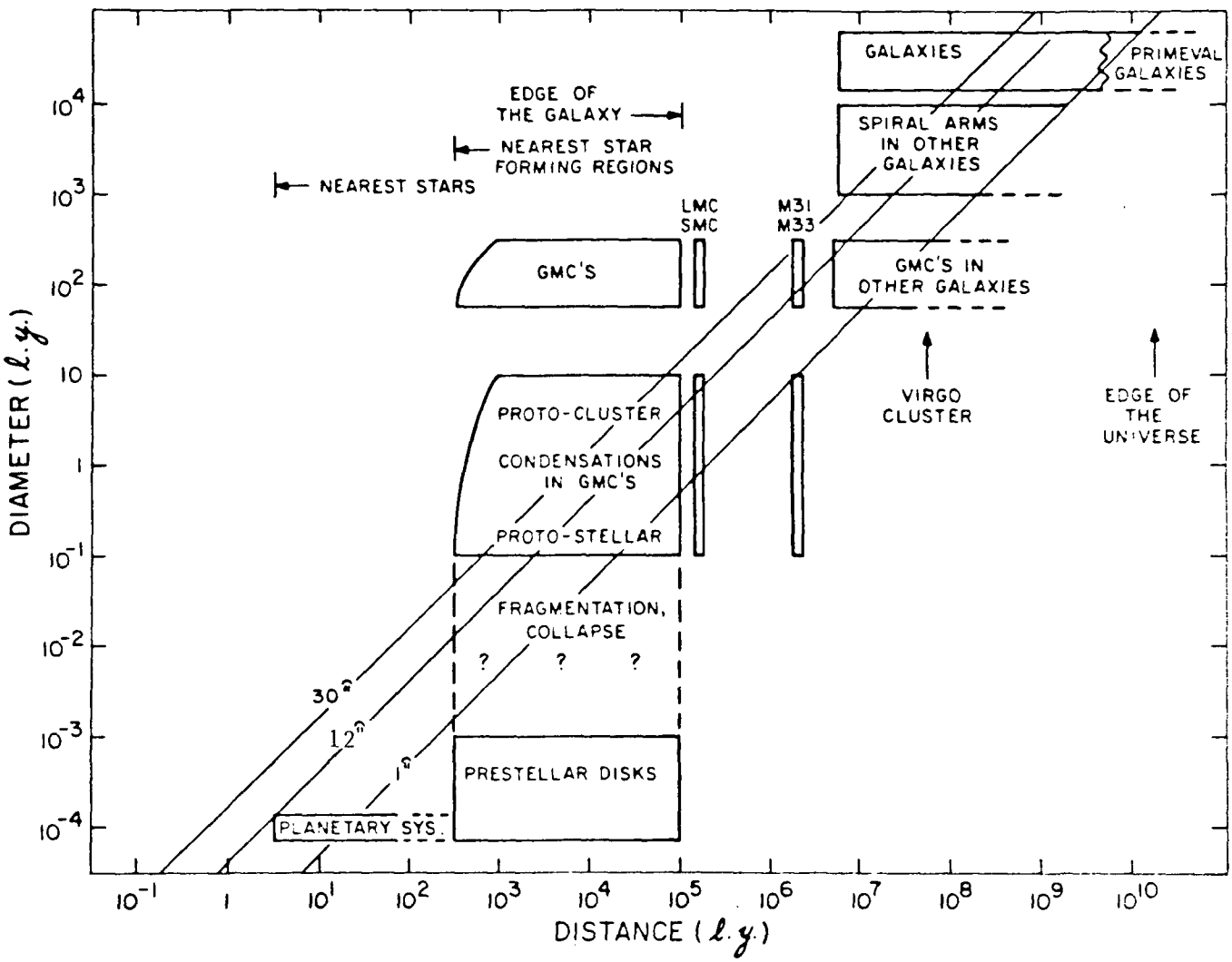

Figure 2.1-1. Typical Sizes of Objects to be Studied by the Two-Meter Balloon-Borne Telescope

2.2 Submillimeter Spectroscopy

2.2.1 Introduction

The discussion that follows is divided into three parts: (1) a review of the most important transitions between 50μm and 1mm, (2) a brief discussion of the method used to model the atmospheric transmission, and (3) the unique science that can be conducted by a balloon-borne telescope.

2.2.2 Far-Infrared and Submillimeter Lines

The spectroscopic features in the far-infrared and submillimeter are expected to be dominated by molecular rotational transitions and by atomic fine-structure lines. From the results of millimeterwave spectroscopy, not only is it known that the interstellar medium contains many molecular species, but also from observations of these various molecules it is clear that the temperature of the gas is typically between 10 and 100 K. Generally, then, it is expected that most of the energy emitted by the medium will be in the range 1mm-100μm.

Most of the lines occurring in the far-infrared and submillimeter may be placed into one of three categories: (1) ground-state, fine-structure transitions in atoms or atomic ions, (2) low-lying rotational transitions in light molecules, such as hydrides, and (3) mid-level rotational transitions in heavy molecules. These transitions are summarized in Tables 2.2-1 - 2.2.4.

(a) Atoms and Ions

Atoms and atomic ions may possess a ground state with a net orbital electronic angular momentum so that the state may be split by spin-orbit effects. Several of the light atoms and ions have a ground state fine structure of this kind which provides transitions in the far-infrared and submillimeter. With increasing atomic weight the transitions move rapidly into the near-infrared and optical.

(b) Light Molecules

These molecules contain hydrogen, incorporated into the structure in such a way that the lowest rotational modes are dominated by the hydrogen mass so that the lowest frequency appears in the submillimeter. For most of the simple hydride molecules this is the case, and they can only easily be observed in the submillimeter.

(c) Heavy Molecules

Although heavy molecules possess transitions which can be observed in the millimeter band, it is most helpful to an understanding of the physical conditions giving rise to the emission to have available the higher energy transitions for comparison.

Species	Transition	Frequency (GHz)	Wavelength (μm)
N^+	$^3P_1 \rightarrow {}^3P_0$	1470.3	203.9
C^+	$^2P_{3/2} \rightarrow {}^2P_{1/2}$	1900.536	157.741
N^+	$^3P_2 \rightarrow {}^3P_1$	2459.553	121.889
O^{++}	$^3P_1 \rightarrow {}^3P_0$	3393.045	88.355
N^{++}	$^2P_{3/2} \rightarrow {}^2P_{1/2}$	5230.428	57.317
O^{++}	$^3P_2 \rightarrow {}^3P_1$	5785.712	51.816

Table 2.2-1. Important Submillimeter Transitions - Atomic Ions

Species	Transition	Frequency (GHz)	Wavelength (μm)
C^o	$^3P_1 \rightarrow {}^3P_0$	492.162	609.134
C^o	$^3P_2 \rightarrow {}^3P_1$	809.350	370.411
O^o	$^3P_0 \rightarrow {}^3P_1$	2060.061	145.526
Si^o	$^3P_1 \rightarrow {}^3P_0$	2311.751	129.682
Si^o	$^3P_2 \rightarrow {}^3P_1$	4378.194	68.474
O^o	$^3P_1 \rightarrow {}^3P_2$	4744.775	63.184
S^o	$^3P_0 \rightarrow {}^3P_1$	5322.830	56.322

Table 2.2-2. Important Submillimeter Transitions - Neutrals

Species	Transition	Frequency (GHz)	Wavelength (μm)
H_2D^+	$J_{K_pK_o} = 1_{10} \rightarrow 1_{11}$	372.421	804.982
AlH	$J = 1 \rightarrow 0$	377.59	793.96
LiH	$J = 1 \rightarrow 0$	443.953	675.280
H_2S	$J_{K_pK_o} = 1_{11} \rightarrow 0_{00}$	452.390	662.685
CH	$^2\Pi\ F_1 \rightarrow F_2 : J = 3/2^+ \rightarrow 1/2^-$	532.726	562.751
	$J = 3/2^- \rightarrow 1/2^+$	536.761	558.521
H_2O	$1_{10} - 1_{01}$	556.936	538.289
NH_3	$J_K = 1_0 \rightarrow 0_0$	572.498	523.657
SiH	$^2\Pi\ F_1 : J = 3/2^- \rightarrow 1/2^+$	624.925	479.726
HCl	$J = 1 \rightarrow 0$	625.919	478.964
SiH	$^2\Pi\ F_1 : J = 3/2^+ \rightarrow 1/2^-$	627.690	477.612
NH	$^3\Sigma^-, N = 1 - 0, J = 2 - 1$	974.63	307.60
H_3O^+	$J_K = 0_0^- \rightarrow 1_0^+$	984.656	304.464
H_2O	$1_{11} \rightarrow 0_{00}$	1113.342	269.273
NH_3	$J_K = 2_0 \rightarrow 1_0$	1214.859	246.771
H_2D^+	$J_{K_pK_o} = 1_{01} \rightarrow 0_{00}$	1370.204	218.794
SH	$^2\Pi_{3/2}\ J = 5/2 \rightarrow 3/2$	1382.928	216.781
		1383.257	216.729
CH	$^2\Pi\ F_1 : J = 5/2^- \rightarrow 3/2^+$	1656.964	180.929
	$J = 5/2^+ \rightarrow 3/2^-$	1661.105	180.478
OH	$^2\Pi_{1/2}\ J = 3/2^- \rightarrow 1/2^+$	1834.760	163.396
	$J = 3/2^+ \rightarrow 1/2^-$	1837.853	163.121
CH	$^2\Pi\ F_2 : J = 3/2^- \rightarrow 1/2^+$	2006.797	149.388
	$J = 5/2^+ \rightarrow 3/2^-$	2010.809	149.091
CH_2	$J = 1 - 1, N_{K_aK_c} = 1_{11} \rightarrow 0_{00}$	2344.697	127.860
OH	$^2\Pi_{3/2}\ J = 5/2^+ \rightarrow 3/2^-$	2509.963	119.441
	$J = 5/2^- \rightarrow 3/2^+$	2514.320	119.234
HD	$J = 1 \rightarrow 0$	2675.023	112.071
OH	$^2\Pi_{1/2 \rightarrow 3/2} : J = 5/2^+ \rightarrow 3/2^-$	3786.132	79.182
	$J = 5/2^- \rightarrow 3/2^+$	3789.216	79.117

Table 2.2-3. Important Submillimeter Transitions - Hydrides

Species	Transition	Frequency (GHz)	Wavelength (μm)
O_2	$N_J = 1_1 \rightarrow 1_0$	118.750	2524.568
CS	$J = 7 \rightarrow 6$	342.883	874.329
CO	$J = 3 \rightarrow 2$	345.796	866.964
HCN	$J = 4 \rightarrow 3$	354.505	845.666
CS	$J = 8 \rightarrow 7$	391.847	765.075
O_2	$N_J = 3_2 \rightarrow 1_2$	424.763	705.788
^{13}CO	$J = 4 \rightarrow 3$	440.764	680.166
CS	$J = 9 \rightarrow 8$	440.803	680.105
HCN	$J = 5 \rightarrow 4$	443.123	676.544
CO	$J = 4 \rightarrow 3$	461.042	650.250
O_2	$N_J = 3_3 \rightarrow 1_2$	487.249	615.276
CS	$J = 10 \rightarrow 9$	489.751	612.132
HCN	$J = 6 \rightarrow 5$	531.712	563.825
CS	$J = 11 \rightarrow 10$	538.689	556.522
^{13}CO	$J = 5 \rightarrow 4$	550.926	544.161
CO	$J = 5 \rightarrow 4$	576.267	520.232
CS	$J = 12 \rightarrow 11$	587.616	510.184
HCN	$J = 7 \rightarrow 6$	620.301	483.302
CS	$J = 13 \rightarrow 12$	636.532	470.978
^{13}CO	$J = 6 \rightarrow 5$	661.066	453.498
CS	$J = 14 \rightarrow 13$	685.435	437.376
CO	$J = 6 \rightarrow 5$	691.474	433.555
HCN	$J = 8 \rightarrow 7$	708.889	422.905
^{13}CO	$J = 7 \rightarrow 6$	771.183	388.744
HCN	$J = 9 \rightarrow 8$	797.433	375.947
CO	$J = 7 \rightarrow 6$	806.652	371.650
^{13}CO	$J = 8 \rightarrow 7$	881.273	340.181
HCN	$J = 10 \rightarrow 9$	885.977	338.375
CO	$J = 8 \rightarrow 7$	921.799	325.225
HCN	$J = 11 \rightarrow 10$	974.475	307.645
^{13}CO	$J = 9 \rightarrow 8$	991.330	302.414

Table 2.2-4. Important Submillimeter Transitions - Heavy Molecules

Species	Transition	Frequency (GHz)	Wavelength (μm)
CO	$J = 9 \rightarrow 8$	1036.913	289.120
HCN	$J = 12 \rightarrow 11$	1062.974	282.032
^{13}CO	$J = 10 \rightarrow 9$	1101.351	272.204
HCN	$J = 13 \rightarrow 12$	1151.443	260.362
CO	$J = 10 \rightarrow 9$	1151.985	260.240
HCN	$J = 14 \rightarrow 13$	1239.882	241.791
CO	$J = 11 \rightarrow 10$	1267.016	236.613
CO	$J = 12 \rightarrow 11$	1381.995	216.927
CO	$J = 13 \rightarrow 12$	1496.924	200.272
CO	$J = 14 \rightarrow 13$	1611.795	185.999
CO	$J = 15 \rightarrow 14$	1726.604	173.631
CO	$J = 16 \rightarrow 15$	1841.346	162.812
CO	$J = 17 \rightarrow 16$	1956.020	153.267
CO	$J = 18 \rightarrow 17$	2070.615	144.784
CO	$J = 19 \rightarrow 18$	2185.136	137.196
CO	$J = 20 \rightarrow 19$	2299.570	130.369
CO	$J = 21 \rightarrow 20$	2413.917	124.193
CO	$J = 22 \rightarrow 21$	2528.174	118.581
CO	$J = 23 \rightarrow 22$	2642.332	113.458
CO	$J = 24 \rightarrow 23$	2756.388	108.763
CO	$J = 25 \rightarrow 24$	2870.342	104.445
CO	$J = 26 \rightarrow 25$	2984.182	100.461
CO	$J = 27 \rightarrow 26$	3097.911	96.772
CO	$J = 28 \rightarrow 27$	3211.521	93.349
CO	$J = 29 \rightarrow 28$	3325.007	90.163
CO	$J = 30 \rightarrow 29$	3438.368	87.190
CO	$J = 31 \rightarrow 30$	3551.593	84.411
CO	$J = 32 \rightarrow 31$	3664.687	81.806
CO	$J = 33 \rightarrow 32$	3777.640	79.360
CO	$J = 34 \rightarrow 33$	3890.446	77.059
CO	$J = 35 \rightarrow 34$	4003.105	74.890

Table 2.2-4 Important Submillimeter Transitions - Heavy Molecules (Continued)

2.2.3 Models of Atmospheric Transmission

Use is made of the Air Force Geophysical Laboratory Atmospheric (AFGL) Absorption Line Parameters Compilation (Rothman et al. 1983) atmospheric absorption-line parameter database to obtain the wavenumber, line strength, pressure broadening coefficient, and energy level of the lower state for over 109,000 known transitions of H_2O, O_3, O_2, CO_2, CO, N_2O, HCl, OH, and CH_4 between about 0.76μm and 3.26mm. At the wavelengths of interest here, 50μm to 1mm, essentially all of the atmospheric interference is due to lines of H_2O, O_3, and O_2. Table 2.2-5 summarizes the molecular abundances, pressures, and temperatures employed in the calculation of atmospheric transparency at 14 and 32 km.

The H_2O abundance at 14 km is an average over many KAO flights (Meyer 1988), while the 32 km value corresponds to an average value measured during balloon flights over Palestine, Texas, during the spring and fall (Chance and Traub 1988). The O_2 abundance is taken from Allen (1973). The vertical distribution of O_3 is taken from the U.S. Standard Atmosphere Supplements. The value for CO is given by Farmer (1974) as 0.06 ± 0.01 ppmv at latitude 30°N and altitudes greater than 10 km. The OH concentrations were obtained from Solomon (1986) and the HCl concentrations are from Farmer et al. (1988).

The model atmosphere used is a three-layer, Curtis-Godson approximation (Goody 1964) with the parameters as given in Table 2.2-5. The effective pressures in Table 2.2-5 are a mean for each layer and are used in the calculation of collision line-broadening. The effective temperatures are taken to be those which actually occur at each effective pressure using the U.S. Standard Atmosphere (1966).

According to Goody (1964), the Curtis-Godson approximation is quite accurate for the weak and strong line strength limits at each point in the absorption line profile. For intermediate line strengths, the transmission error appears to be at worst about 5% at the line core, and much smaller elsewhere. Inspection of the comparison calculations reported in Goody's book suggests that for species that are well-mixed, the error in average transmission across a line should be well under 1%. Some further support for the Curtis-Godson approximation can be derived from experiences in fitting theoretical line profiles to high resolution observations of the terrestrial O_2 near 7635 Angstrom (Carleton and Traub 1972) and 1.27μm (Noxon et al. 1976) and H_2O lines near 8197 Angstrom (Traub and Carleton 1974); in all cases the experimental and calculated profiles were identical to within the noise level of the data, which was typically less than 5% of the continuum.

Validation of the calculated atmospheric transmission profiles at balloon altitudes in the far-infrared have been obtained more recently by Chance and Traub (1987), Robbins et al. (1988), and Murcray et al. (1988). Very good qualitative agreement between calculated and observed atmospheric transmission profiles is also seen in the far-infrared at airplane altitudes; however, the absence of a reliable line-of-sight water vapor content limits our ability to quote an exact measure of agreement.

Parameter	Layer 1	Layer 2	Layer 3
		14 km	
Effective altitudes (km)	15.16	18.42	25.50
Effective number density (cm^{-3})	3.9×10^{18}	2.4×10^{18}	7.6×10^{17}
Column densities (cm^{-2})	1.4×10^{24}	1.4×10^{24}	1.4×10^{24}
Effective pressures (mbar)	118.08	70.85	23.61
Effective temperatures (K)	217	217	226
H_2O concentration †	5.5×10^{-6}	5.5×10^{-6}	5.5×10^{-6}
O_2 concentration	2.1×10^{-1}	2.1×10^{-1}	2.1×10^{-1}
O_3 concentration	8.0×10^{-8}	3.0×10^{-7}	7.0×10^{-6}
CO concentration	6.0×10^{-8}	6.0×10^{-8}	6.0×10^{-8}
OH concentration	1.0×10^{-13}	4.0×10^{-13}	4.0×10^{-11}
HCl concentration	2.6×10^{-9}	2.6×10^{-9}	2.6×10^{-9}
		32 km	
Effective altitudes (km)	33.24	36.82	45.05
Effective number density (cm^{-3})	2.3×10^{17}	1.3×10^{17}	4.2×10^{16}
Column densities (cm^{-2})	9.0×10^{22}	9.0×10^{22}	9.0×10^{22}
Effective pressures (mbar)	7.41	4.45	1.48
Effective temperatures (K)	232	242	258
H_2O concentration †	4.0×10^{-6}	4.0×10^{-6}	4.0×10^{-6}
O_2 concentration	2.1×10^{-1}	2.1×10^{-1}	2.1×10^{-1}
O_3 concentration	6.0×10^{-6}	8.0×10^{-6}	6.0×10^{-6}
CO concentration	6.0×10^{-8}	6.0×10^{-8}	6.0×10^{-8}
OH concentration	1.0×10^{-11}	5.0×10^{-11}	2.0×10^{-10}
HCl concentration	2.6×10^{-9}	2.6×10^{-9}	2.6×10^{-9}

† Corresponds to 7.0 μm at 14 km and 0.32 μm at 32 km of precipitable H_2O along a 45° elevation line-of-sight.

Table 2.2-5. Parameters Used in Three-Layer Atmospheric Approximation

The calculating grid is chosen to have points spaced by $0.0002cm^{-1}$ at both 14 and 32 km levels. The pressure-broadened full-width (FWHM) expected for a typical molecule at 14 and 32 km levels is 0.007 and $0.0008cm^{-1}$, respectively; thus these calculations should accurately represent the true width of the atmospheric features.

2.2.4 Unique Balloon Altitude Science Programs

To determine which of the transitions given in Tables 2.2-1 - 2.2-4 are accessible only from a balloon-borne platform, and not from an airborne platform, the atmospheric transmission within about ±1000 km s^{-1} of each of the listed transitions was examined. This range of velocities was selected to include all bright galactic H II regions and planetary nebulae (see Table 2.2-6) as well as many of the brightest nearby star forming galaxies (see Table 2.2-7). For simplicity, the results discussed below are divided into two categories: (1) the transmission of the atmosphere within 100 km s^{-1} of the line center, which includes the V_{LSR}'s of most galactic sources, and (2) the atmospheric transmission greater than +100 km s^{-1} and less than -100 km s^{-1} from the line center, which corresponds to the V_{LSR}'s of most of the nearby, infrared bright extragalactic sources. These results are summarized in Tables 2.2-8 and 2.2-9. Examples of a few cases are shown in Figures 2.2-1 - 2.2-6.

The main result is that a balloon-borne telescope permits observations of several ionic, atomic, and molecular transitions from galactic sources that are inaccessible from an airborne telescope. Because of the narrowing of all atmospheric features at 32 km compared to 14 km combined with the relatively large Doppler shifts of many extragalactic sources, a balloon-borne telescope offers particularly impressive advantages for the study of other galaxies.

The greatest advantage to galactic spectroscopy of a balloon-borne telescope is the significantly increased observability of the [OI] 145.526μm fine-structure line (Figure 2.2-3). Measured in conjunction with the widely observed [OI] 63.184μm fine-structure line, the ratio of these line strengths can be used to determine the neutral gas temperature. Further, when the [C II] 157.741μm line is also measured, the ratio of these three line strengths can be used to tightly constrain both temperature and density (cf. Watson 1985). Likewise, the [N II] 121.889μm fine-structure line (Figure 2.2-4), which is only observable at or above an altitude of 32 km, could be combined with the [N II] 203.9μm and the [N III] 57.317μm fine-structure lines to study the electron density, nitrogen abundance, and ionization structure of galactic H II regions.

In recent years, airborne spectrometers have achieved the sensitivity needed to study galactic molecular emission other than CO, such as OH, CH, and NH_3. In principle, accounting for the line strengths of two or more transitions from the same molecule is a powerful means of limiting the range of density, temperature, and, in some cases, the radiation field strength in the emitting region (cf. Melnick et al. 1987). Whereas OH, CH, and NH_3 have several transitions which occur at far-infrared and submillimeter wavelengths, not all of the lowest transitions are free from atmo-

Source	V_{LSR} (km s^{-1})
NGC 7538	−60
G 333.6-0.2	−48
W3	−40
IRC +10216	−26
Eta Carina	−18
BD +30 3639	−13
NGC 6357	−4
NGC 6720 (Ring Neb.)	0
DR 21	+1
M 8	+3
W 49	+9
NGC 2024	+8
Orion-KL	+10
NGC 2071	+10
M 17	+18
NGC 7027	+24
Sgr A	+50
W 51	+58
Sgr B2	+66

Table 2.2-6. V_{LSR}'s of Selected Galactic HII Regions and Planetary Nebulae

Source	V_{LSR} (km s^{-1})
IC 342	+30
NGC 6946	+55
M82 (NGC 3034)	+220
NGC 253	+250
M83 (NGC 5236)	+490
Cen A (NGC 5128)	+500
NGC 2146	+865
NGC 1068 (M77)	+1120
M51 (NGC 5194)	+1470

Table 2.2-7. V_{LSR}'s of Nearby, Gas-Rich Star Forming Galaxies

Species	Transition	Frequency (GHz)	Wavelength (μm)
CO	$J = 10 \rightarrow 9$	1151.985	260.240
NH_3	$J_K = 2_0 \rightarrow 1_0$	1214.859	246.771
CH	$^2\Pi\ F_1 : J = 5/2^- \rightarrow 3/2^+$	1656.964	180.929
O°	$^3P_0 \rightarrow {}^3P_1$	2060	145.526
N^+	$^3P_2 \rightarrow {}^3P_1$	2459.553	121.889
OH	$^2\Pi_{1/2 \rightarrow 3/2}\ J = 5/2^+ \rightarrow 3/2^-$	3786.132	79.182
	$J = 5/2^- \rightarrow 3/2^+$	3789.216	79.117

Table 2.2-8. Some Important Transitions Observable from a Balloon, but not an Airplane, for $+100 \leq V_{LSR} \leq -100$km s^{-1}.

spheric interference at 14 km. At balloon altitudes, the full spectrum of lower transitions from these molecules is observable.

Perhaps the greatest contribution of a balloon-borne telescope would be to significantly expand the ability to observe important molecular cloud coolants in extragalactic sources such as H_2O and O_2. As is shown in Figures 2.2-5 and 2.2-6, at an altitude of 32 km the terrestrial counterparts to these ground-state H_2O and O_2 lines become sufficiently narrow that any source with a V_{LSR} greater than ± 300 km s^{-1} will be clear of any atmospheric interference. This would also apply to potentially interesting higher-lying H_2O lines not indicated in Table 2.2-9. As shown in Figure 2.2-8, H_2O and O_2 compete with CO as the most important coolants of the denser portions of molecular clouds.

Most of the energy emitted by neutral atomic gas with temperatures in the range 10-5000 K and densities below about 10^8 cm^{-3} is radiated in the [OI] 63.184μm and [C II] 157.741μm fine-structure transitions, making them the brightest lines in the infrared spectrum of gas-rich galaxies (cf. Crawford et al. 1985; Lugten et al. 1986). At an altitude of 14 km, the [OI] 63.184μm line cannot be observed from sources with V_{LSR}'s much greater than +200 km s^{-1} (Figure 2.2-1). At an altitude of 32 km, this line can be observed from most of the sources in Table 2.2-7.

Species	Transition	Frequency (GHz)	Wavelength (μm)
O_2	$(1,1) \rightarrow (1,0)$	118.750	2524.568
O_2	$(3,2) \rightarrow (1,2)$	424.763	705.788
O_2	$(3,3) \rightarrow (1,2)$	487.249	615.276
H_2O	$1_{10} \rightarrow 1_{01}$	556.936	538.289
H_2O	$1_{11} \rightarrow 0_{00}$	1113.342	269.273
CO	$J = 10 \rightarrow 9$	1151.985	260.240
SH	$^2\Pi_{3/2}\ J = 5/2 \rightarrow 3/2$	1382.928	216.781
		1383.257	216.729
N^+	$^3P_1 \rightarrow {}^3P_0$	1470.3	203.9
CH_2	$1_{11} \rightarrow 0_{00}$	2344.697	127.860
N^+	$^3P_2 \rightarrow {}^3P_1$	2459.553	121.889
O°	$^3P_1 \rightarrow {}^3P_2$	4744.775	63.184
S°	$^3P_0 \rightarrow {}^3P_1$	5322.830	56.322

Table 2.2-9. Some Important Transitions Observable from a Balloon, but not an Airplane, for -100km $s^{-1} \geq V_{LSR}$ and $V_{LSR} \geq +100$km s^{-1}.

Because sulfur has an ionization energy of 10.36 eV, the [SI] 56.322μm fine-structure will arise almost exclusively from well shielded neutral gas regions - regions not entirely probed by the [C II] 157.741μm line which exists within a photon energy range of 11.26 and 24.38 eV. As such, this line, along with its companion fine-structure line at 25.246μm and the fine-structure lines of [CI], can be used to study deeper (i.e. higher A_v) portions of extragalactic photodissociation regions (cf. Tielens and Hollenbach 1985)(Figure 2.2-7).

Thus, much as ground-based radio astronomy has spent the past three decades successfully studying a large variety of galactic and extragalactic phenomena in the lines of a few important atomic and molecular species (eg. CO, HI, OH, CS, NH_3), opening the skies to regular study in the lines discussed above will complement the scientific contributions from the KAO and SOFIA and will fill a unique niche in far-infrared and submillimeter astronomy until LDR is a reality.

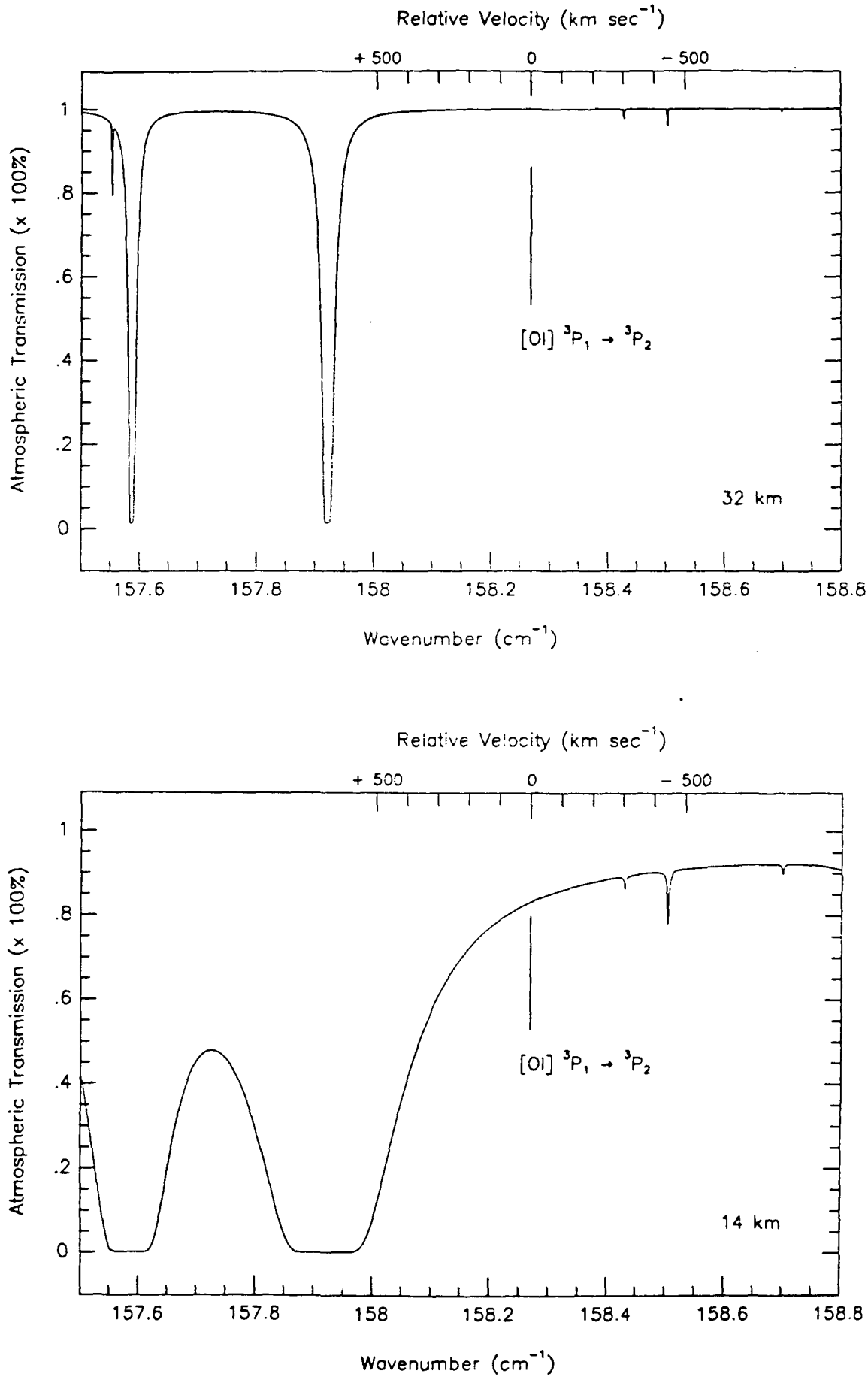

Figure 2.2-1. Atmospheric transmission at 14 and 32 km in the vicinity of the [OI]63.184μm line

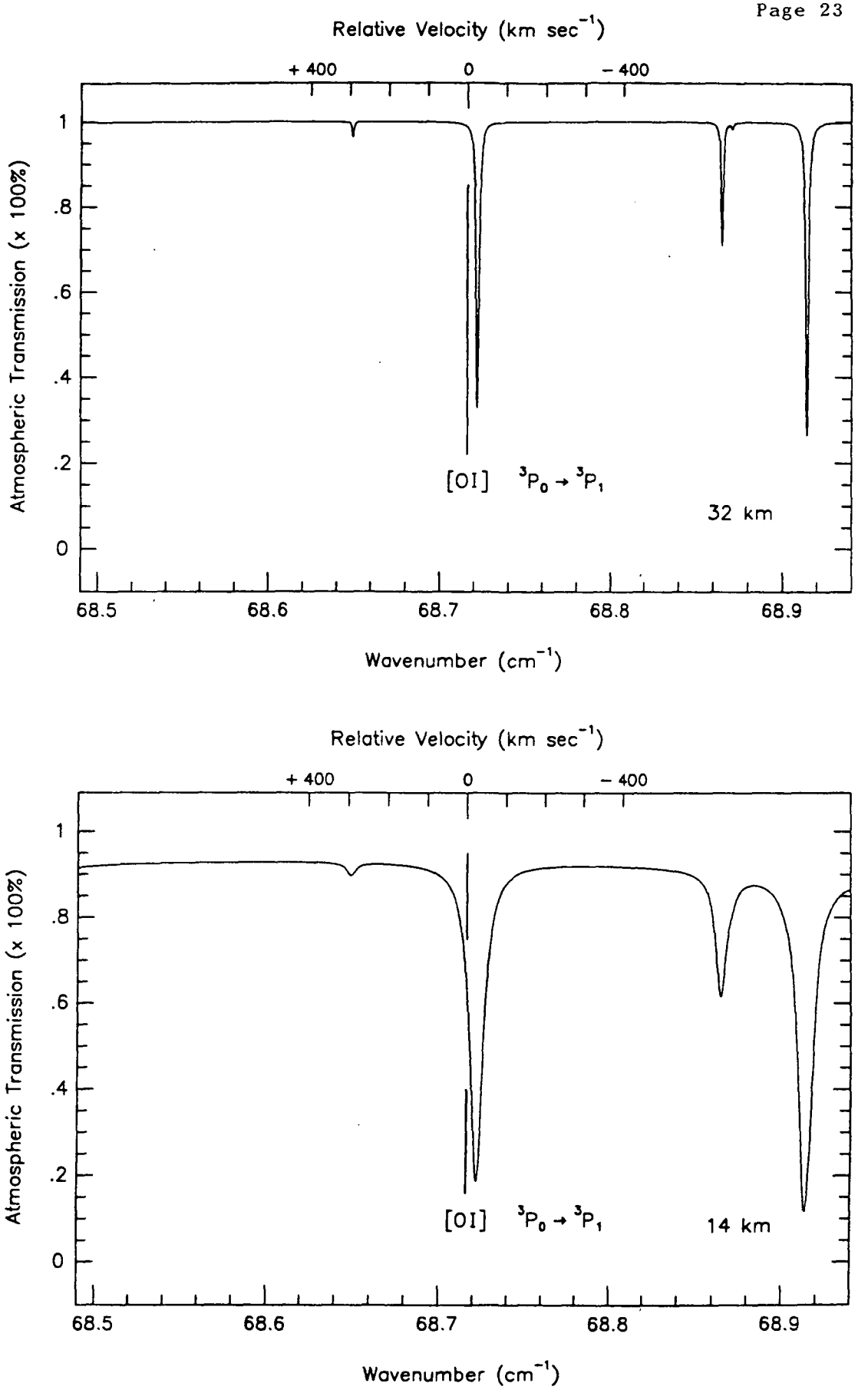

Figure 2.2-2. Atmospheric transmission at 14 and 32 km in the vicinity of the [OI]145.526μm line

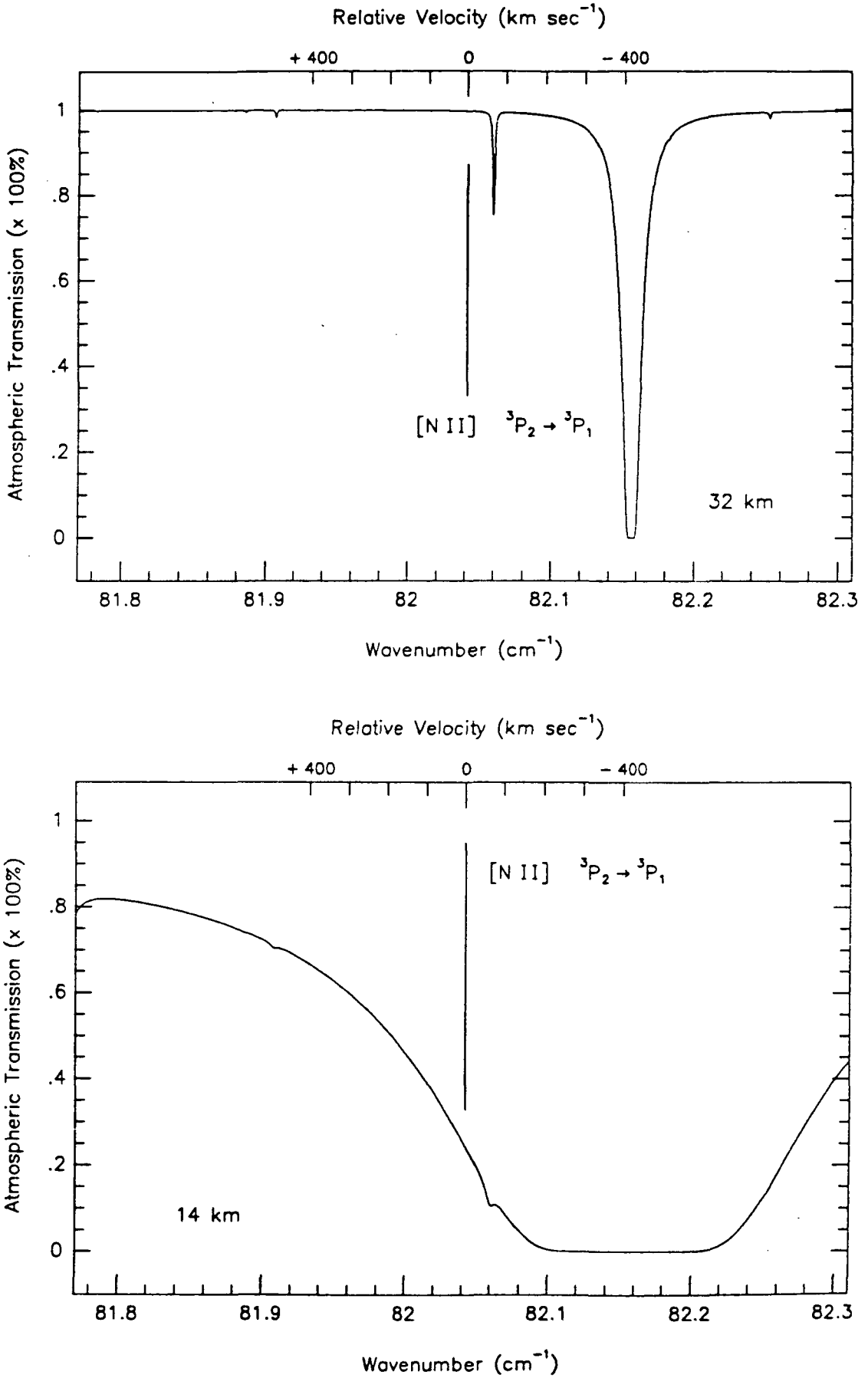

Figure 2.2-3. Atmospheric transmission at 14 and 32 km in the vicinity of the [N II]121.889μm line

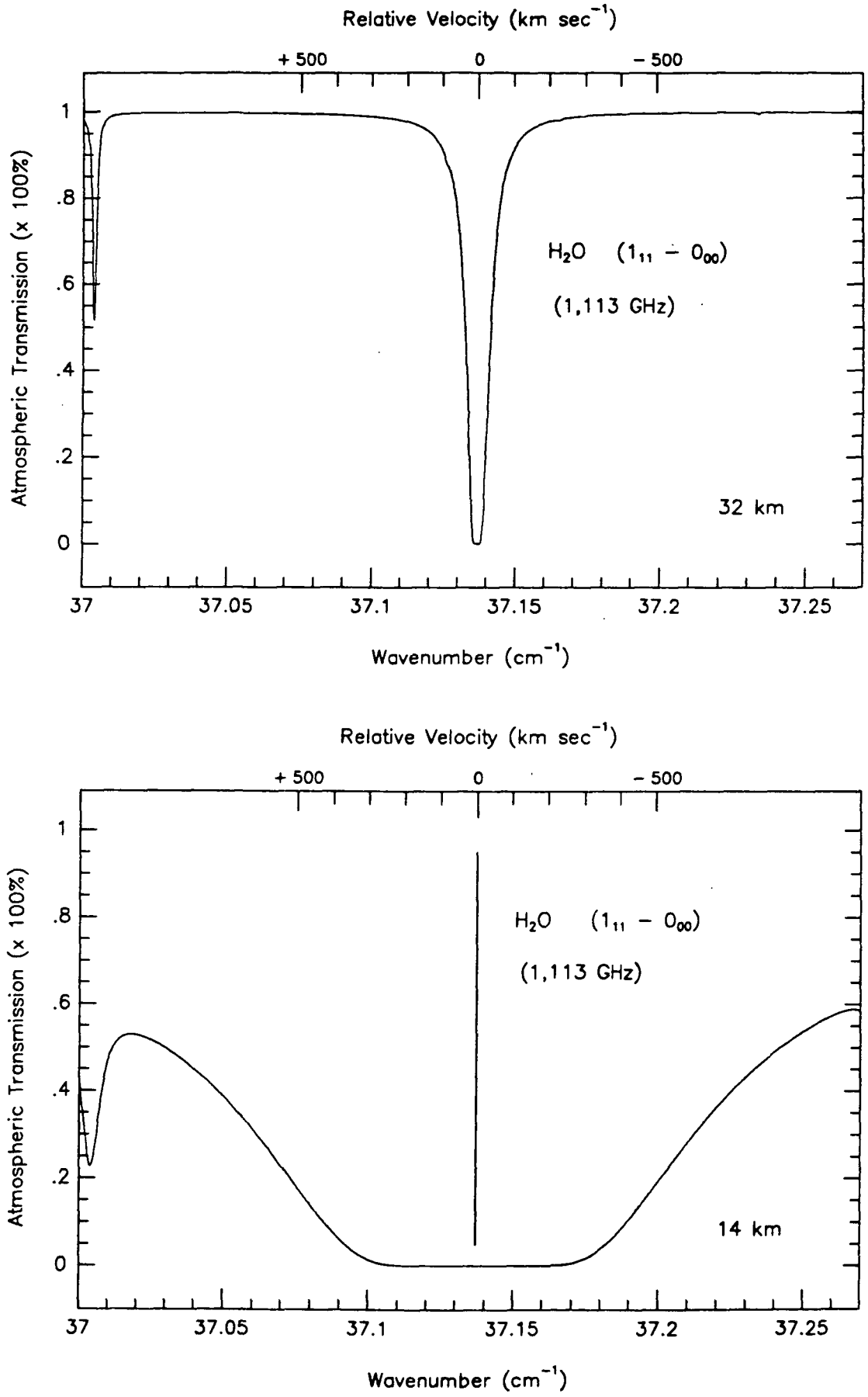

Figure 2.2-4. Atmospheric transmission at 14 and 32 km in the vicinity of the ground-state transition of para-H_2O

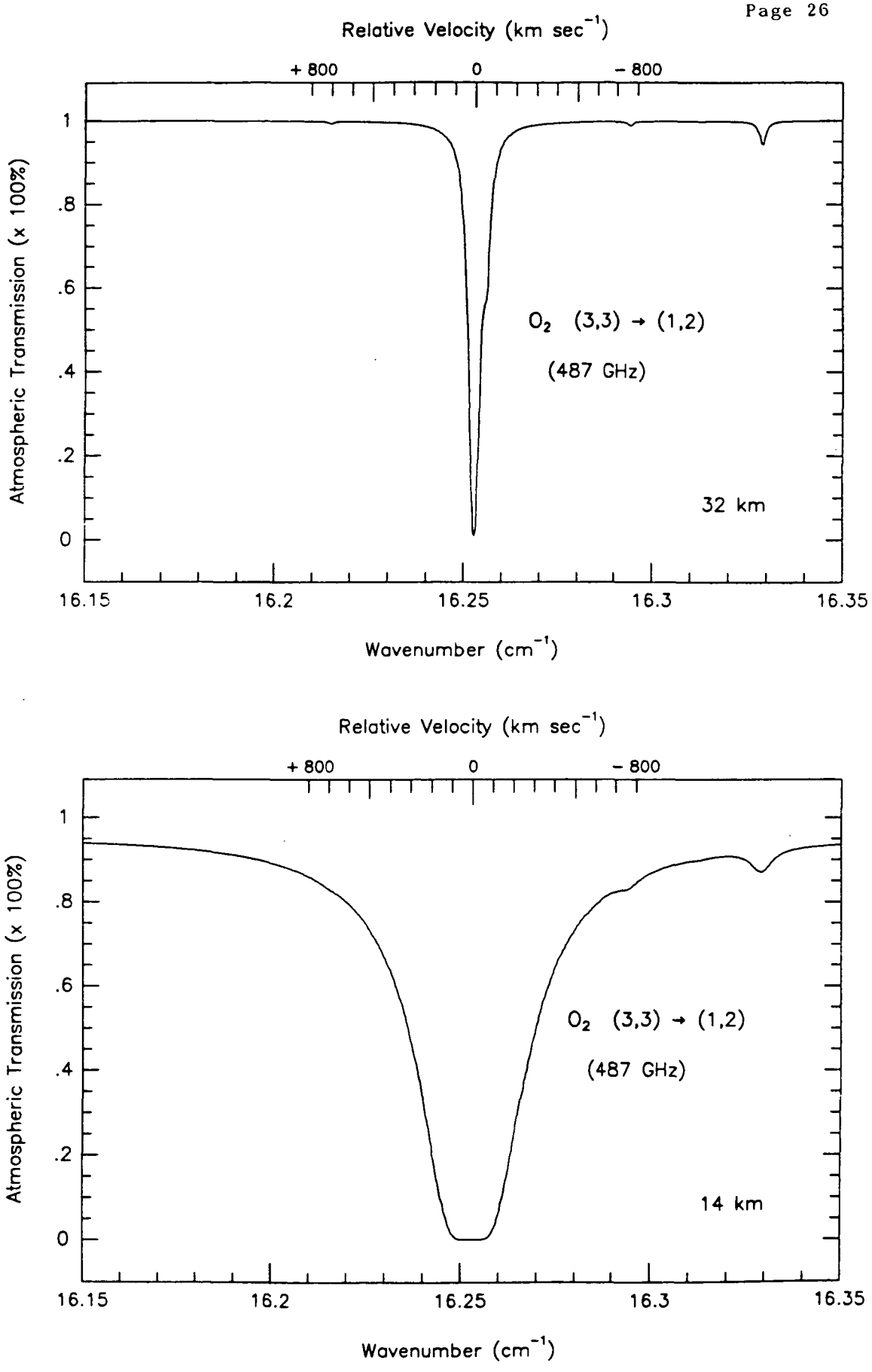

Figure 2.2-5. Atmospheric transmission at 14 and 32 km in the vicinity of the O_2 487 GHz line

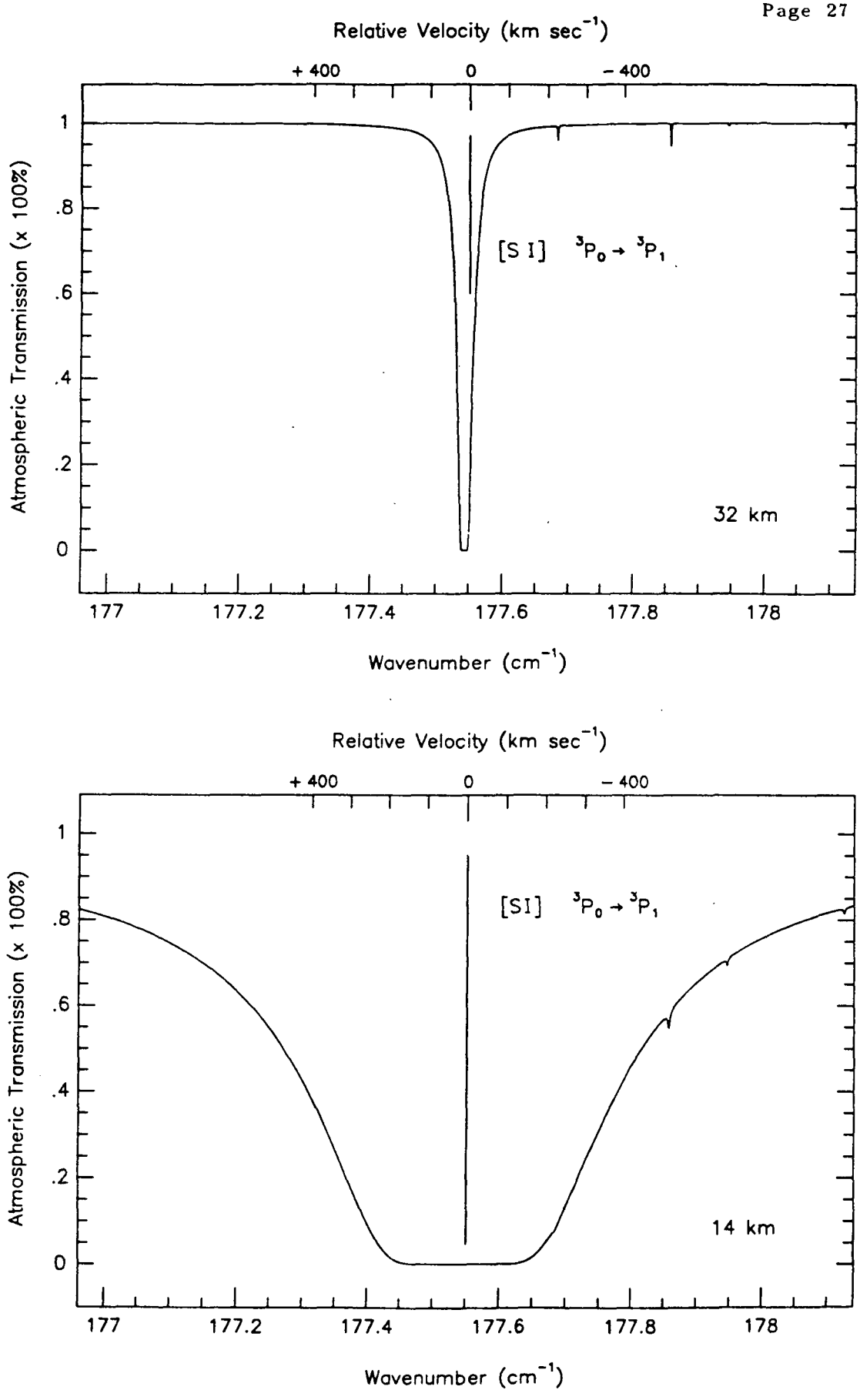

Figure 2.2-6. Atmospheric transmission at 14 and 32 km in the vicinity of the [SI] 56.322μm line

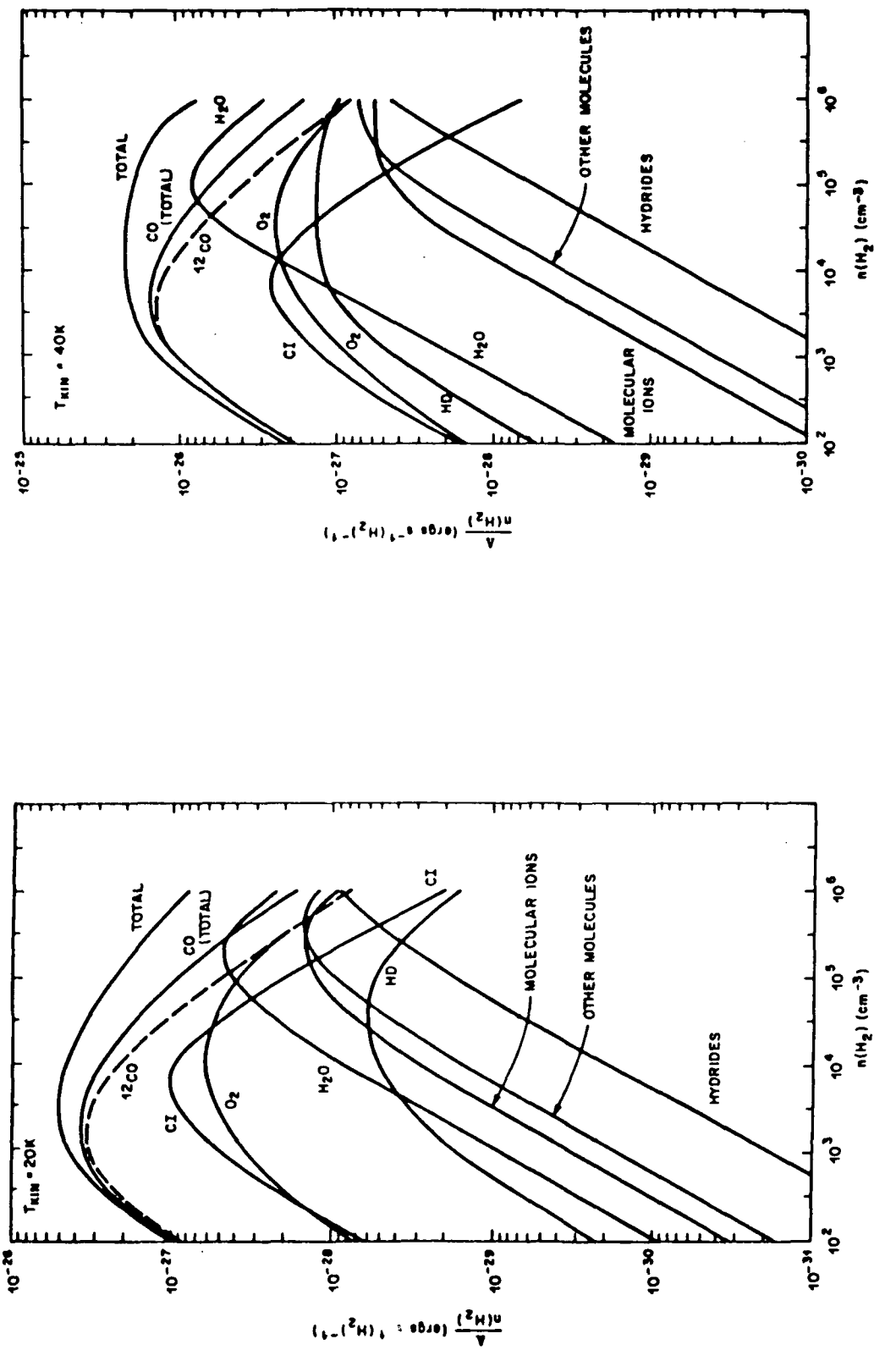

Figure 2.2-7. Total cooling per H_2 molecule as a function of H_2 density for kinetic temperatures of 20 K and 40 K. A fractional abundance of 3 and 1 × 10^{-6}, respectively, has been assumed for ortho- and para-H_2O (after Goldsmith and Langer 1978).

2.3 Photometry

2.3.1 Star Formation and the Interstellar Medium

Far-infrared observations provide a unique set of tools for studying star formation: first, because stars form in dense clouds that heavily attenuate radiation at shorter wavelengths and, second, because many important processes occur in gas and dust clouds with temperatures between a few tens and a few hundreds of degrees Kelvin. Most of the cooling for such clouds is provided by far-infrared continuum and line emission.

Perhaps the most fundamental quantity provided by far-infrared measurements is the total luminosity of dust-embedded energy sources. Very little dust is required to completely absorb stellar ultraviolet and optical emission, and this energy is subsequently re-emitted in the far infrared.

Most far-infrared investigations of active regions of star formation have been limited not by instrumental sensitivity but by source confusion. The mean projected separation of stars in nearby open clusters (for which membership is fairly complete) is of the order of 0.1 pc. Separations within the most compact parts of the youngest clusters (e.g., the Trapezium and KL clusters in the Orion Nebula) may be smaller by a factor of 3-10. Other phenomena relevant to the process of star formation (e.g., Jeans' lengths for gravitational collapse in dense molecular clouds, the sizes of the high-velocity molecular flows seen in Orion and other sources, and the projected thickness of shock and ionization fronts) also have scale sizes in the range of .01-.1 pc. Since the nearest star-forming regions are typically a few hundred pc away, only the closest sources and the largest scales can be adequately resolved by current far-infrared telescopes (Figure 2.1-1).

In addition to extending our knowledge of regions such as the Orion/BN/KL complex, the two-meter telescope should provide a powerful tool for studying lower-mass protostars and their relationships and interactions with their natal clouds. The ability to image structures with angular scales of 10 arcseconds to 10 arcminutes at wavelengths between 30 and 300 microns is crucial to an understanding of the nearest dark-cloud complexes (150-200 pc). Recent observations with the University of Chicago 32-channel far infrared and submillimeter cameras on the 0.9-meter telescope of the Kuiper Airborne Observatory and the three-meter telescope of the NASA Infrared Telescope Facility have begun to probe these regions with beam sizes of 45" and reference-beam (chopper) spacings of 5'. At this beam size, it is possible to detect clouds which are externally heated by the ambient interstellar radiation field. Imbedded sources of the order of on solar luminosity can just be clearly distinguished against this background surface brightness. This is also the level at which it should be possible to study regions which have been mechanically heated by gaseous outflows from active protostars.

Another area of star formation that can be best studied at submillimeter wavelengths by a two-meter balloon-borne telescope is large "infrared quiet" molecular clouds. Observations of the $J = 1 \rightarrow 0$ rotational transi-

tion of CO near the galactic plane in Monoceros (l = 216 degrees) reveal a molecular cloud with unusually low peak CO temperatures (T < 2 K) but wide lines (7 km/s) typical of much warmer clouds (Maddalena and Thaddeus, 1985). At the assumed distance of 3 kpc, the cloud is large (250 x 100 pc), has a mass of 7 - 11 x 10^5 $M_\odot$, and is well removed from the galactic plane (130 pc). Except for a possible H II region, all the signs of star formation usually shown by clouds of comparable mass are missing. The cloud was not detected in the IRAS survey, and unlike cloud complexes of similar size, it is a single, continuous object that apparently has not been torn apart by star formation. Clouds with such properties are rare in the Galaxy; only two other similar objects have been found. Large area (3 x 4 degrees) mapping at submillimeter wavelengths could determine if the cloud is young and has not yet formed stars, but will evolve into a typical cloud complex once star formation begins.

These studies are currently limited to a small class of sources which are sufficiently small, isolated, and geometrically simple that the 5' reference-beam spacing does not seriously affect the interpretation of the far infrared and submillimeter data. The two-meter balloon telescope would be able to simultaneously provide better angular resolution at far infrared wavelengths, larger reference-beam spacings, and larger scanned areas than is practical with airborne or ground-based measurements. Thus the balloon telescope will fill a crucial niche between facilities like SOFIA and 10-meter class ground-based telescope which can provide good data on smaller structures and IRAS sky-maps which provide excellent data on structures larger than a few arcminutes at wavelengths less than 120 microns. It is impossible to completely understand the complex relationships between molecular clouds, ambient stars and low-mass protostars without thorough coverage of this range of spatial scalelengths.

2.3.2 Galactic Structure

The major unsolved problems of galactic structure are how galaxies form, how they evolve through successive generations of star formation, and the nature and significance of energetic events in their nuclei. A full-scale attack on these problems in the far infrared will require the very large collecting area and high angular resolution of space-based instruments such as LDR -- particularly for attempts to observe galaxies at very high redshifts. However, the Two-Meter Balloon-Borne Telescope could contribute substantially to our understanding of processes occurring in the nearest galaxies, thereby laying the groundwork for later work with larger instruments.

At 100μm the Two-Meter Balloon-Borne Telescope can resolve an object about 180 pc in size at a distance of approximately 3 Mpc. This is a sufficiently large distance to include the nearest field galaxies and groups beyond the Local Group. One-to-two pc is comparable to the scale sizes of individual giant molecular clouds, to the thicknesses of the disks of spiral galaxies, and to the scale of "circum-nuclear" structure in our own galaxy (e.g., to the major features in far-infrared maps made with angular resolutions of a few arcminutes). This is the scale required, for example, to distinguish low-lumin sity "nuclear" sources from nearby,

luminous molecular cloud complexes. It is also the scale at which one can begin to test hypotheses concerning star formation in spiral arms and circum-nuclear "rings" (Figure 2.1-1).

As in the studies of star formation described in Section 2.3.1, the balloon telescope can play a crucial role by virtue of its ability to image large areas at a variety of scale sizes, wavelengths, and angular and spectral resolutions. It will be particularly valuable for examining the nearest galaxies, which are inconveniently large for airborne and ground-based instruments but which offer the best opportunities for examining the detailed structure of spiral arms, nuclear regions, bars, and individual star-forming complexes.

2.4 *Cometary Science with a Two-Meter Balloon-Borne Telescope*

Comets are of interest because they are the least modified bodies remaining from the formative phase of our planetary system. The compositions and physical structure of cometary nuclei are central data for interpreting the chemical and physical processes which accompanied their formation. A few comets may be visited in future by spacecraft for in-depth investigation, but the vast majority can only be studied remotely, and it is certain that the taxonomy of cometary classes can only be established by characterizing many of them. Several decades of observations at ultraviolet, visual, and radio wavelengths have provided a wealth of information on the dissociation products of the primary molecules, and even detection of a few trace constituents (e.g. S_2, CO, HCN). However, the general detection of the dominant species has only become possible with the development of the theory of solar infrared fluorescence (cf. Weaver and Mumma 1984) and the extension of infrared spectroscopic instrumentation to the cometary problem, particularly at airborne and spacecraft altitudes. Recent spectroscopic measurements of H_2O and CH_4 from the KAO and of H_2O, CO_2, the organic grain feature, and possibly H_2CO from the Vega spacecraft have established the feasibility of characterizing both the volatile and solid phase fractions of the cometary nucleus at infrared wavelengths (Mumma et al. 1986, Weaver et al. 1987, Larson et al. 1988, Combes et al. 1988). Theoretical modelling of the far infrared spectrum of water demonstrates that the strongest rotational transitions become optically thick at $\sim 1 \times 10^5$ km from the nucleus, thus those lines can be used to probe the kinetic temperature throughout the coma, if their line shapes are measured.

While many important investigations can only be carried out from airborne telescopes, and a few with ground-based instrumentation, there are several which require a balloon-borne telescope. First is the detection of CO_2, near 4.3 microns. This is not possible from 12 km altitude, owing to opacity of the terrestrial atmosphere. However, the opacity is reduced enough at 30 km to permit its detection when the geocentric doppler shift is favorable, similar to the present situation for H_2O from airborne telescopes. Second is obtaining a complete inventory of water lines in the 2.7 micron band, part of which is obscured by the 101-000 band of CO_2 at aircraft altitudes. This will permit a highly accurate measurement of the ortho-para ratio, which may be a cosmogonic invariant in comets, preserving a record of the temperature of formation of the primordial water molecules.

Third is the measurement of the far-infrared spectra of comets, which promises to be exceedingly rich for detection of new species, and for probing the physics of the cometary coma through fully resolved spectra of the water lines (e.g. 110-101).

The ability to measure the 3.0-2.5 micron region, free of the obscuring effects of CO_2 and H_2O should permit complete characterization of the competing forms of the OH stretch found or suspected to be present in Halley's comet (prompt emission and solar fluorescence from gas-phase OH, nu-3 and hot-band stretch in H_2O, OH in hydrated minerals, and possibly OH stretch in water cluster molecules). In addition, complete freedom from obscuration in the other bands will provide similar gains for other molecular species, and will assist in separating molecular and solid phase contributors to the 3.4 micron feature, for example.

2.5 Scientific Performance

The infrared performance of the Two-Meter Balloon-Borne Telescope is determined by the aperture, effective telescope emissivity, and the telescope temperature, the same items that determine the LDR performance. With the exception of the aperture, the values for these quantities on the gondola should be similar to those of the LDR. This telescope will operate at an ambient temperature of about 230°K and should have an emittance near 10%. A lower value of the mirror emittance may be achievable. Figure 2.5-1 gives the broadband sensitivity at 100μm vs. the diffraction-limited beam size for existing and planned instruments. The highest sensitivity is at the top. Figure 2.5-1 shows clearly the effectiveness of the Two-Meter Balloon-Borne Telescope for follow-through of 100-μm sources at the limit of IRAS sensitivity, a task of which the KAO is not capable. The Two-Meter Balloon-Borne Telescope has substantially less sensitivity than SIRTF for broadband photometry because of its higher temperature. It is superior to SIRTF only in angular resolution and in high spectral resolution observations limited by detector noise.

The sensitivity of the two focal-plane instruments proposed for the 2-meter balloon-borne telescope, the photometric infrared camera and the heterodyne submillimeter receiver, are discussed in Sections 5.2 and 5.3.

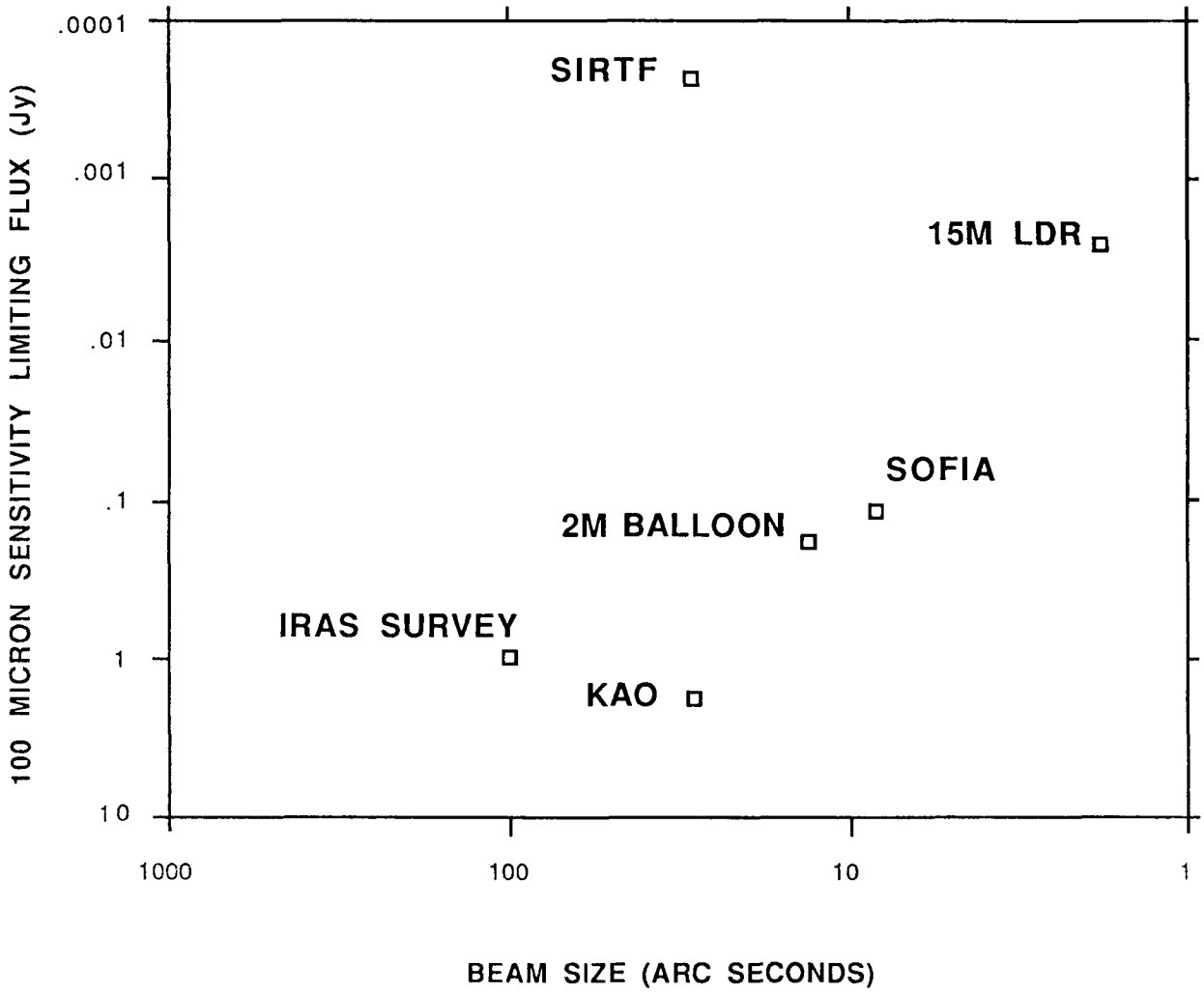

Figure 2.5-1. Broadband Sensitivity at 100μm vs. the Diffraction-Limited Beam Size. For the pointed telescopes, the limiting flux is given for a signal-to-noise of 10σ, bandwidth $\Delta\lambda/\lambda$ = 0.5, beam size of 1.22 λ/D, photoconductor detective quantum efficiency of η = 0.5, and integration time of 30 minutes with half of the time on the source. For the Two-Meter Balloon-Borne Telescope and LDR, the telescope emissivity and instrument efficiency are each taken to be 0.1 and the telescope temperature 220°K. For the KAO and SOFIA, the telescope emissivity, sky emissivity, and transmission are taken to be 0.2, 0.2, and 0.8 respectively. The IRAS survey limiting flux is taken from IRAS results.

3.0 GONDOLA DESIGN

3.1 Telescope Design

3.1.1 Telescope Requirements

Four important scientific requirements of the telescope which dictate the optics specifications are: 1) to cover the spectral range not observable or only poorly observable from the ground from 30μm to 1 mm; 2) to provide a collecting area much larger than now available from 1-meter size balloon-borne and airborne telescopes for high resolution far-infrared and submillimeter spectroscopy; 3) to provide a major advance in far-infrared spatial resolution; and 4) to take advantage of the potential sensitivity obtainable from the low thermal background at balloon altitudes. The optics specifications resulting from these requirements are given in Table 3.1-1. The resulting preliminary design is shown in Figure 3.1-1 and in the photograph in the frontispiece.

The two-meter aperture provides the a large step in collecting area and spatial resolution, and is compatible with current U.S. balloon launch facilities. The spectral range and angular resolution requirements imply diffraction-limited optical performance at a wavelength of 30μm. This means a half-power full-width of the central diffraction fringe of 3.9 arcseconds, which determines the acceptable image blur from optical design aberrations, misalignment, and fabrication errors. Conventionally, with optical (visible light) telescopes, this is taken to mean total effective rms surface errors of 1/26 of the wavelength. This yields a Strehl ratio (the ratio of the peak intensity of a point source to that produced by an ideal diffraction pattern) of 0.8. For radio telescope design, the rule of thumb is to require a surface half as accurate yielding a Strehl ratio of 0.5. Thus we interpret a 30-μm diffraction-limited performance to mean an image diameter (HPFW) of 3.9 arcseconds and a total surface error of 1- to 2-μm rms. Since much of the most important science done on this telescope will come from observations at 50 and 100μm and beyond, the 2-μm rms surface accuracy appears adequate.

The specification for operation at visible wavelengths is determined by the desire to use the main telescope to image stars for guiding purposes. This places additional constraints on the character of the optics surface error and polish. We intend to make every effort to meet this constraint and will relax it only if it cannot be achieved at reasonable primary mirror cost.

The unvignetted infrared field of view of 6 arcminutes is chosen to provide 1½ full Airy disk diameters (diameter to the first diffraction zero) at the longest wavelength of operation (1 mm).

Achieving maximum possible sensitivity requires an effective noise-free mechanism for subtracting the thermal background due to the telescope and sky from the observations. The most successful technique to date for doing this is beam switching by oscillating the secondary mirror through an angle either with a square wave or a linear scan. While the use of arrays of detectors in the far infrared may provide an alternative background

Optical Design	
Aperture	2 Meters
Spectral Range	Visible to millimeter
Optics Design	Cassegrain
Focal Ratio	f/13.5
Back Focus	93 cm from primary mirror vertex
	52 cm from instrument mounting plate
Interoptic Spacing	180 cm
Angular Resolution	Diffraction limited to 30μm (Raleigh Criterion 3.9")
Infrared Field of View	6' diameter unvignetted with ± 3' chop and diffraction spillover at 1 mm
Optical Field of View	15' vignetted only by the primary
Secondary Chopper	
Chop Rates	16 Hz up to 1' throw
	2 Hz at 6' throw
Deadtime	20% (6ms) at 16 Hz
Position settability	3% of total throw
Position repeatability	0.25"
Position drift	< 1"/hour
Chop axis rotation settability	1°
Focus settability	10% of depth of field
Pointing Stability	
Inertial Mode	1" rms
Magnetometer Mode	± 10' azimuth, ± 5' elevation
Source Offset	± 1/2° (Magnetometer Mode)
Slew Rate	10'/S
Thermal Stability	
Telescope	-40° ± 10° C
Mirror Stabilization Time	< 1 Hour
Command and Telemetry	
Number of IRIG User Channels	6
Useful Range	To limit of standard NSBF telemetry
IRIG VCO Channels Available	1/3/5/7/8/9/10/11/12/B/E/H/HH
PCM Bit Rate	81 KBpS; expandable to 256 KBpS
Video Bandwidth	4.5 MHz
Gondola Characteristics	
Total Weight	1731 kg (3809 lbs.)
Overall Height	5.8 Meters (19 Feet)
Overall Width	2.9 Meters (9 Feet 6 Inches)
Overall Depth	2.5 Meters (8 Feet 2 Inches)
Experiment Accommodations	
Power	140 W typical; 425 W maximum
Weight	125 kg at focal plane

Table 3.1-1. Telescope and Gondola Specifications

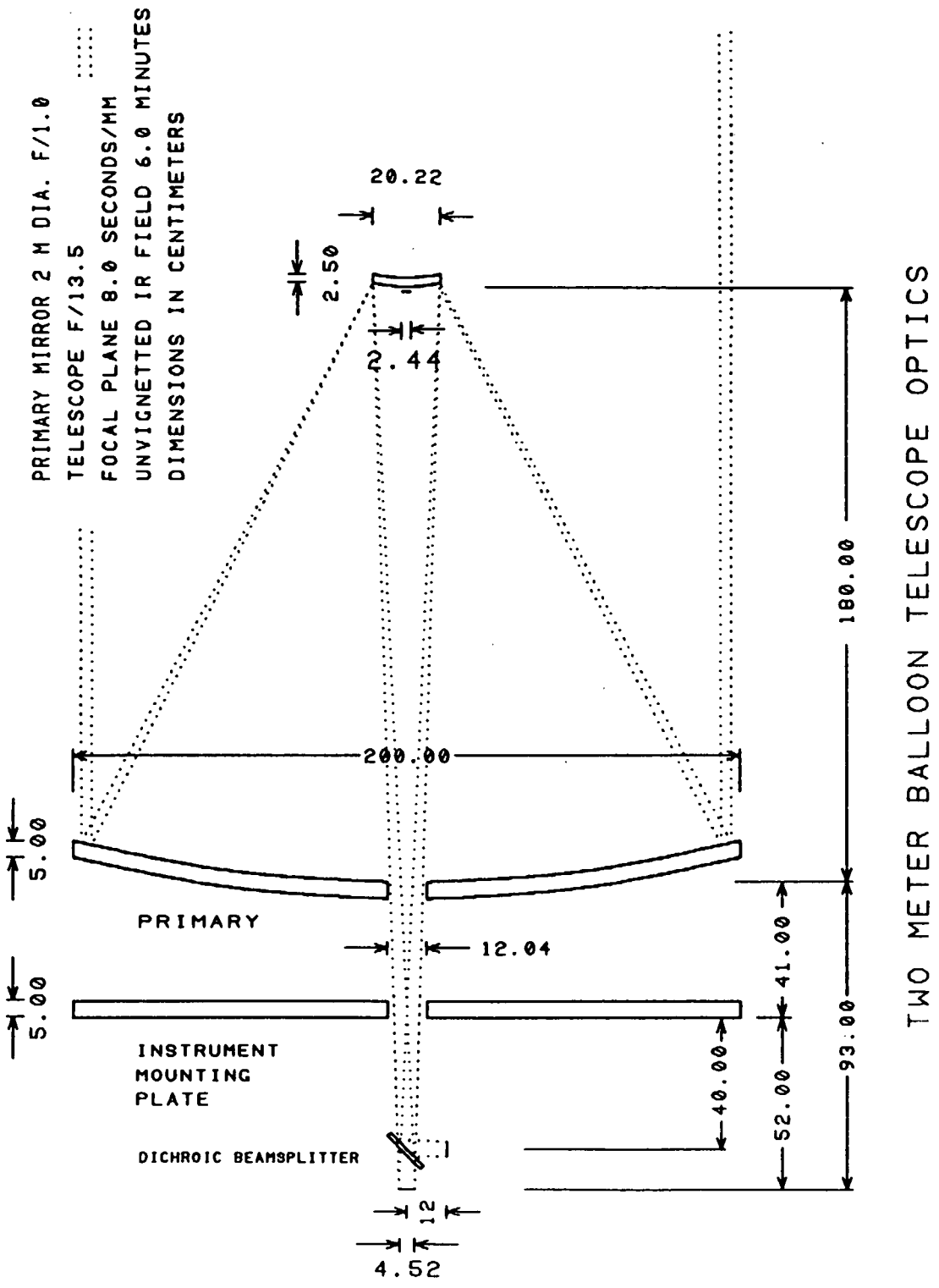

Figure 3.1-1. Optical Design of Two-Meter Balloon Telescope

subtraction technique for some observations, the secondary chopper still appears necessary for this telescope. Maintaining quality images while tilting the secondary places major demands on the optical design.

A second aspect of the high sensitivity requirement is minimizing the thermal emission of the telescope by minimizing obscuration from the secondary mirror and the secondary mirror support structure and maintaining very low emissive surfaces on the optics. Both the chopper and the low obscuration requirements dictate a small secondary mirror.

3.1.2 Description of the Cassegrain Telescope

a) Optics Design

Figure 3.1-1 illustrates the design of the telescope optics and specifications. The optical design is based on third order analytic aberration theory as presented by Gascoigne (1973). The telescope is a classical Cassegrain with a paraboloidal primary and hyperboloidal secondary. The secondary is undersized relative to the primary so that it provides the optical stop of the system. The undersizing of the secondary and the hole in the primary are selected so that for the full field size, the maximum chop amplitude, and the full diffraction width (diameter of Airy disk first zero) at the maximum design wavelength (1 mm) the field of view of a detector at the focal plane will "see" only the secondary, the cold sky, and the primary, but not the warm periphery of the primary nor the edge of the hole in the primary. The rays from the focal plane which would be reflected from the center of the secondary into the hole in the primary are deflected by a button on the secondary to the primary and hence to the sky (very much out of focus).

The minimum wavelength (30 microns) and associated diffraction HPFW determines the diffraction-limited performance of the telescope. The maximum HPFW is defined at the longest wavelength expected to be used (1 mm). The diffraction size of the beam at this wavelength contributes to the required secondary undersize. The secondary undersize ratio is set to assure that it is the optical stop of the telescope for all normal use.

The optical design parameters are chosen to provide no spherical aberration or other third order aberrations in the image at the nominal focal plane on axis. Figure 3.1-2 shows how the coma, astigmatism, and field curvature affect the image size as a function of field radius. Figure 3.1-2 also gives the miscollimation coma length due to secondary chopper tilt as a function of image displacement in the focal plane. The chop angle (in terms of focal-plane displacement), back focus, and field radius for which the image blur (or coma length) is 1.8 arcsecond in size are also given in Table 3.1-1. The greatest image degradation comes from the chopper tilt. This is a basic problem for this method of sky subtraction with a fast primary Cassegrain telescope. Shown on the coma length curve in Figure 3.1-2 are points for a Strehl ratio of 0.9 at 30μm wavelength and for 3.0 arcminutes chopper amplitude. When coma is the only optical aberration, the Strehl ratio (ratio of peak intensity of a point source to that produced by an ideal diffraction pattern) is .9 when the coma length equals

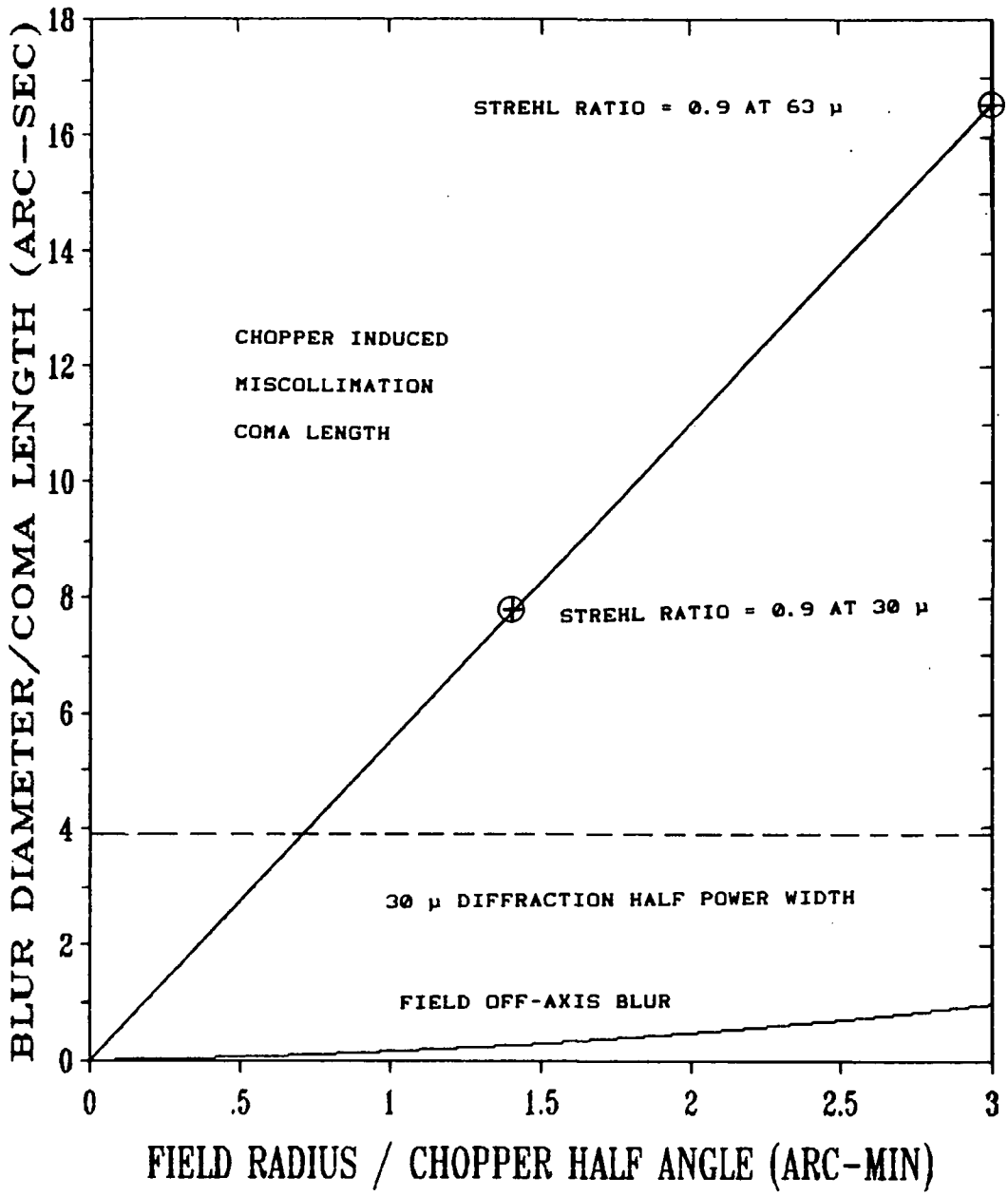

Figure 3.1-2. Image Blur vs. Field Position and Chopper Angle

the Airy disk full diameter. For this telescope the coma length equals the 30μm Airy disk diameter of 7.8 arcseconds at a chopper angle of 1.4 arcminutes. The coma length equals the 63μm Airy disk diameter of 16.6 arcseconds at a chopper angle of 3.0 arcminutes. At a chopper field amplitude of 3.0 arcminutes, the Strehl ratio is 0.9 at 63μm. Thus, for a Strehl ratio of 0.9, at all wavelengths the maximum focal-plane displacement due to secondary chopper tilt is 22 resolution elements (1.22 λ/D). The coma length is nearly independent of telescope aperture for a given chopper field angle, primary focal ratio, Cassegrain focal ratio, and back focus. The coma length varies inversely as the square of the primary focal ratio for a given chopper angle, Cassegrain focal ratio, and back focus.

b) Alignment Tolerances

The design in Table 3.1-2 and the desire for a diffraction limited (3.8-arcsecond) beamwidth determine the acceptable alignment tolerances for the secondary tilt, decenter, and axial motion. This includes both initial alignment when the gondola reaches float altitude and the stability of alignment during observing. Initial alignment has far greater tolerances than alignment stability because of the adjustments which can be made in secondary axial motion (focus) and secondary tilt after the gondola reaches float.

Meinel has pointed out that precision centering of the secondary of a Cassegrain telescope is not essential. The miscollimation coma created by a secondary decenter can be corrected for by a compensating secondary tilt. For this reason this telescope requires only a remote controlled secondary tilt adjustment, not a centering adjustment, for adjusting the collimation of the telescope after it reaches float altitude. This adjustment can best be made by observing the symmetry of the aperture illumination with an out-of-focus image of the bright star utilizing the focal-plane tracking camera.

c) Initial Alignment

With the exception of decenter, the driver for the optical stability tolerance requirements on reaching float altitude is the necessity of insuring rapid and efficient alignment of the telescope at the beginning of observation. It is necessary to have a star image appear in the field of the main focal-plane camera when it is centered on the boresighted acquisition guide telescope and to have the telescope focus close enough to correct the result in a detectable star image. The decenter tolerance is limited by the amount of decenter that can be compensated by secondary tilt before the resulting tilt of the focal plane blurs images at the edge of the field of view unacceptably.

With regard to decenter, we have assumed that the initial defocus tolerance results in an image four times the full diameter of the 30-μm central diffraction fringe, that is, 30 arcseconds; and tilt and decenter result in a coma of 15 arcseconds. Also, we have assumed an angular offset due to initial tilt and decenter equal to the focal-plane infrared camera field radius, 3.0 arcminutes. Finally, the initial decenter is limited by requiring an image defocus blur of less than 1.8 arcsecond at the edge of the field due to focal-plane tilt after secondary tilt compensation. The

Table 3.1-2. Telescope Optics Design and Performance

Aperture (cm)	200
Cassegrain focal ratio (f/)	13.5
Primary secondary separation (cm)	180
Primary focal-plane separation (cm)	93
Infrared field radius (')	3
Chop field amplitude (')	3
Minimum wavelength (μm)	30
Maximum wavelength (μm)	1000
Visible field radius (')	7.5
Diffraction HPFW min (")	3.9
Diffraction HPFW max (')	2.1
Secondary undersize	.040
Cassegrain focal length (cm)	2590
Focal-plane scale ("/mm)	7.96
Field diameter (cm)	4.52
Primary focal length (cm)	201.2
Primary focal ratio (f/)	1.00
Primary sagitta (cm)	12.4
Primary departure from sphere (cm)	.20
Primary hole in IR min (cm)	12.04
Primary hole in IR max (cm)	12.09
Primary hole visible min (cm)	14.34
Secondary diameter (cm)	20.22
Secondary focal length (cm)	-22.99
Secondary conic constant ($-e^2$)	-1.365
Secondary sagitta (cm)	1.10
Secondary departure from sphere (cm)	.013
Secondary button min (cm)	2.44
Secondary button max (cm)	2.99
Secondary axial magnification	-167
Secondary angular magnification	.210
Range for 1" blur of 1.8"	
Chop (')	.33
Back focus (cm)	9.5
Field coma (')	26.8
Field astigmatism (') quadratic	17.4
Field curvature (') quadratic	4.8
Total field aberrations (')	4.7

resulting initial tolerances are given in Table 3.1-3.

If there is a predictable and repeatable focus shift from ground to float altitude, it can be removed by the initial focus setting. For example, a carbon-fiber-reinforced plastic secondary truss support with a coefficient of thermal expansion of 2×10^{-6}°C will result in a secondary

defocus motion of 0.23 mm due to a temperature change of 65°C from ground to float altitude. The tolerances in Table 3.1-3 cover the remaining mechanical and thermal uncertainties of such a correction. They should be treated as maximum tolerances. Smaller errors will result in faster telescope realignment during the flight.

Table 3.1-3. Telescope Optics Alignment Tolerances

Alignment for blur of 1.8"	
Secondary decenter (mm)	-.095
Secondary tilt (')	-1.55
Secondary axial motion (mm)	.018
Alignment for motion 1.8"	
Secondary decenter (mm)	-.019
Secondary tilt (')	.14
Initial Alignment	
Secondary defocus blur of 36" (mm)	.35
Secondary decenter for coma of 18" (mm)	.95
Secondary decenter corr. blur of 1.8" (mm)	2.05
Secondary decenter for motion of 3' (mm)	2.86
Secondary tilt for motion of 3' (')	21.3
Secondary tilt for coma of 18" (')	15.5

d) Operating Alignment Tolerance

The operating tolerances for secondary tilt, decenter, and axial motion each defocusing the image by 1.8 arcsecond are also given in Table 3-1.3. These tolerances are for telescope stability between realignment on a reference star, an activity which should take place as little as possible during the flight. The defocus blur is minimized by refocusing on a bright star. The decenter blur can be corrected by examining an out-of-focus star image and tilting the secondary to restore collimation. The decenter and tilt shift tolerance affect the stability of the bore sighting with a tracking telescope. If the gyros are updated by images in the main telescope these tolerances can be substantially relaxed.

3.1.3 Optics Design Trade-Offs

a) Tradeoff Approach

The telescope design is a compromise between the largest aperture compatible with the National Scientific Balloon Facility and a size and shape providing affordable construction, ease of transport, and minimum launch constraints. We have chosen an aperture of two meters which meets the requirements and is at a breakpoint in the available equipment and cost of fabricating light weight carbon fiber reinforced plastic mirrors. In the design study we have chosen as the variable parameters the Cassegrain focal ratio, primary-secondary separation, and primary-to-focal-plane

distance. We have considered the required field radius, chopper field amplitude, and maximum operating wavelength to be fixed. The tradeoff studies investigate the impact of varying the input parameters on the focal-plane scale, primary focal ratio, secondary diameter, back focus range, field aberrations, chopper-induced aberrations, and alignment tolerances. These impacts were examined for five different values of each of the three parameters while the other two were held fixed at the chosen design values. The calculations were based on the third order analytic aberration referred to in Section 3.1.2. The tradeoff approach and explanations of the items in Tables 3.1-2 and 3.1-3 are given in PDR Appendix A.

b) Interpretation of Trade-offs

The advantage of reducing the primary to the focal plane distance is to simplify the telescope structure design and reduce its weight. The back focus distance is constrained both by instrument requirements and the required depth of the primary mirror backup structure.

The significance of the items investigated is as follows:

Focal-Plane Scale. This along with the field size determines the minimum possible size of the instrument dewar window and the scale of the instrument cold optics and is especially important at the longest wavelengths where even a small number of elements of an imaging array cover the full six-minute-diameter field. For a small field diameter, the focal plane scale should be large.

Primary Focal Ratio. Optically ground and polished, paraboloidal primary mirrors of large size have been made only to f/2. New methods utilizing a computer controlled flexible lap promise to extend this to much shorter focal ratios. Replicated primary mirrors have been fabricated with focal ratios as short as f/.35. In general, the larger the primary focal ratio, the easier the fabrication and testing of the primary is, although this is not considered a major constraint for this tradeoff.

Secondary Diameter. The secondary obscuration which impacts the effective emissivity of the telescope increases as the square of the diameter. The secondary moment of inertia that dominates the secondary chopper performance increases as the fourth power of the secondary diameter. A major driver for the telescope is to keep the secondary as small as possible.

Back Focus Range. Since instruments are to be designed for operation at the design focus, the back focus range is not a significant consideration.

Field Angle for One-Arcsecond Blur. The field aberrations are well within the specifications for image blur at the specified 6-arcminute infrared field diameter for all designs examined. The field aberrations are dominated by the field curvature.

Chop Amplitude. Chopper-induced coma is by far the largest optical aberration of the telescope as shown in Figure 3.2-2. Hence, the chopper-induced image blur is a critical item to minimize over the tradeoff range.

Secondary Axial Motion for 1.8-Arcsecond Blur and Secondary Decenter for 1.8-Arcsecond Blur. These two items indicate the tolerances the telescope must maintain during observations without refocusing or adjusting the secondary tilt to compensate for decenter. The 1.8-arcsecond blur increases the image half power width by about 10% over the 30 micron diffracted image. While it appears from the mechanical design analysis that these tolerances are acceptable and can be met, clearly trade-offs that increase the tolerances are preferable.

c) Conclusions

The most critical goals of the design tradeoff are in descending order of priority:

1. Minimize the secondary diameter.

2. Minimize the chopper induced coma length.

3. Minimize the size of the 6-arcminute field diameter at the Cassegrain focus.

These impact the free parameters as follows:

1. Cassegrain focal ratio. This should be small for maximum chopper amplitude and minimum field size. It should be large for minimizing the secondary diameter. A focal ratio of f/13.5 is a compromise choice. It is also identical to the NARO 13 meter millimeter telescope at Kitt Peak for which a number of high frequency heterodyne receivers have been built.

2. Overall length (secondary vertex-focal plane). Reducing this reduces the secondary diameter and the gondola size but requires a faster primary and increases the chopper induced coma. For a given chopper angle the coma length is inversely proportional to the square of the primary focal ratio. The overall length has no effect on the field diameter. The chosen design favors low weight and ease of transportation at the expense of a fast primary and chopper induced coma. Chopper induced coma can be reduced at the expense of producing field coma by altering the secondary figure.

3. Back focus (primary vertex-focal plane). Reducing the back focus improves the chopper amplitude and the field diameter and has no effect on the secondary diameter. The smallest back focus is best for the optical performance. The design value is chosen to accommodate expected instrument configurations.

3.1.4 Telescope Mechanical Design

The optical design characteristics and optical positioning tolerances were given in Tables 3.1-2 and 3.1-3. The telescope mechanical design is aimed at achieving these optical positioning requirements in an efficient manner. The design for the two-meter telescope is based directly on the three-meter telescope design presented in the PDR. Our goal in the redesign was to produce a gondola of minimum practical weight. The reduction in size and the selection of a faster (f=~1.0) primary significantly reduces the telescope's weight, inertia and length. Positional requirements for the secondary mirror are tightened by a factor of two, however, due to the change in optical design. Fortunately, the reduction in truss length offsets this tighter positional tolerance.

Primary Mirror and Cell. The primary mirror cell serves as a pedestal from which to erect the telescope including its aspect cameras, stabilization components, mirror protection cover and experiments. Table 3.1-4 lists the major telescope components along with their expected weights. The primary cell will be a monocoque structure fabricated from graphite-epoxy composite in a fashion similar to that proposed for the primary mirror. This affords maximum structural stiffness per unit of weight while minimizing mirror distortions created by temperature-induced differential expansions between the mirror, its mounting system, and the cell. The cell is directly attached to the cross-elevation gimbal via a set of centrally aligned flexpivots. This interface is insensitive to temperature effects between cell and gimbal. The mirror cell also provides mirror mounting and protection while serving as a base for the secondary truss. The primary mirror mounting technique will most likely follow techniques developed by Dornier-System GmbH for mounting large-diameter graphite-epoxy millimeter wavelength radio astronomy telescope primary reflectors.

Mirror protection is accomplished in two ways. First, the mounting cell has a forward skirt that protrudes beyond the mirror, thereby placing the mirror in a protective cavity. This skirt can be removed to provide access for mirror mounting. Second, a retractable mirror cover, presently conceived as a rolled curtain of strong plastic woven mesh, is mounted on the skirt. The cover will be used during testing and during recovery to prevent tools, telescope components, tree branches, and the like from striking the mirror.

The quadrupod secondary mirror truss mounts at four points just forward of the primary mirror. This is a departure from the standard infrared telescope design of a circular head ring with four thin secondary vanes and was chosen to minimize the overall gondola weight while guaranteeing the positional accuracy required by the optical design. The telescope truss is designed to place the natural vibrational frequencies of the truss well beyond the pointing and stabilization servomechanism systems' bandpass to minimize coupling sensitivity to secondary chopper motion and other vibrational inputs.

The secondary mirror assembly truss mounting must allow positioning of the secondary to $\leq$.002cm and support re-entry loads without failure. Secondary mounting designs of similar characteristics have been developed for

Subsystem	Unit Weight (pounds)	Total Weight (pounds)	Total Weight (kilograms)
I. Secondary Mirror Assembly			
Mirror	10		
Focus Drive	22		
Chopper	25		
Tilt System	5		
Truss and Attachments	125		
		187	85
II. Primary Mirror Assembly			
Mirror	140		
Mirror Cell	250		
Mirror Cover	30		
5° FOV Aspect TV	15		
1° FOV Camera	25		
Focal Plane Camera	40		
Cross-Azimuth Servo	20		
Offset Pointer	20		
Miscellaneous	20		
		560	255
III. Cross-elevation axis			
Cross-Elevation Drive System	60		
Elevation Drive System	40		
Gimbal Frame	85		
Cross-elevation Reaction Wheel	25		
Elevation Reaction Wheel	25		
Electronic Interface	10		
Wire Harness	10		
Miscellaneous	25		
		280	127
IV. Experiment Package			
Tailpiece	50		
Submillimeter Spectrometer	125		
IR Camera	50		
Experiment Selector	12		
Combined Electronics	100		
Trim Weights	5		
		342	155
TOTAL TELESCOPE WEIGHT		1369 lbs.	622 kg.

Table 3.1-4. Two-Meter Telescope Subassembly Weight Summary

ground-based telescopes and should not pose any technical problems for this program.

The telescope is capable of making observations from 10 degrees below the horizon to an elevation of 65 degrees. The truss must therefore maintain the position of the secondary mirror over this observational range.

The truss structural characteristics are calculated to be:

Natural frequency, gravity axis	$\geq$210cps
Natural frequency, chopped axis	$\geq$234 cps
Natural frequency, individual member	$\geq$137 cps
1 g deflection (zenith to horizon)	2×10^{-4} in ($\geq 5\times10^{-4}$ cm)
Gravity deflection Hr^{-1} at fixed pointing	5×10^{-5} in ($\approx 1.2\times10^{-4}$ cm)

The truss is also subjected to a large thermal excursion from launch to altitude with a small fluctuation occurring at altitude. A temperature difference of 54°C (130°F) and $\pm$5.6°C ($\pm$10°F) fluctuation was used to determine the material characteristics required to minimize the need to actively refocus the telescope during an observation. This requirement mainly influenced the selection of graphite-epoxy as the truss material, although its strength-to-weight ratio and natural damping qualities are also highly desirable. The temperature defocus was calculated to be 0.0094 cm over this range which implies an in-flight defocus equal to 0.008 cm. These values are attained by using a coefficient of thermal expansion of $1.0\times10^{-6}/F^{\circ}$ which is conservative for this material.

3.1.5 Telescope Thermal Design

Minimizing telescope distortion induced by the adverse thermal environment at float altitude is the major criterion for thermal design of the Three-Meter Balloon-Borne Telescope. Active control of telescope optics and structure at the original launch ambient temperature during flight is impractical because of the complexity of doing so and the very large heater power requirements. Fast stabilization of the telescope at a quasi-equilibrium temperature (at which heat exchange with the environment is minimized) and maintenance of this condition throughout the observation period is the primary goal of this design. Thermal gradients across the mirror face and through its thickness must be minimal, focal length must be within tolerance, and quadrupod temperatures must be equal and stable.

The Two-Meter Balloon-Borne Telescope will utilize the enhanced convection environment of the ascent phase and the low air temperatures of the tropopause to cool critical elements to the desired temperatures, about -40°C. Although little investigation of convection conditions in a balloon environment has been reported, our own work (summarized in Section 2.2.4 of

the PDR) shows that convection coefficients on exposed surfaces of order 10 W/m^2K or greater can be expected during a large portion of ascent, and about 5 W/m^2K at float altitude.

It is readily calculated that a lightweight glass mirror of density 70 kg/m^2, with both surfaces exposed to such a convective environment of temperature 20°C below itself, will reach -40° during ascent. Such a calculation is conservative with respect to both convection and air temperature, so there is adequate reserve cooling capability; enough, in fact, that a provision to prevent overcooling may be needed. We have also verified that radiative heat transfer in the cellular construction of a lightweight Pyrex mirror permits the mid-plane to stabilize with a time constant of less than a half hour. A composite mirror would stabilize even more rapidly because of higher thermal conductivity as demonstrated in the cooled test chamber.

During observation an exposed primary mirror would radiate to space at 10-15 W/m^2, depending on the emittance of its polished surface. However, a protective tube surrounding the optical path will reduce the solid angle of exposure to space, reducing the net radiation to 2-3 W/m^2. This radiation will be balanced by convection to the front surface from the air near the surface and by conduction and radiation from the rear surface to the front. This second mode would result in a temperature difference between front and back which would distort the figure, and must therefore be kept to a minimum by radiative and convective isolation of the back surface (coatings, insulation, or both), allowing convection at the front to dominate. It is not yet clear what the convective environment will be inside the telescope tube (partially shielded from relative motion between the gondola and surrounding air) and a scaled-down experiment is planned for the near future to help determine this.

Structural elements such as the quadrupod legs will respond to the ascent convective environment with a time constant of a few minutes. Overcooling in the tropopause will occur, and response will slow as the experiment nears float, but these elements will be within a few degrees of final temperature within a half hour of achieving altitude. At stable altitude, and therefore stable air temperature, the quadrupod will be stable as well except for changing radiative environment. Controlled-emittance coatings will be used on critical structural elements; detail design will determine whether coatings of high emittance (giving faster response but greater excursion) or low emittance (yielding the opposite) are best.

3.1.6 Chopping Technique

Telescope specifications call for a secondary chopper with a beam switching angle referred to the sky of 6 arcminutes at a frequency of 16 Hz and a dead time of 20%. The secondary mirror diameter is 20.2 cm. It will be lightweighted. Several options exist such as beryllium, glass, composite, and foamed silicon carbide.

High performance servo-controlled secondary choppers have been developed by Steward Observatory for the Multiple Mirror Telescope, by Kitt Peak

National Observatory (KPNO), and by several balloon and aircraft infrared groups. The Two-Meter Balloon-Borne Telescope secondary design will take advantage of these developments. It will have a reactionless drive with high permeability core "loud speaker" type drives pushing against a reaction plate. The drive will permit remote control of the chopper throw and frequency.

Properties of the secondary chopper are given in Table 3.1-1.

3.2 Support Structure Design

3.2.1 Mechanical Concept

The Two-Meter Balloon-Borne Telescope design concept is shown in Figure 3.2-1. Two major assemblies, the telescope and support structure, form the overall gondola.

The support structure is a yoke frame that serves five major functions:

- Telescope structural attachment to the balloon.
- Telescope azimuthal orientation and coarse stabilization.
- Telescope elevation reference frame.
- Packaging for all electronics and gondola support systems.
- Launch, landing and recovery protection.

A yoke frame has been selected as the best method of telescope support given NSBF size and weight restrictions. The telescope weighs 623 kg (1,734 lbs.) and measures 3.24 meters along the optical axis (including experiments), 2.9 meters in width, and 2.5 meters in depth. The yoke frame requires only 342 kg (755 lbs.) to meet the telescope's structural load-carrying requirements while only increasing the overall gondola size to 5.8 meters in height and 3.9 meters in width with no change in depth. Deployable crash rings are needed to protect the telescope on landing. These add to the gondola's width and depth but not sufficiently to cause a handling problem with the NSBF launch vehicle or staging building.

A momentum transfer device is used at the point of balloon attachment. It provides 360 degrees of angular rotation for azimuthal orientation and is decoupled except for the friction required to transfer momentum for azimuthal stabilization.

The gondola yoke frame will align itself with the earth gravity vector. The elevation servo system uses this gravity alignment for determining the telescope elevation angle and for stabilization purposes.

The telescope will be locked in place during launch. Locking is necessary to ensure maximum telescope and experiment protection for all

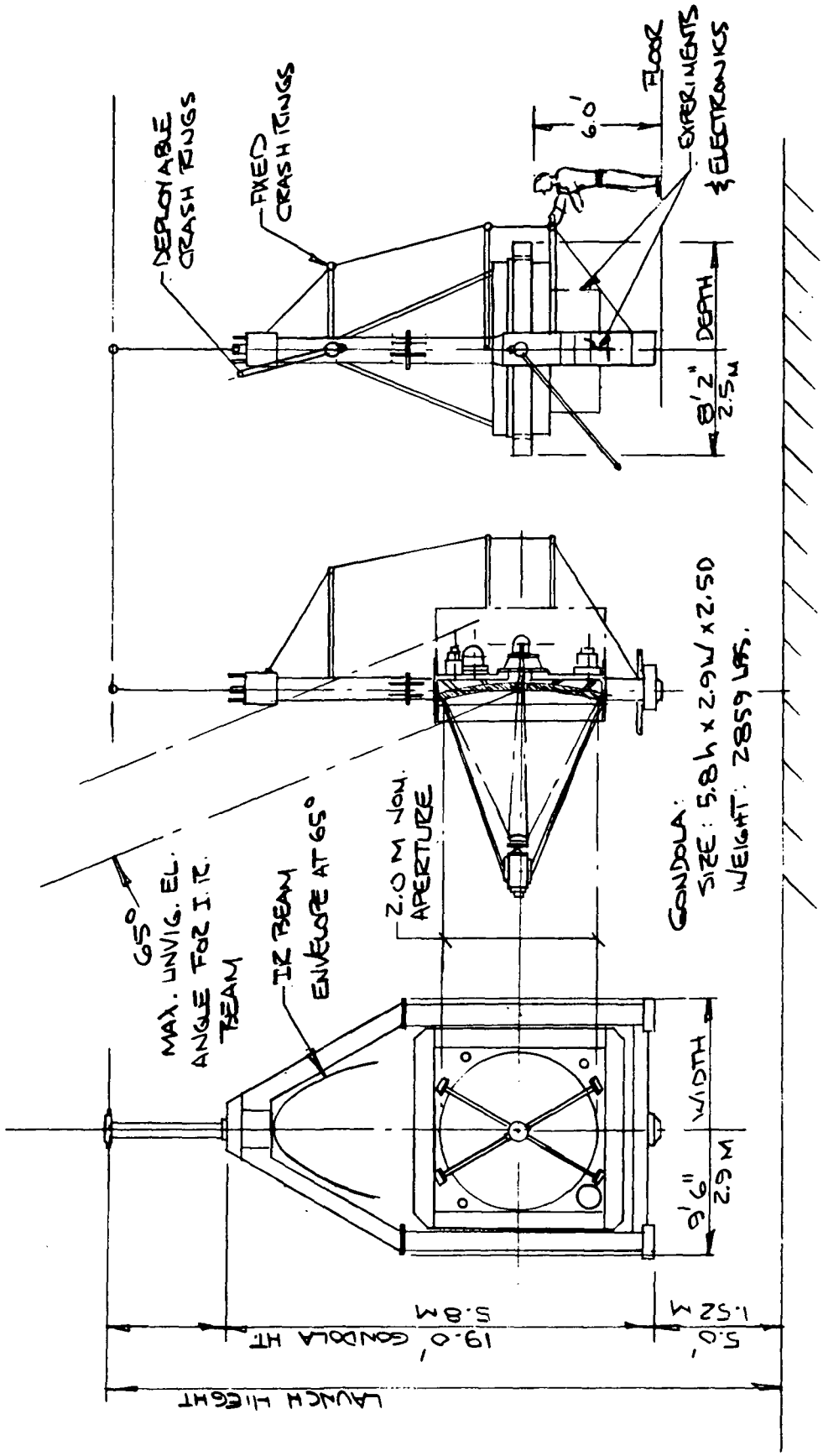

Figure 3.2-1. Three Views of Gondola

times when it is exposed to impact loads. The locking device will be thoroughly tested with redundant schemes for activation so that the highest probability exists for achieving the locked configuration. Since telescope locking can not be absolutely guaranteed, the structural members were sized to carry the full loads of an unlocked telescope. Stress levels were allowed to rise to within 80% of the materials' yield strength, thereby yielding a minimum factor of safety equal to 1.5 for structural failure.

The diagonal and side column members were designed as thin-walled, deep-section aluminum beams.

3.2.2 Launch, Landing, and Recovery Considerations

Launch requires that the gondola be suspended from the launch vehicle for transportation to the launch area and subsequent launch. The gondola will be exposed to low level mechanical vibrations during this activity. Experience indicates these levels to be less than the vibration levels experienced during nominal handling in test and experiment integration phases. Therefore, we will design the gondola for no detectable performance degradation when exposed to nominal handling. This is specified as not to exceed 3 g's rms over the spectral range of 20-2,000 Hz. The NSBF requires five feet minimum for ground clearance and various radial clearances at elevations below the launch arms. This relatively light payload can be supported well in front of the vehicle allowing adequate ground and vehicle clearance. The crash rings have been stationed at the secondary to allow proper radial clearance with the launch arms. All sensitive equipment and experiments are fully protected during launch.

Damage is most likely during landings. The gondola will descend in its normal (upright) flight attitude. On impact, one or both side columns will contact the ground, absorbing energy via crushable pads and structural stressing. The structure is designed to sustain these impact loads and will roll over either naturally or be pulled over by the parachute pulling on it. The crash rings are designed to absorb this rollover energy by distortion. The crash rings should maintain a reasonable ground clearance, even if nominal (50') parachute dragging occurs, to protect the telescope and experiments. All electronics are completely protected because they are mounted inside the frame.

Recovery is difficult at best from the various terrains into which balloon payloads descend. Therefore, the yoke frame as well as the telescope are modular designs. This allows field disassembly into manageable components if necessary. The gondola can be transported on a standard flat-bed trailer for transport back to the NSBF without the need for special roadway routing and/or variances.

Subsystem	Unit Weight (pounds)	Total Weight (pounds)	Total Weight (kilograms)
I. Telescope Assembly (See Table 2.2-3)		1374	625
II. Structure and Subsystems			
Structure (Yoke Frame)			
Upper	175		
Telescope Mounting Interface	50		
Side Columns	400		
Stabilizer Beams	50		
Miscellaneous Structure	80		
		755	343
Stabilization and Pointing*			
Momentum Transfer Unit	50		
M-T Reaction Wheel	35		
Magnetic and Gravity Sensors	20		
Elevation Drive	35		
		140	64
Electronics			
Command	25		
Control	50		
Batteries	120		
Cables and Connectors	65		
Enclosures	120		
Miscellaneous	30		
		410	186
Re-entry Devices			
Telescope Latch	30		
Crash Rings	110		
Crash Pads	40		
		180	82
III. NSBF Equipment			
Ballast	400		
Electronics	55		
120-Ft. Parachute	430		
Suspension Ladder	65		
		950	432
TOTAL GONDOLA WEIGHT		3809 lbs.	1731 kg.

*Remaining items not attached to telescope

Table 3.2-1. Gondola Weight Summary

Table 3.2-2. Gondola and Telescope Products and Moments of Inertia

Gondola Inertial Properties about Its Origin (kg-m×m)

Axis	X	Y	Z
X	3532.	0.	0.
Y	0.	2690.	-116.
Z	0.	-116.	2679.

Telescope Inertial Properties about Its Origin (kg-m*m)

Axis	X	Y	Z
X	461.	0.	0.
Y	0.	478.	-25.
Z	0.	-25.	342.

3.3 Pointing System

3.3.1 Pointing Requirements

The pointing and structural specifications shown in Table 3.1-1 are dominated by the 30-μm wavelength beam size, the slewing and scanning requirements, the maximum allowable gondola weight, the thermal environment, and the operational requirements of balloon flights. The pointing stability specification of 1-arcsecond rms is set so as not to compromise the imaging quality of the optics.

The telescope is suspended in gimbals within the gondola frame and is oriented in two orthogonal control axes, elevation and cross-elevation. Telescope motion in the cross-elevation axis is limited to about $\pm 3^{\circ}$. Coarse azimuthal control is achieved by rotating the entire gondola at its attachment point to the balloon.

3.3.2 Operating Modes

Sources are acquired initially in the Magnetometer Mode which provides coarse telescope positioning. The gondola is first rotated about the azimuthal axis, using the Earth's magnetic field as reference, to a positional accuracy of about 30 arcminutes. Then, telescope rotation about the elevation axis, using the gondola gravitational alignment as reference, to a positional accuracy of about 10 arcminutes brings the desired source direction within the range of motion of the cross-elevation axis.

Once the source is acquired in the Magnetometer Mode, the gondola is switched to the Inertial Mode, the fine pointing mode, for science data acquisition. Pointing stability in the Inertial Mode will be better than 1 arcsecond rms. In addition to fixed pointing, which stabilizes the telescope on a given celestial target, the inertial mode can also be used to step or scan the telescope with respect to a celestial object. For mapping of extended sources a raster pattern can be generated by scanning in cross-elevation and stepping in elevation at the end of each scan line. The angular size of such rasters and the scan rates can be varied on command. In addition to the commanded scan rates and directions, a joystick control at the ground station can be employed for telescope positioning.

3.3.3 Gimbal Design

Two types of gimbal designs were evaluated during the program. The first with the baseline flex-pivot design described in the PDR; the second, the active-gimbal ball bearing concept described in Semiannual Report #6.

The advantages of the flex-pivot designs were detailed in the PDR. Further examination of the concept revealed several design weaknesses all of which relate to the limited rotation range of the flex-pivot. A long period of undisrupted tracking requires a large stiff flex-pivot which is difficult and expensive to fabricate. The flex-pivot design also requires a secondary actuation system to unwind the flex-pivots accumulated rotation due to tracking and to move the telescope through large angles when acquiring a new source. Recent experience on an SAO balloon borne spectrometer also revealed that a flex-pivot based design would require precise alignment across the telescope frame at a level difficult to maintain in the field.

The active gimbal ball-bearing design provides unlimited angulation without the need for a secondary drive system. The graininess and slip-stick which they exhibit in slow-speed servos is compensated for by using a feed-forward path in the torque motor servo loop driven by bearing torque measurements. The torque sensor, which has an appropriate torsional spring rate, permits telescope rotation while the ball-bearings are locked by graininess or slipstick friction. While this design does have certain inherent non-linearities which the baseline design avoided, the feed forward servo incorporated in the design can compensate for them more than well enough to achieve the desired pointing accuracy and stability.

The mechanical design of the ball-bearing gimbal is shown in Figure 3.3-1. A backplate acts as a pedestal on which the servo components are mounted. The torque sensor is rigidly attached to the backplate on one end and is machined on the other to mount a matched pair of angular contact bearings. These bearings provide the required rotation via a spindle which has the servo motor stator and position resolver armature mounted to it. It also provides the bolt pattern for attachment to either the telescope or X-elevation frame. The backplate also has provisions for mounting the servo motor armature and position resolver stator.

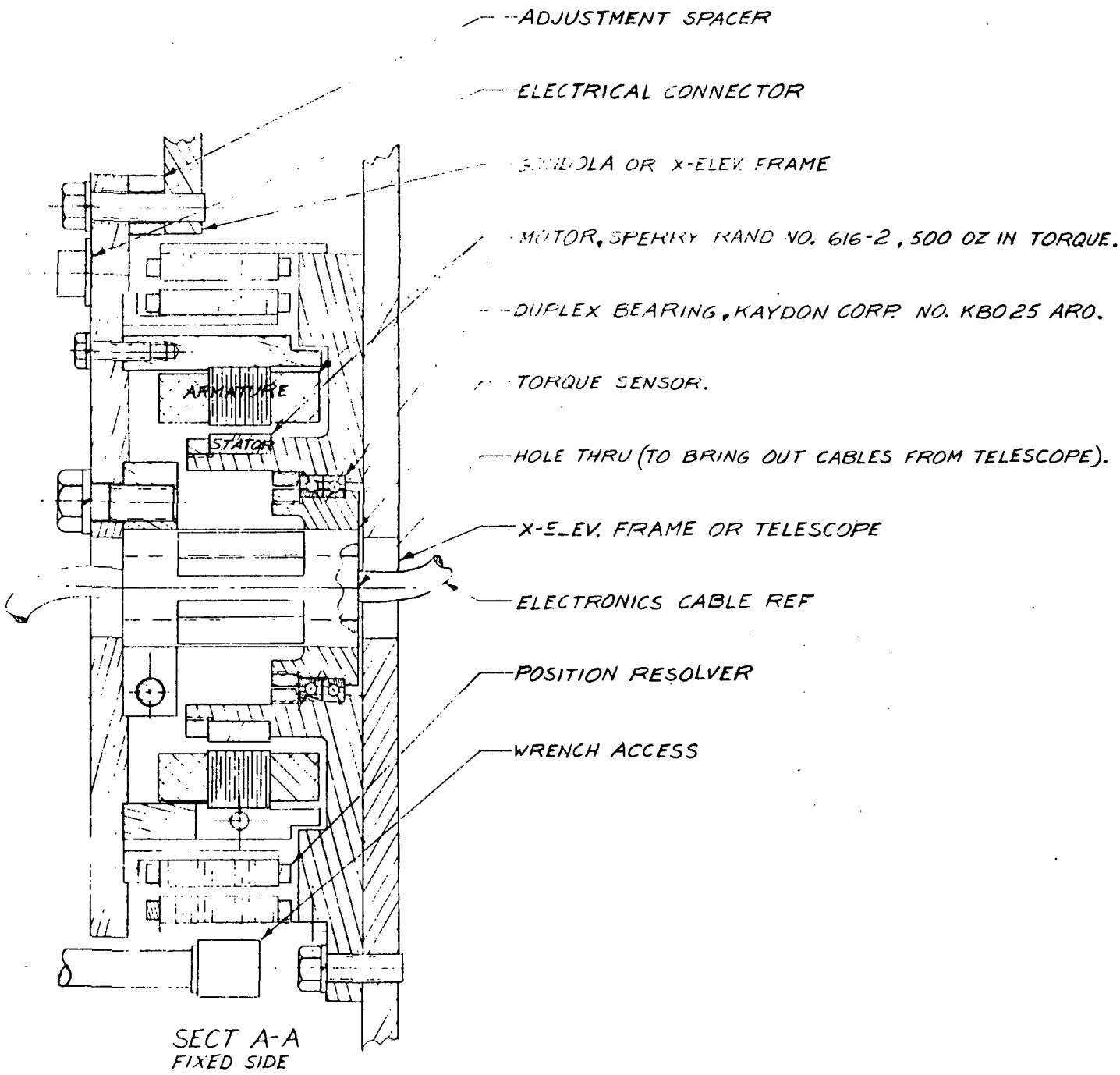

Figure 3.3-1. Gimbal Assembly

The torque sensor is a commercial device which has the appropriate structural load capacity for all normal operational situations. During severe load applications (parachute deployment and crash landing for example) the torque sensor will deflect until the diameters of the servomotor mount and bearing spindle come into contact. This contact will then carry all such severe loads with a factor of safety ≥ 3 insuring that rupture and/or separation between the telescope and gondola cannot occur.

This design allows complete assembly and functional checkout of the gimbal to occur at the sub-assembly level. Two completed gimbals are then installed between the Telescope X-elevation frame and gondola X-elevation frame (one per side) to form the telescope elevation mount. This installation is easily accomplished by centering the telescope in the frame and attaching the gimbal assemblies to each by using the appropriate hardware. All hardware required is accessible from the outside to facilitate this attachment. The same gimbal design is used in the cross-elevation servo.

3.3.4 Azimuth Servo

The Azimuth Servo is the outermost control loop. It is a coarse pointing loop which contains the cross-elevation, or fine loop, within it.

In Magnetometer Mode, the Azimuth Servo is used for the initial acquisition of a targeted celestial object, and points the gondola to within ± 30 arcminutes of the commanded location. This is close enough to allow recognition of the star field in the aspect TV camera. Azimuth reference in this mode is the earth's magnetic field, as sensed by a Schonstedt fluxgate magnetometer. The inner (cross elevation) gimbal is driven to its center position and locked while the target is being acquired.

In Inertial Tracking Mode, the error input which drives the Azimuth Servo is switched from the magnetometer to the inner gimbal position sensor and the inner gimbal is unlocked, allowing the cross-elevation fine servo to become active. The Azimuth Servo then maintains coarse orientation of the gondola so that the target object remains well within the limited range of the cross-elevation gimbal. A threshold, or dead-banding, feature will be included so that the outer loop becomes active only when the inner gimbal moves away from its center position more than some minimum angle. This will reduce the amount of activity in the Azimuth servo, and result in fewer disturbance torques for the pointing control to cope with.

The coarse Azimuth servo also serves as a means of dissipating momentum built up in the cross-elevation reaction wheel. When this momentum is dumped (by torquing the cross-elevation gimbal motor) a component of it, proportional to the cosine of the elevation angle, is coupled into the gondola azimuth axis. The azimuth reaction wheel responds by taking on a velocity and this energy is removed by the azimuth loop twisting against the suspension lines.

A full explanation of the overall system concept with descriptions of the subsystem elements is contained in the PDR.

3.3.5 Elevation and Cross-Elevation Servos

The elevation and cross-elevation servos are the positioning systems used only in the inertial pointing mode for precise (1 arcsecond) telescope pointing.

(a) Elevation Servo System

During inertial tracking the elevation servo control loop consists of four elements*:

1) The prime attitude control loop,

2) The gyro update arm,

3) The momentum management loop, and

4) The active bearing assembly.

The elevation servo takes into account telescope inertia, reaction wheel behavior, and gyroscope behavior using designed-in control laws to stabilize the telescope. A simple proportional plus derivative controller implemented in software was selected for the inertial loop. Its projected bandwidth is 2 Hz with a 0.7 damping ratio. Integral feedback is not required as steady state errors are implicitly corrected within the momentum management loop. Gyroscopes are used as the primary inertial reference and are drift corrected by a coaligned startracker. These positional updates take place every 1 to 5 seconds, too slowly to use this information directly within the fine control loops, however, more than fast enough for updating the gyros.

Space Telescope wheels were selected for the reaction wheels. The reaction wheel momentum is transferred from the telescope structure to the gondola by the gimbals' brushless torque motor. The reaction wheel velocity is monitored and is used to generate a proportional torque from the torque motor in the same direction. This causes the telescope to angulate. The change in position is noted by the prime inertial loop which, while compensating for this motion, causes the reaction wheel to slow down. The operation of the momentum management system is mathematically similar to integral feedback and therefore acts to correct steady state errors.

Finally, the active bearing assembly operates as a torque-free gimbal for the telescope. The gimbal consists of a ball-bearing, torque sensor, and a brushless torque motor (the same one used in the momentum management system). As the telescope elevates, the bearings generate friction torque, which is measured and compensating torques fed into the gimbal by the torque motor. This is not a closed loop system and the torque motor reac-

---

* See also Section 2.4 of the PDR for a complete block diagram and analysis of the elevation servo.

tion time is important. By keeping this time as short as possible the effects of bearing "graininess" or slip-stick behavior are minimized and the chances of an interaction between the telescope attitude control loop and the active bearing are avoided. In order to successfully cancel the torque generated by the bearing the torque motor constants must be well understood. The motor will be calibrated at all orientations and conditions of expected operation. If necessary, a look-up table of torque constants will be used in demanding torque from the motor.

Each gimbal assembly cancels the torque created by its own bearing. This prevents the bearing torque from distorting the mirror cell.

Which gimbal assembly to select for momentum management is still an open question. Both are equally capable of dealing with the momentum transfer, but whether to split the load equally between the gimbals assemblies or give the duty to one of them alone has not yet been determined.

(b) Cross-Elevation Servo System

The cross elevation servo system is virtually identical to the elevation servo, however its range of travel and interaction with the gondola and coarse loop are different. The cross elevation axis has less than $\pm 3^{o}$ of motion. The gimbal is kept centered within this range by occasional activation of the azimuth coarse loop. The cross-elevation gimbal, as it moves, changes orientation with respect to the gondola, since it is the inner gimbal. Therefore, when cross elevation momentum is dumped into the gondola it will excite a complex gondola motion which is not necessarily around an axis parallel to the cross elevation gimbal. Passive methods for damping this gondola momentum will be required.

(c) Selected Components

Components to implement this system including the gimbal motors and reaction wheels are readily available. Semiannual Report #6 describes candidate components for this gondola.

(d) System Response

A full analysis of this system is presented in Semiannual Report #6. System behavior was simulated using the computer program "TF" written at Stanford University. This program provided a Bode plot (see Figure 3.3-2) and an impulse response (Figure 3.3-3) for the modelled system. The impulse assumed for the sake of the analyses was 5×10^{-3} Nms as mentioned above, applied at T=0, it resulted in a maximum predicted excursion of the telescope from its commanded position of .075 arcsec. At such a small angle the system behavior begins to be quantized by the digital-to-analog converters and cannot be considered strictly linear, so the response shown in Figure 3.3-3 may not be a realistic prediction of system response. However, we do see that the "snapping" of the ball-bearing has little effect on the telescope pointing.

The rest of the model behavior is nearly identical to the system described in the PDR. The new gimbal model predicts that the telescope is completely isolated from the gondola. This is different from the earlier

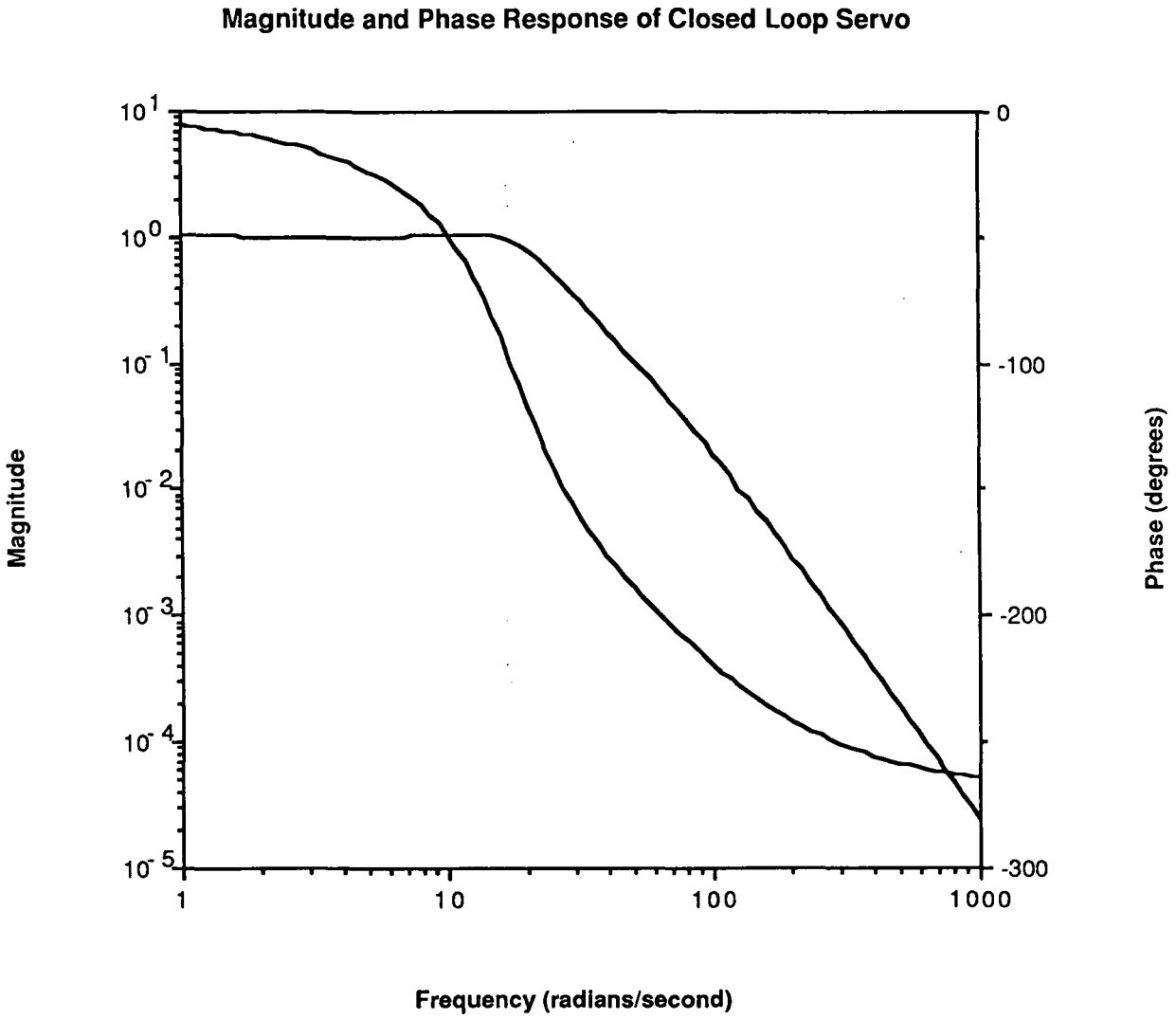

Figure 3.3-2. Fine-Pointing Control System Response to a Sinusoidal Command Signal

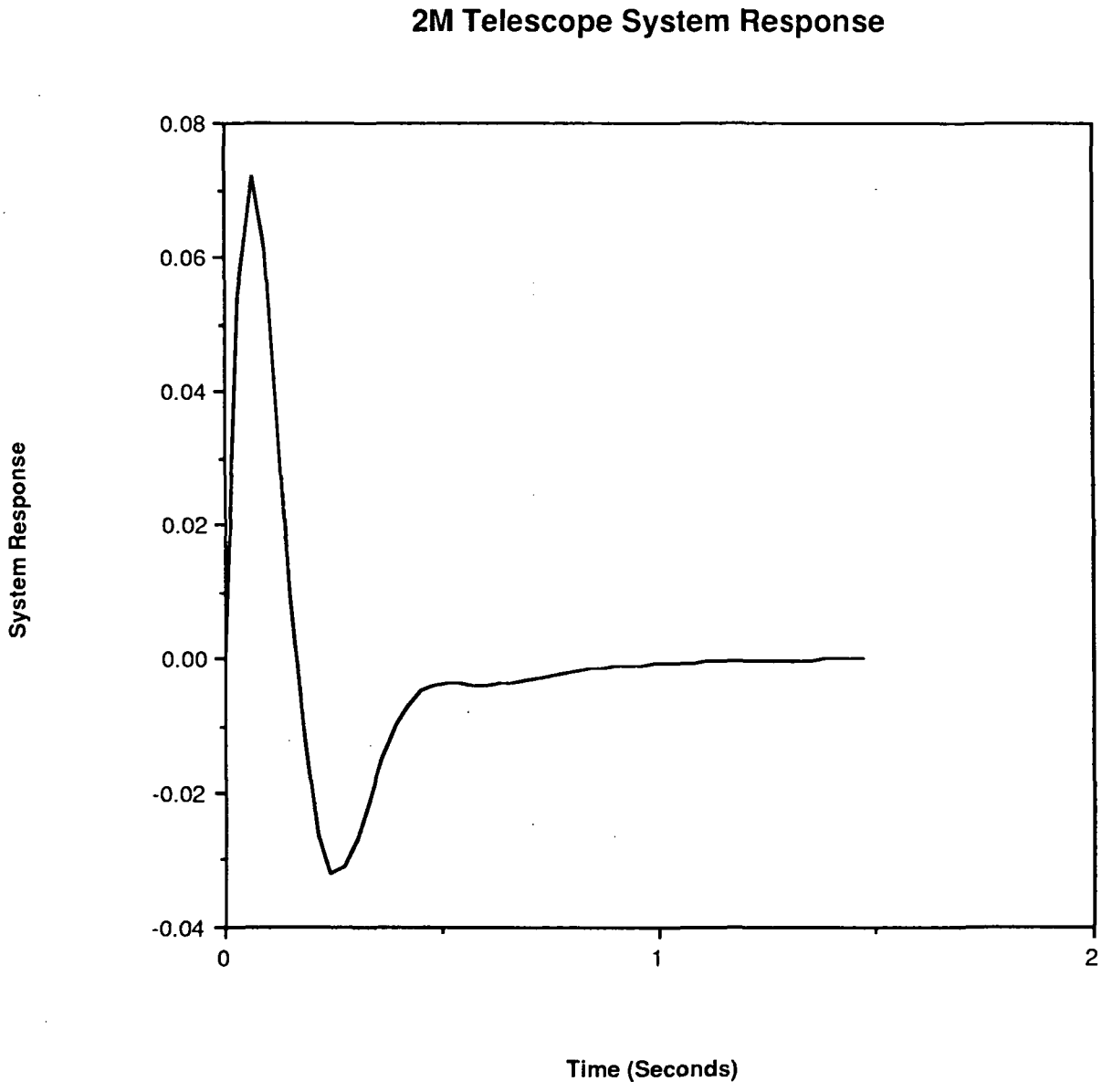

Figure 3.3-3. Telescope Point Response to a $5x10^{-3}$ Nms Torque Pulse

system model in which the telescope was explicitly coupled to the gondola behavior by the flex-pivot. In practice, the gondola will excite some telescope motion through the nonlinearities in the gimbal.

3.3.6 Aspect System

Pointing of the telescope at a desired astronomical object is achieved through the use of three intensified-CCD television cameras. One camera is used for acquisition, one for fine guiding, and one can be used for both if necessary. The primary acquisition camera, with a 5° field of view (FOV) and a limiting stellar magnitude of approximately 8, is used to identify the initial star field. The primary tracking function is performed by a focal plane camera, with approximately the same field of view as the main telescope. A backup camera having a 1° FOV is also used.

The focal plane camera will be used to compute the rotation angle (after determination of a constant offset) with sufficient accuracy to permit single-star tracking. Two-star tracking and scans over large angular fields would also be possible. Gyro drift rates should be small enough to permit tracking for time scales of minutes without updating from the star sensors, if required.

The sensor being considered at this time for each of these cameras is the Fairchild intensified CCD camera Model CCD 3000I. This camera has a pixel format of 488 lines by 380 columns. The wafer-type intensifier used increases the camera sensitivity by a factor of 1,000. The camera has two types of outputs. One is a standard composite video signal; the second provides the timing waveforms and video level for each pixel. The latter output, when coupled to a computer can be used by centroiding, to determine the image coordinates of the guide star to at least 1/10 pixel accuracy (0.2" position accuracy). The intensified CCD camera offers the advantages of fixed pixel structure, high sensitivity, insensitivity to magnetic fields, lack of high voltage requirements, and small size, all of which make it ideal for this application. Such a camera is presently being evaluated in the OIR Division of the Smithsonian Astrophysical Observatory.

Advances in technology (lower readout noise) may also make it possible to use unintensified CCD cameras in this application at a later date. This approach is currently being investigated at the University of Chicago on ground-based telescopes. The ASTROS CCD tracker, developed by Jet Propulsion Laboratory (JPL) for operation from the Space Shuttle bay on the Instrument Pointing System (IPS), provides extremely precise measurements of star image coordinates as inputs to the Image Motion Compensation system used to stabilize the science instrument focal planes. ASTROS can determine star image position to an accuracy of 0.2" over a field of view of 2°2 x 2°5. This requires consistent star image position determination to an accuracy of 1/100 pixel. The ASTROS tracker will be used in early 1986 on the first Astro mission of the Space Shuttle to observe Halley's Comet and a variety of other astronomical targets. If it is possible to approach this performance, the 1° camera could track as accurately as the focal plane camera.

3.3.7 Estimate of Total Pointing Performance

An error analysis has been performed for two different focal plane camera configurations:

1) Optical beamsplitter camera at the focal plane;

2) Direct IR focal plane measurement by a high resolution imaging instrument.

These calculations are based on error magnitudes that have been taken from the PDR or, if unavailable there, assigned on the basis of best engineering judgement. All calculations assume that the system is boresighted prior to each observation. The contribution of image blur to the image position error was reviewed, found to be minor and thus not included. The two errors resulting from each source are first added together algebraically before root-square-summing these values with errors resulting from other uncorrelated sources. The precisions assigned to the secondary mechanisms and the primary mirror to housing motion are estimates.

Following the methods presented in Semiannual Report #6, we project total rms stabilities of 1.0 arcseconds for an optical camera beamsplitter fed at the focal plane and 0.64 arcseconds for a direct fed infrared image instrument. (See Table 3.3-1.)

	Using Resolving Instrument	Using Optical Tracker
Fixed Errors		
Control System	---	0.60
Star Camera	---	0.20
Focal Plane CCD	---	0.20
Unremovable Decenter	---	0.10
Focal Plane Knowledge	0.10	0.10
Total Fixed Error (RSS)	0.10	0.68 arcsec.
Operational Errors		
Star Tracker Misalignment	---	0.40
Star Tracker Centroiding	0.20	0.20
Control System	0.60	0.60
Total Operational Error (RSS)	0.63	0.75 arcsec.
TOTAL ERROR (RSS)	0.64	1.01 arcsec.

Note: All values are for apparent image motion at the focal plane

Table 3.3-1. System Error Performance for Two Star Tracker Configurations

3.4 Electrical Systems Design

3.4.1 Command and Telemetry System

The command and telemetry system will be very similar to the system already in use at NSBF and compatible with it. The heart of the telemetry system is the NSBF Consolidated Instrument Package (CIP II) (see Figure 3.4-1). It consists of subcarrier oscillators used to FM/FM modulate the UHF L BAND telemetry transmitters for efficient use of the authorized bandwidth. Standard IRIG VCO channels of 1, 3, 5, 7, 8, 9, 10, 11, 12, B, E, H, or HH are used. The channel HH (referred to as wide band H or WBH) is used on most flights for PCM data rates of up to 80 kilobits of NRZ or 40 kilobits biphase. There are six of the IRIG channels available for the user.

The main PCM command system provides for 80 discrete functions and a 16-bit parallel data word with strobes. These would be used for control of the gondola. A second command decoder can is provided with a different address. This provides 48 discrete commands and a 16-bit parallel data word with strobes for the experiments.

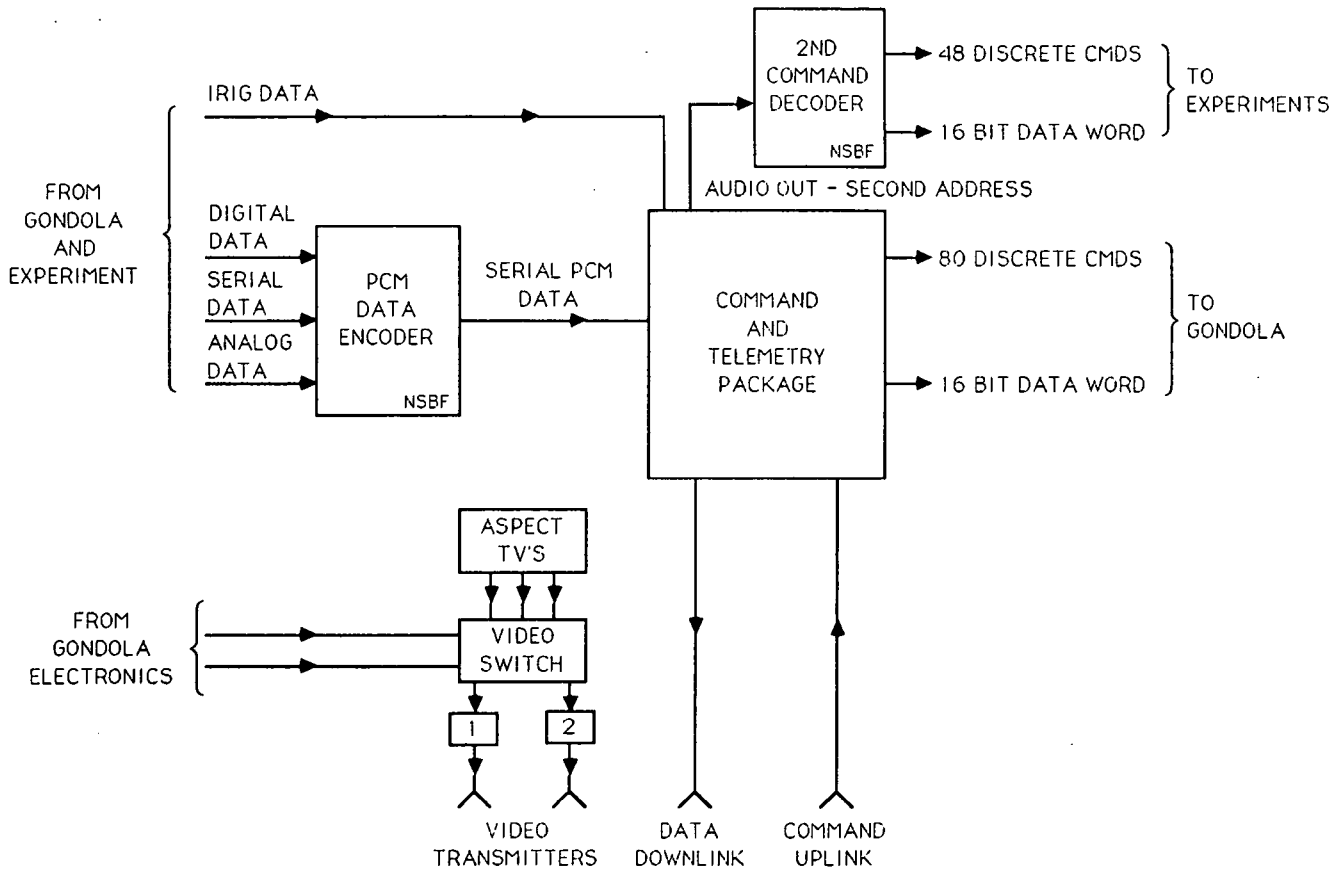

Figure 3.4-1. On-Board Command and Telemetry System for the Balloon-Borne Three-Meter Infrared Telescope

The PCM data encoder format is controlled by an EPROM. There are 128 inputs available, which can be programmed for either analog single ended, analog differential input, parallel digital input or serial digital input. The bit rate is 80.92-kilobits under internal control and 256-kilobit under external control (planned for the future). The gondola would require about 50 digital inputs (5 at 10 bits each) and 30 analog inputs. The remaining 48 inputs would be available for the experimenter.

3.4.2 Gondola Electronics System

Conceptual design of the most critical of these systems, the pointing and stabilization systems, is complete and discussed in detail in Section 3.3 of this report. The balance of the systems are straightforward extensions of existing designs in use on the Smithsonian One-Meter Balloon Infrared Telescope. For flexibility, the designs of the primary experiment controller will be microprocessor based. Low power technology will be used throughout the gondola electronics systems. A block diagram of these systems is shown in Figure 3.4-2.

3.4.3 Gondola Power Requirements

Power requirements are summarized in Table 3.4-1. For the first flights the primary power will come from lithium/sulfur dioxide cells. Power Conversion, Inc., produces a lithium pack rated at 36 volts open circuit and 30 volts under rated load (2a) and at rated capacity (35 ampere-hours). The gondola would require seven packs in parallel. The battery complement for each mission will depend on the experiments flown. When the Two-Meter Balloon-Borne Telescope becomes fully operational, a silver-zinc battery set is planned which would greatly reduce the cost per flight without a significant weight increase.

3.4.4 Electronics Packaging

The yoke frame has been sized to provide an electronics cavity on each side of the gondola that can be thermally controlled, maintain atmospheric pressure and utilize standard 19-inch electronic racks. These enclosures begin just below the telescope elevation drive at a level easily accessible for ground maintenance and checkout. The volume available $0.34 m^3$ ($12 ft^3$) is more than sufficient to hold all system electronics, including any NSBF batteries which must be flown. The left side will be used for gondola equipment while the right side will be dedicated to experiments/hardware.

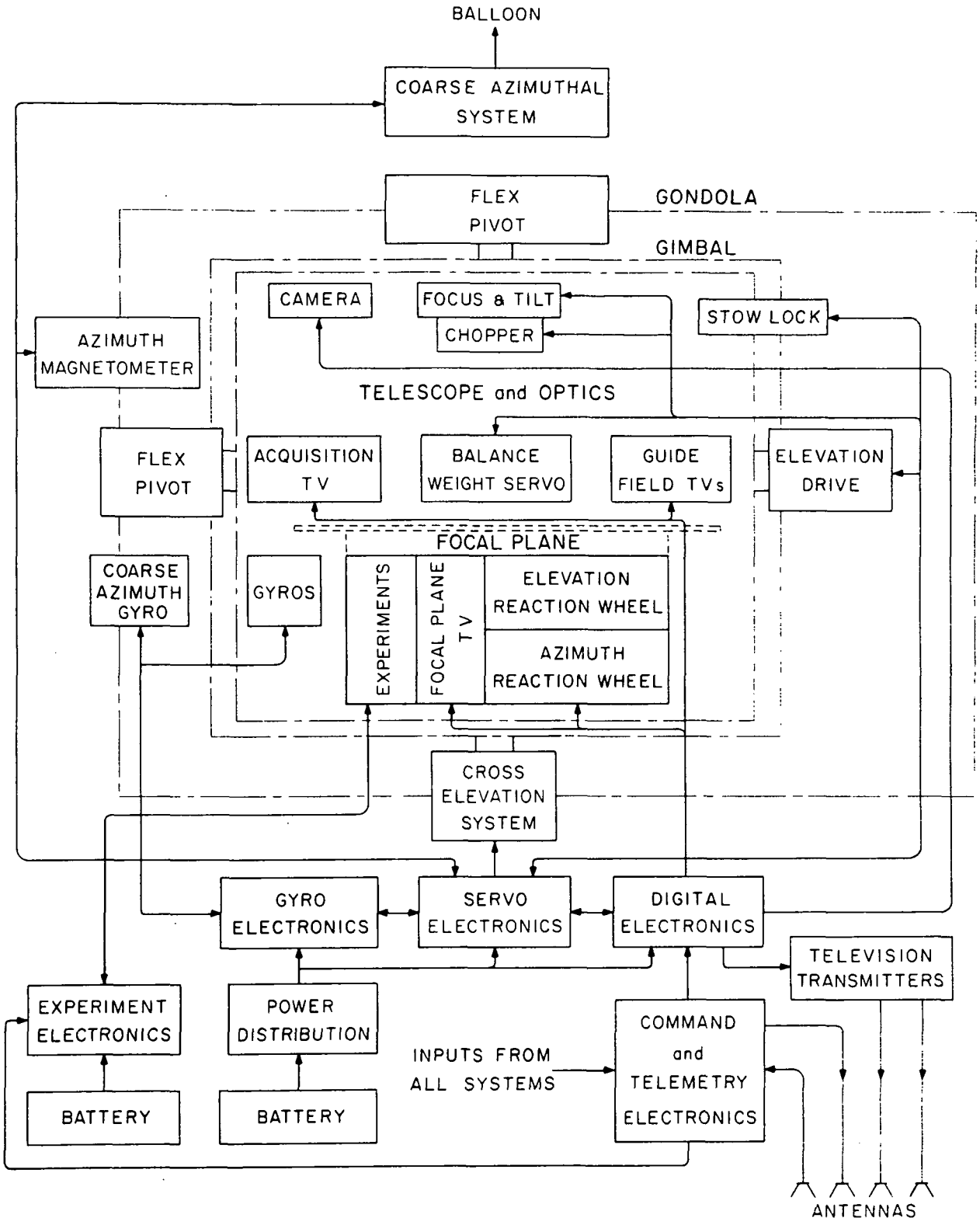

Figure 3.4-2. Gondola Electronics Systems

Table 3.4-1. Estimated Power Requirements

Assembly	Average Steady-State Power (Watts)
Azimuth Stabilization Drives	168
Elevation Stabilization Drives	56
Pointing and Guidance	84
Command System	28
Experiments	140*
Other Systems	84
. Chopping Secondary	
. Focus Drive	
. Heaters	
. Miscellaneous (Power Supply, Losses, etc.)	
Total Steady-State Power	560 watts

Estimated Power per Flight	
. Preflight Checkout	1 hour = 560 watt-hours
. Ascent Power	1.5 hours = 252 watt-hours
. Experiment Power	11 hours = 6160 watt-hours
Total Energy Required	6972 watt-hours at 28 volts (249 ampere-hours)

*Will vary with experiment packages; quoted number is for dual photometer instrument, but can be as high as 425 watts for a heterodyne spectrometer.

4.0 MIRROR DEVELOPMENT PROGRAM

4.1 Approach and Scope

A number of unique requirements for the Two-Meter Balloon-Borne Telescope primary mirror have caused it to be identified as one of the critical items for attention during the definition study. It must:

1. be very lightweight. Preferably approximately 31 kg (10 kg per square meter).

2. maintain its figure at room temperature for testing and at an operating temperature of -45°C.

3. come to rapid thermal equilibrium during a two hour ascent from high summer temperatures through the tropopause to the operating temperature at 30-km altitude.

4. survive the high gravity loading during launch and at the time of parachute opening on descent and survive the landing impact shock.

An additional unique feature of this telescope is its 30-μm diffraction-limited performance requirement which places it in a domain between radio reflectors of considerably lower accuracy and optical telescopes of considerably higher accuracy, a domain which has had little attention for either ground-based or space applications. Because of the very similar reflector requirements for the Large Deployable Reflector (LDR), the balloon telescope development and test effort has potential impact on that future space facility.

The thrust of the mirror development program has been to measure the low temperature performance of state-of-the-art lightweight mirror materials and to work with manufacturers to further develop the technology. In addition we have pursued improvements both in the surface figure as replicated and in techniques for optically figuring composite mirrors for further figure improvements. Our activities include:

1. Designing and constructing a thermally controlled test chamber for optical evaluation of very lightweight mirrors at low temperatures. This is described in detail in the PDR, Section 3.3.

2. Testing a series of nine 0.5-m replicated Carbon Fiber Reinforced Plastic (CFRP) 6-cm-thick aluminum honeycomb core sandwich mirror panels made by Dornier Systems of West Germany. The panels are replicated from a convex Pyrex template with a 10-m radius of curvature. They were tested both for low temperature distortion and for deformation under mechanical load. These were variously obtained by procurement by this project, procurement by JPL in a complementary development effort, and by loan as part of a cooperative project with Dornier.

3. Testing a series of five lightweight replicated CFRP panels made by Hexcel Corp. in a collaborative JPL/Hexcel/University of Arizona (UA) program.

4. Testing a CFRP sandwich panel with additional pyrex facesheets made by Mitsubishi Corp.

5. Collaborating with United Technology Research Center in the development and testing of two very lightweight "egg crate" mirror panels made of carbon fiber reinforced glass (TSC).

6. Procuring for testing an aluminum facesheet, foamed aluminum core mirror made by Energy Resources Group.

7. Experimenting with optically polishing the composite facesheet as fabricated.

8. Experimenting with vacuum deposition of silicon monoxide on the composite for subsequent optical polishing.

4.2 Conclusions from Mirror Development Program

4.2.1 The Dornier Mirrors

The Dornier 0.5 meter octagonal mirror showed spectacular improvement during the course of the nine mirror development program. The surface replication accuracy has improved by a factor of two and the thermal stability by a factor of twenty-five. Figure 4.2-1 shows the figure as replicated of Dornier Quad 25, which was tested March 11, 1987. The surface figure departs from a best fit sphere by 2.5μm rms. With the astigmatism which is the dominant figure error, removed, the residual is 0.8μm rms. Figure 4.2-2 shows the change in focus, XY astigmatism, spherical aberration and rms residual (calculated after subtracting these Zernike terms plus coma) from room temperature to -60°C. The numbers are the peak-to-valley surface change for the particular Zernike terms. The total change over a temperature change of 82°C is .99μm rms.

The Dornier replication accuracy of the 0.5 meter mirror comes close to meeting our required accuracy (1-2μm rms). The thermal stability equals our requirements. Dornier and other manufacturers have made many CFRP two-meter panels for submillimeter radio astronomy. The remaining uncertainty is how the thermal performance scales to this size. At present the CFRP sandwich panel reflector is the baseline mirror approach.

4.2.2 The Hexcel/JPL Mirrors

The five Hexcel mirrors ranging in size from 15 to 40 cm square have had relatively low replication accuracy. The significant achievement of the JPL/Hexcel/UA development program is the validity of the JPL modelling for predicting the UA measured panel performances. Figure 4.2-3 shows the predicted and measured thermal changes in focus, astigmatism, spherical aberration, and coma for the 0.4 meter square mirror Hexcel-4.

4.2.3 The Pyrex Face Sheet Composite Mirror

The Pyrex/CFRP composite demonstrated excessive low temperature deformation and is not a useful balloon-borne telescope mirror candidate.

```
Filename:  ave.2              16:52:48      03-02-87
Quad 25 Figure II 19.5°C Pixel P.Error=.009
            Wavelengths per band= 0.378
        Fraction of band printed= 0.500
Number of half wavelength shifts= 0.000
Coefficients removed: Piston Tilt Focus
```

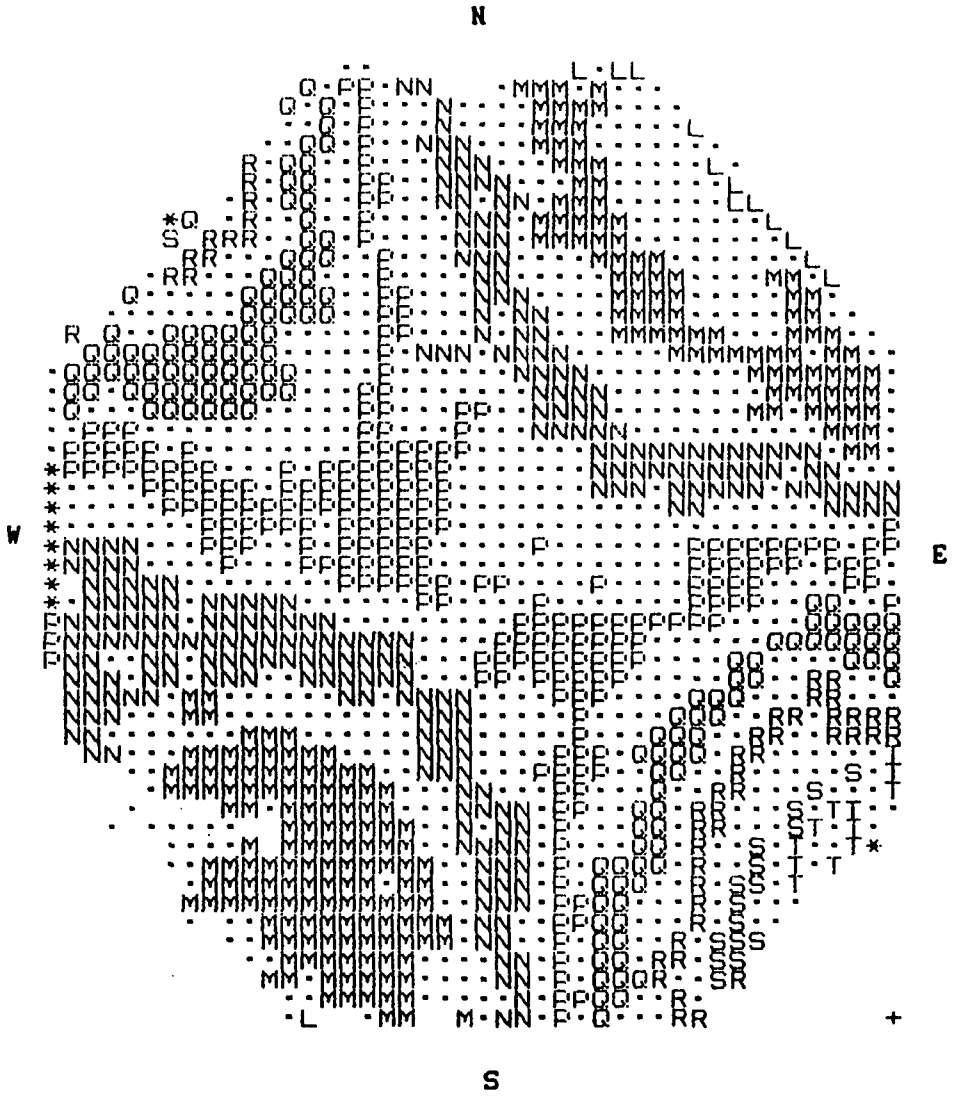

Figure 4.2-1. Dornier Quad 25 As Replicated Surface Figure Error Contour Level 2μm

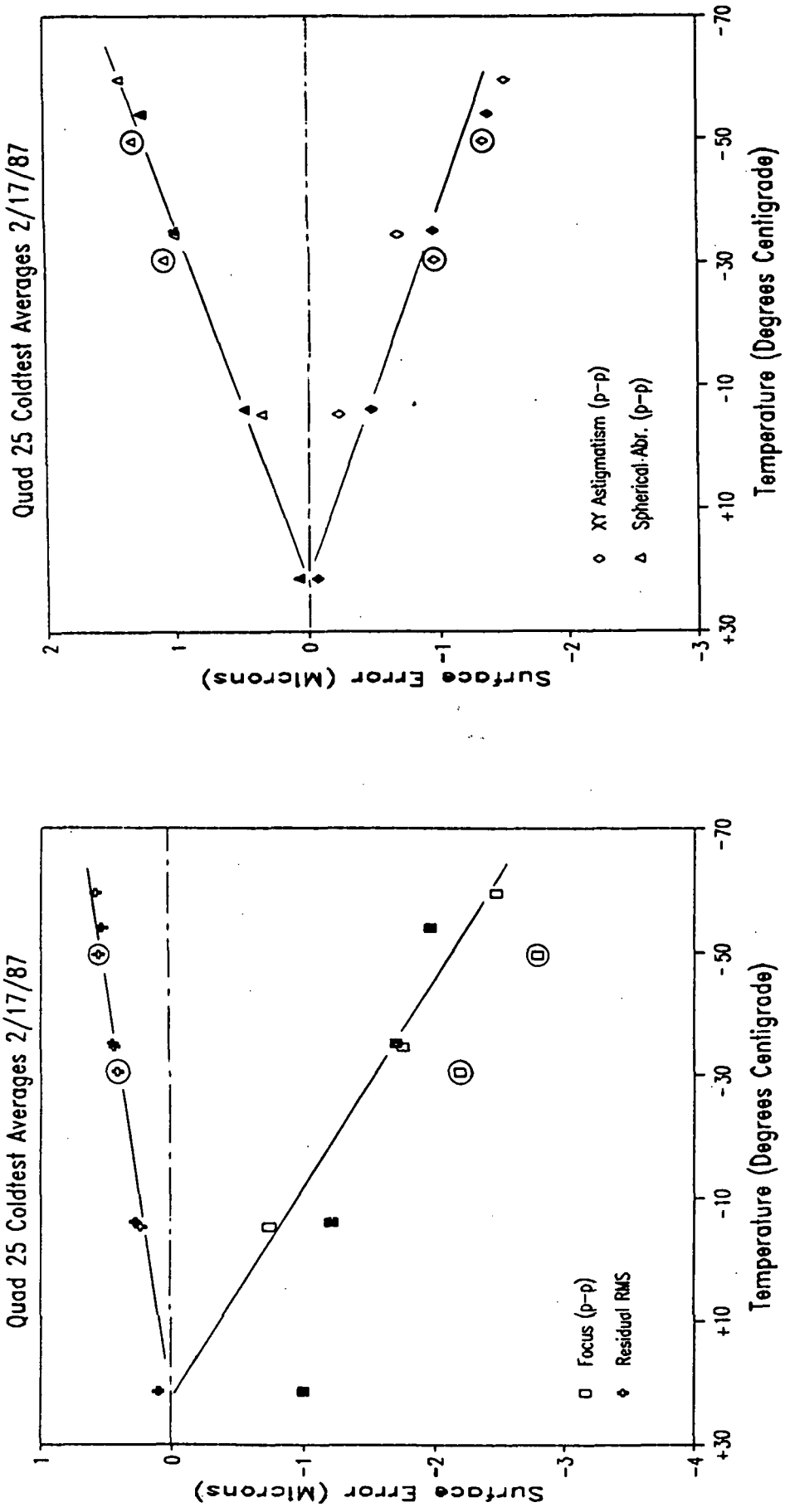

Figure 4.2-2. Quad 25 Peak-to-Valley Change in Figure over 82°C Temp. Change

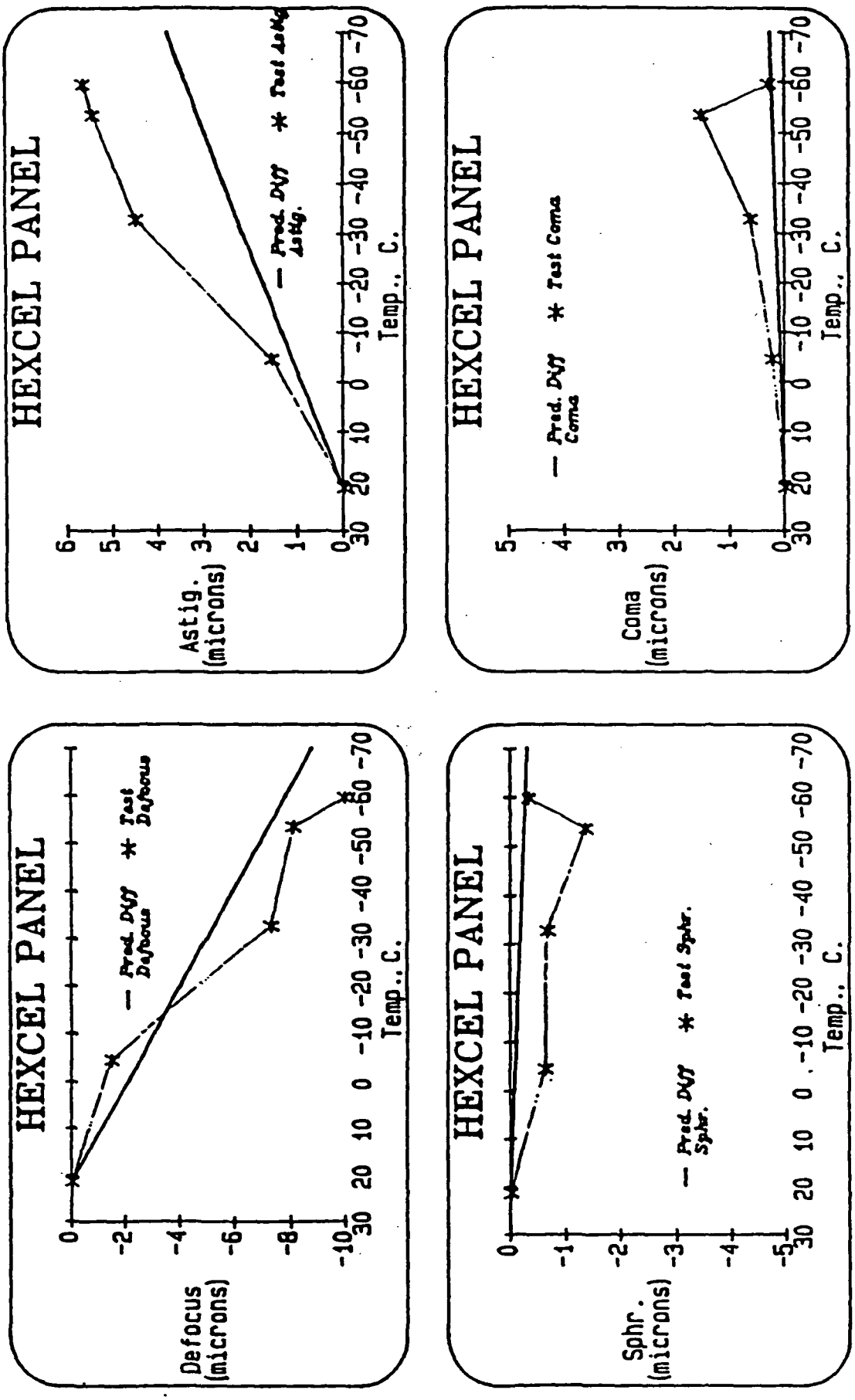

Figure 4.2-3. Hexcel 4 Comparison of JPL Model

4.2.4 The United Technology Graphite/Glass Mirrors

Graphite glass has considerable promise for fabricating optics because of its high strength-to-weight, chemical inertness, freedom from moisture absorption, and low coefficient of thermal expansion of the laminate ($\sim .5\times10^{-6}/°C$). However, the techniques for fabrication of the laminates and assembling these into an egg-crate structures are in their infancy, resulting in deformations due to material non-uniformity. The UTRC 27cm diameter mirror NPM-2 distorted by 0.74μm rms over a 82°C temperature changing largely from focus change. With the focus term removed, the distortion was .41μm rms. While graphite/glass is promising, it is premature to incorporate it into the balloon telescope design.

4.2.5 Foamed Aluminum Core Mirror

A 0.5 meter lightweight mirror has been fabricated by Energy Resources Group, Inc. (ERG) by dip-brazing aluminum facesheets to a foamed aluminum core forming a lightweight homogeneous aluminum structure. The mirror has an areal density of approximately 20 kg/m^2. The mirror is presently being diamond turned in preparation for figure and thermal stability tests.

4.2.6 Optical Polishing Composite Facesheets

We have successfully improved the figure of a 0.5 meter Dornier CFRP mirror by optically polishing an epoxy rich front surface. This was done using an aluminum tool with a pitch face covered with a Pellan pad. The polishing was done with diamond dust suspended in oil. The only limitation to this technique appears to be breakthrough of the thin epoxy surface to the underlying fibers.

4.2.7 Silicon Monoxide Over Coating and Polishing

We have investigated evaporation coating of a CFRP mirror with silicon monoxide and polishing it to improve the mirror. The initial experiments successfully achieved a 6.5μm polishable layer with excellent adherence and stability. We are currently carrying out a systematic effort to develop the technique for thicker (25μm) coatings without overheating the mirror with a goal of achieving optical image quality by polishing this coating. For this purpose we have rehabilitated a vacuum system for evaporative coating and are constructing a chamber large enough for a one-half meter square mirror. The chamber is shown in Figure 4.2-4.

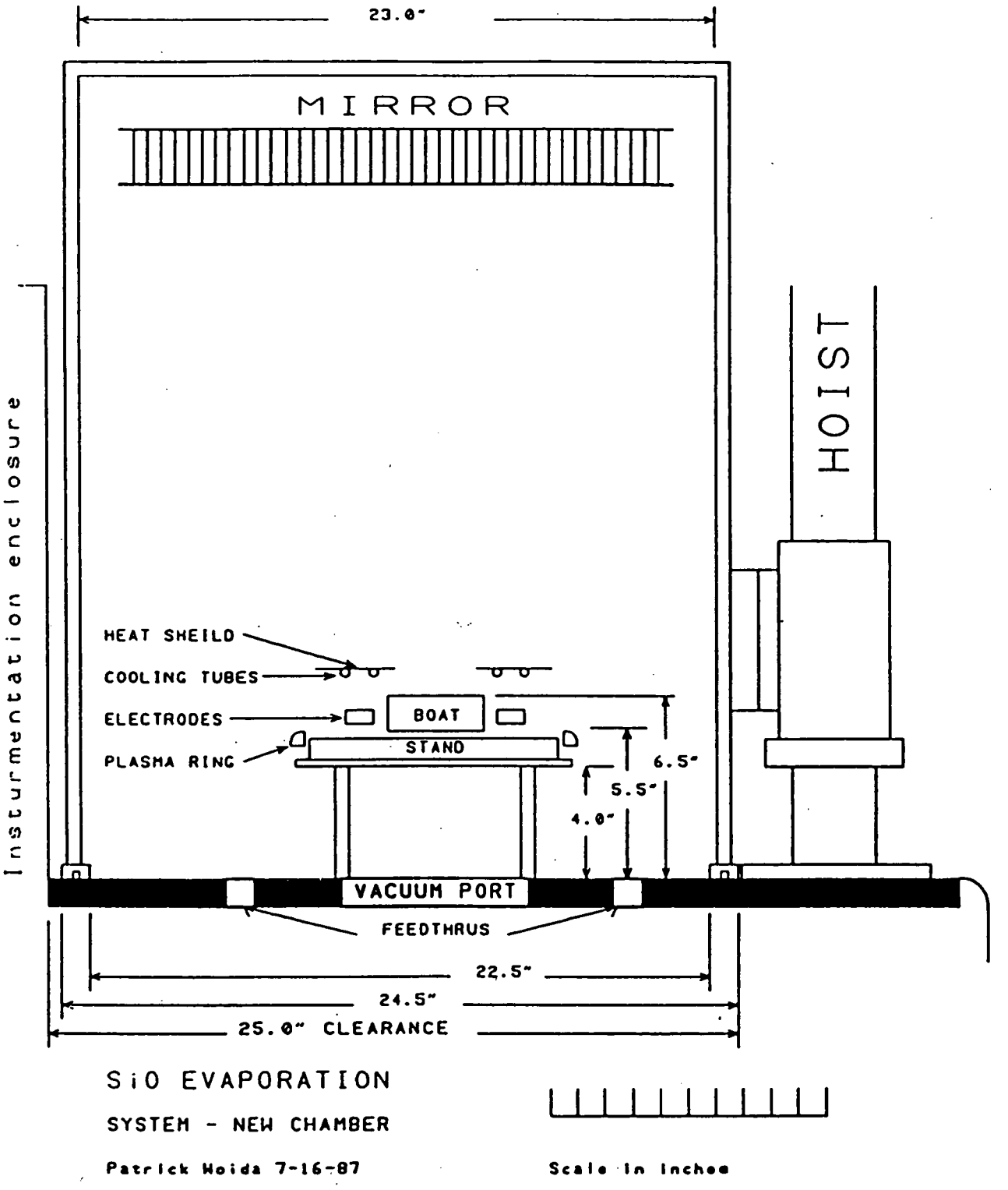

Figure 4.2-4. Silicon Monoxide CFRP Mirror Coating Chamber

5.0 EXPERIMENT ACCOMMODATIONS

5.1 Focal Plane

A rotating dichroic beamsplitter will permit switching of the IR/submillimeter between the IR photometer and the submillimeter spectrometer. Simultaneously, continuous viewing of the sky will be provided an intensified CCD camera for closed loop bore-sight pointing and offset pointing.

5.2 Photometric Infrared Camera

5.2.1 Instrument Description

The proposed far-infrared imager will be based on a 60-channel spatial array of He^3-cooled silicon bolometers (an 8×8, rectangular, close-packed array with unused corner positions). The system will be similar to a 60-channel camera now under construction for the Kuiper Airborne Observatory and to 32-channel systems which have been used extensively on the Kuiper Airborne Observatory at submillimeter wavelengths at the NASA Infrared Telescope Facility and the Caltech Submillimeter Observatory at Mauna Kea. Interchangeable re-imaging lenses will permit discrete changes of the apparent pixel size over a range of ~15"-60".

The spectral sensitivity of the camera will be set by He^4-cooled interference filters mounted in a multi-position turret. Additional spectral blocking will be provided by fixed, low-pass, interference filters, crystalline re-imaging lenses, and a polyethylene pressure window coated with diamond dust. The system will be provided with a standard set of filters with $\lambda/\Delta\lambda \sim 0.3$ covering the range 40-400μm. Additional (e.g., narrowband) filters may be added for special observing projects. It will be possible to change both filters and re-imaging lenses during flight.

Cooling for the detectors will be provided by a two-stage He^3 refrigerator with stages operating at approximately 0.25 and 0.4K. Each detector will be mounted in an integrating cavity behind a 0.25K Winston light concentrator. Other optics and band-limiting filters will be cooled to He^4 temperature.

Detector signals will be amplified by N_2-cooled JFET source-followers and warm preamplifiers, filtered to remove high frequencies and demodulated with a digital sampling system consisting of a commutating analog-to-digital converter, variable-gain amplifier, and controlling microprocessor. Required telemetry bandwidth will be <20 Kbaud.

5.2.2 Limits to Sensitivity

The system should be limited by thermal background noise. The photon-noise-limited NEP for a system for which the total efficiency of detector plus all cold optics and filters is η, for which the warm telescope and atmosphere have about the same temperature T and a combined emissivity ϵ, and for which θ is the diameter of the field of view of each detector is approximately equal to

$$(\mathrm{NEP})_p \approx (1+\epsilon\eta M)^{1/2}(8\mathrm{E}{-14})[(\Delta\lambda/\lambda)T\eta\epsilon]^{1/2}\ (\theta/\theta_0)[\lambda/(\mu m)]^{-1}\ \mathrm{W/Hz^{1/2}}$$

where $\theta_0 = 1.22\ \lambda/D$, D is the telescope diameter, and $M=(e^{h\upsilon/kT}-1)^{-1}$. For T=230 K, λ=100μm, η=0.25, ϵ=0.1 $(\Delta\lambda/\lambda)$=0.3, and (θ/θ_0)=1.

$$[\mathrm{NEP}]_p \approx 1.25\ \mathrm{E}{-15}\ \mathrm{W/Hz^{1/2}}$$

The corresponding NEFD (in $\mathrm{Jy/Hz^{1/2}}$) is

$$[\mathrm{NEFD}]_p \approx 2^{1/2}(3.3\ \mathrm{E}11)[\mathrm{NEP}]_p\ [\lambda/(\mu m)]/[\eta\tau A(\Delta\lambda/\lambda)]$$

where A is the telescope collecting area, $\eta\tau$ is the total transmission efficiency of the combination of telescope, detector system, and atmosphere, and where we have assumed the usual sort of double-beam chopping and beam-switching. For the 2-m balloon telescope, A=3m^2. Thus, for the parameters quoted above and τ=0.7,

$$[\mathrm{NEFD}]_p \approx 0.7\ \mathrm{Jy/Hz^{1/2}}$$

For a point source, only half of the source energy falls with θ_0, so

$$[\mathrm{NEFD}]_p \approx 1.4\ \mathrm{Jy/Hz^{1/2}}\ \text{(point source)}$$

Except for the quantum statistical factor $(1+\epsilon\ \eta M)^{1/2}$, which is close to unity for the parameters and wavelengths of interest here, the NEFD at a constant θ/θ_0 and constant $\Delta\lambda/\lambda$ should be independent of wavelength.

$$[\mathrm{NEFD}]_p \propto \frac{(T\epsilon)^{1/2}(\theta/\theta_0)}{\eta^{1/2}\tau A(\Delta\lambda/\lambda)^{1/2}}$$

5.3 Heterodyne Submillimeter Receiver

The photometric infrared camera will be a powerful instrument for studying continuum radiation from astronomical objects. We also propose to develop and fly a heterodyne receiver having the high spectral resolution necessary to study line radiation; with this complementary capability, a significant new class of scientific problems may be addressed.

The astrophysically richest area of molecular line emission happens to lie in the least-studied part of the electromagnetic spectrum, the far-infrared/submillimeter. There have been three main impediments to advances in this field: (1) the atmospheric transmission is poor and is limited to

a few wavelength windows even at the best high, dry observing sites; (2) sensitive submillimeter detector systems involve difficult and recent technology; and (3) suitable telescopes are only now being built. The atmospheric limitation is largely overcome by working at balloon altitudes, while submillimeter receiver technology has now reached a stage of refinement sufficient to make balloon-borne heterodyne instruments desirable. We expect that our ongoing research programs in receiver instrumentation for this project and others will further advance the state of the art in submillimeter detection, and a balloon-borne telescope in particular will provide an invaluable test-bed for the mission concepts needed for future space-borne submillimeter instruments.

Two distinct technological approaches to heterodyne submillimeter receivers are currently feasible: they are SIS and Schottky-diode systems, and take their names from the devices employed to perform the first mixing of local oscillator and signal radiation. SIS receivers take advantage of the behavior of Superconducting-Insulating-Superconducting tunnel junctions when illuminated by microwave radiation, and of the superior mixing properties of the sharp nonlinearity in the SIS device I/V characteristic curve near the onset of quantum tunneling.

SIS receivers have already emerged as the dominant technology at millimeter wavelengths, and are progressing rapidly to higher frequencies. In addition to superior sensitivity, an SIS instrument has a number of operational advantages over Schottky-diode-based alternatives. Chief among these advantages is the relatively low local oscillator power required by SIS junctions (microwatts rather than milliwatts), permitting the use of low-voltage, high-reliability solid-state harmonic generators utilizing Gunn diodes as the fundamental source. Schottky receivers at short submillimeter wavelengths have required complex and unwieldy molecular lasers, optically pumped by CO_2 lasers, as local oscillator sources. Remote (eg. balloon-borne) operations in particular dictate the use of a receiver based on SIS junctions and solid-state local oscillators. To date, harmonic generators have been built with output powers of about 0.1 milliwatts at almost 500 GHz (in the sixth harmonic) utilizing Gunn oscillators as the fundamental source (Zimmermann 1988, personal communication; Millitech 1988, personal communication). Such local oscillator sources are suitable for current SIS junctions, and we can expect that the frequency range will expand in the next few years.

Theoretical analyses of SIS detectors have shown them to be capable of quantum-limited noise performance in both incoherent and coherent detection modes. Experimental tests performed on SIS junctions have demonstrated this performance at frequencies near 36 GHz (Shen et al. 1980, Richards et al. 1980). Currently, SIS heterodyne (coherent mode) receivers are being built and used consistently at 115 GHz and 230 GHz (Sutton 1984). These receivers, although not yet operating at the fundamental quantum noise limit, outperform Schottky-diode receivers operating at the same frequencies; Figure 5.3-1 shows a comparison of receiver sensitivities reported for the competing technologies. This sensitivity advantage enjoyed by SIS increases both the quantity and quality of science that can be done.

Work on SIS receivers is proceeding at a rapid pace in a number of laboratories around the world, including Caltech/Bell Labs (Ellison and

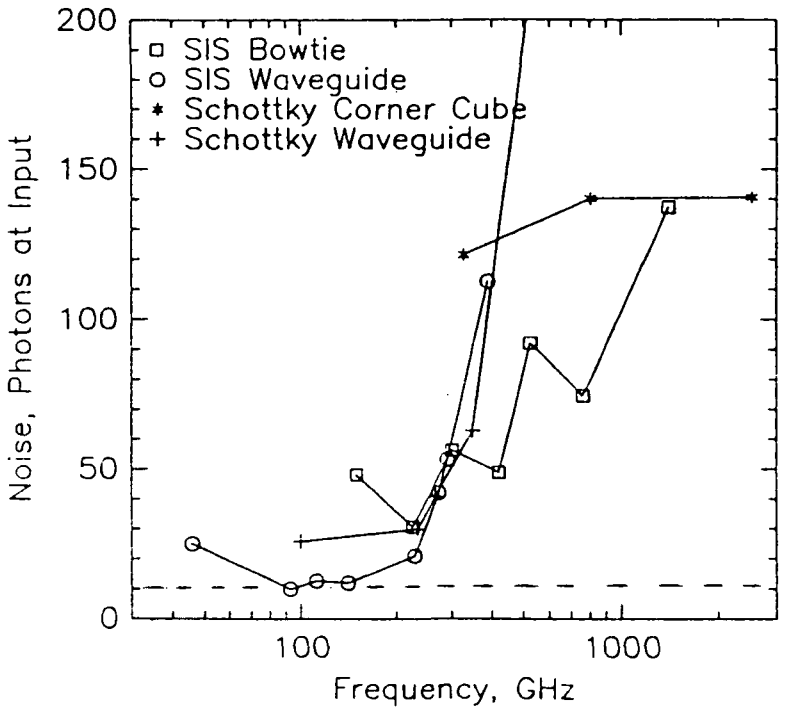

Figure 5.3-1. Comparison of actual receiver performances in terms of number of noise photons at the input. The dashed curve represents the best achieved result of a 10% quantum efficiency, of 10 photons of noise.

Miller 1987), NRAO (D'Addario 1985; Pan et al. 1987), IRAM (Gundlach et al. 1982), Chalmers University (Rudner and Claeson 1979), NASA-Goddard Institute (Pan et al. 1983), and Berkeley (McGrath et al. 1985).

The traditional approach to constructing SIS receivers at lower frequencies has been to place the junction in a resonant waveguide structure for maximum coupling to local oscillator and signal radiation. At frequencies beyond about 350 GHz, fabrication of such small tuned structures becomes extremely difficult, and the use of open, "quasi-optical" structures becomes more attractive (Wengler et al. 1985).

Instead of using waveguide components, such a receiver employs a system of lenses to focus the radiation collected by the telescope onto an antenna connected directly to the SIS junction, and fabricated on the same substrate. The antenna pattern used by Wengler et al. is referred to as a "bowtie", after its shape, and provides a good impedance match to the junction up to ~500 GHz. Hence, the same SIS detector and front-end block can be operated from ~2 mm to ~600μm. The frequency of observation is determined by the local oscillator frequency, while the receiver's bandwidth is limited only by the intermediate frequency (IF) amplifier. Other quasi-optical structures are being tested by various groups, including spirals, log-periodic structures, and end-fired dielectric horns. (Compton et al. 1987).

The frequency flexibility of a quasi-optical SIS receiver is a particularly attractive feature for flights on the two-meter balloon facility, as observations will be conducted from altitudes at which much of the submillimeter spectral band is accessible. Since waveguide receivers are inherently narrow-band, a separate receiver would have to be built for each spectral region of the band. If multiple transitions of a particular molecule (eg. CO) are to be observed on the same flight, then a number of receivers that can be rapidly switched in and out of operation would be required. The cost and complexity of this type of system might prove to be prohibitive. However, since a single open-structure SIS receiver can be used from 2mm to 600μm, the cost and difficulty of switching between different parts of the submillimeter band are dramatically reduced.

For these reasons (sensitivity and broad frequency coverage), open-structure SIS heterodyne receivers are now being developed at UA's Steward Observatory and at SAO. Bowtie antenna/junction structures fabricated by R. E. Miller of Bell Laboratories for the current Steward Observatory SIS receiver are shown in Figure 5.3-2. These are essentially the same as those used by Wengler et al. at Caltech (who also used junctions fabricated by Miller) except that the size has been scaled down to provide optimum performance at 345 GHz.

We have tested a single-element version of the receiver both in the lab and on the NRAO 12 meter telescope. The lab results indicate that at 345 GHz the receiver has a double-sideband noise temperature of $\sim$350 K. A plot of the DC and local-oscillator-pumped I/V curve of an SIS junction operating at 345 GHz at SAO is shown in Figure 5.3-3. The sensitivity of the system can be computed by comparing the IF power output obtained when hot and cold loads are placed in the beam of the receiver; these IF powers are also plotted in Figure 5.3-3. As expected, the junction is most sensitive in the vicinity of the "knee", or non-linear region, of the I/V curve. The 345 GHz tests on the 12 meter telescope indicate that the bowtie and optics produced a main beam with a half-power size $\leq$ the diameter of Jupiter (45" during our run). Poor weather precluded measuring the beam on a smaller source. Further tests of this system will be made on the Steward Observatory 1.5 meter telescope in the spring of 1988.

In the near future, we will begin testing the performance of first-generation receivers using 2- and 4-element SIS/bowtie arrays. Such array receivers are needed to make the most efficient use of flight time. We are also investigating the broad-band characteristics of other types of antenna structures that may provide better performance than the bowtie, including log-periodic, spiral, and V-shaped designs. We propose to combine the results of these studies to construct an SIS array receiver for the two-meter balloon-borne telescope.

A block diagram of the proposed heterodyne receiver system is shown in Figure 5.3-4. Beams from the telescope and from the local oscillator are combined in a diplexer of the Martin-Puplett design, using wire-grid elements as the polarizing mirrors. Local oscillator power at each observing frequency will be provided by a Gunn diode multiplied in a harmonic generator; phase stability is provided by a phase-locked loop using a multiplied crystal oscillator as the reference. The combined signal and local oscillator beams enter a cryogenic dewar housing the SIS mixer, and far-infra-

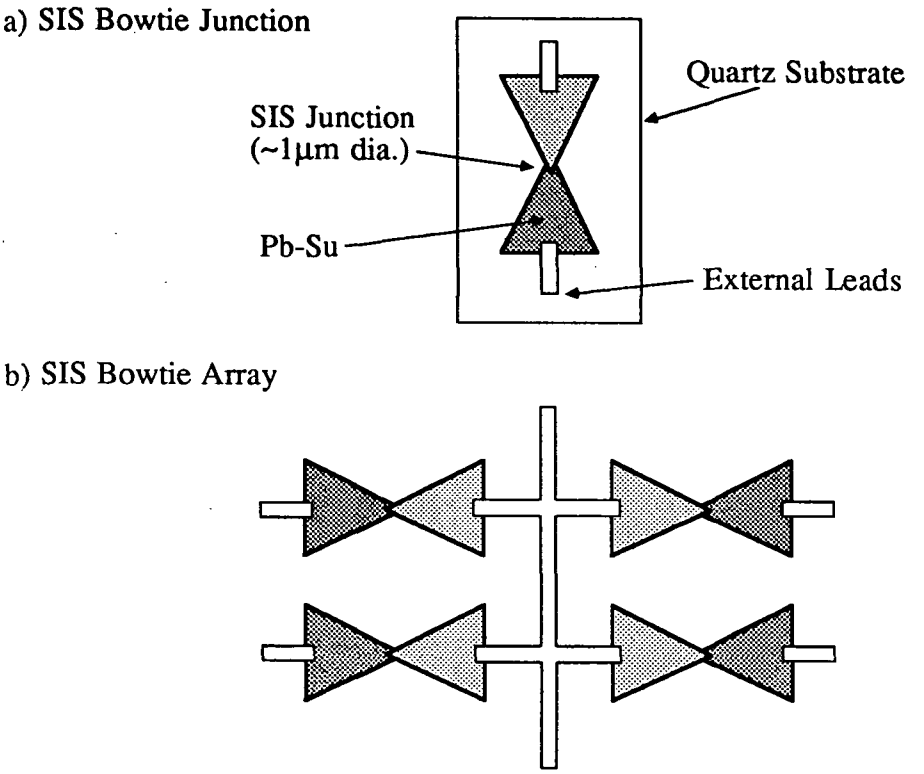

Figure 5.3-2. Bowtie and Bowtie-Array SIS Junctions

red-transmissive optical components couple the optical beam to the junction. For ground-based work we have developed a hybrid design which utilizes a 4-liter liquid-helium reservoir and CTI-22 cold head for the shields; the hold time is about 10 days. For a balloon-borne receiver we will construct a simpler batch-fill liquid-helium and -nitrogen cryostat, since cycle times can be shorter, and simplicity and total weight are important considerations. A superconducting magnet is provided to apply a modest field to the junction in order to suppress undesirable Josephson effects. The first IF amplifier will be a HEMT mounted directly on the cold work surface of the dewar.

Following additional processing outside the dewar, the signal is eventually fed into a backend spectrometer. This may be a filter bank, a digital autocorrelation spectrometer, or an acousto-optic spectrometer (AOS); we currently favor the AOS, as it will be cheaper, lighter, and more flexible than the alternatives. We expect the AOS to have 2048 spectral channels and 1 GHz total bandwidth (1.5 GHz may be possible on the time scale of this project, but 1 GHz is current technology). Spectral resolution will be 0.5 km/s at λ = 1mm and 0.3 km/s at λ=600 μm. Total bandwidth will be 1000 km/s or 600 km/s respectively. The signals from the spectrometer will be read at a relatively modest data rate and passed to

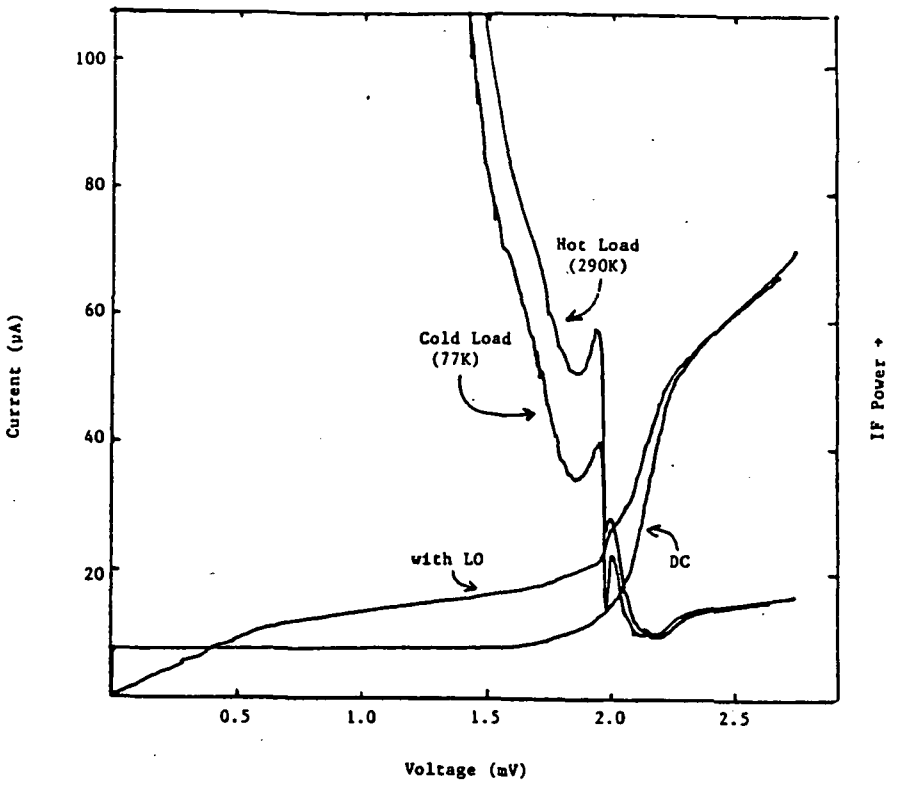

Figure 5.3-3. Laboratory SIS results at 345 GHz. The lower two curves are the I-V curves of the SIS junction with and without local oscillator power. The upper curves are the IF power output versus bias voltage when the detector sees a cold or hot load (vertical scale on the right). The system sensitivity is given by the ratio of the hot/cold IF curves.

the gondola telemetry electronics for relay to the ground control station.

A preliminary estimate for the total weight of the heterodyne submillimeter receiver, backend, and associated interface electronics is 140 pounds. The total power consumption will not exceed 140 Watts.

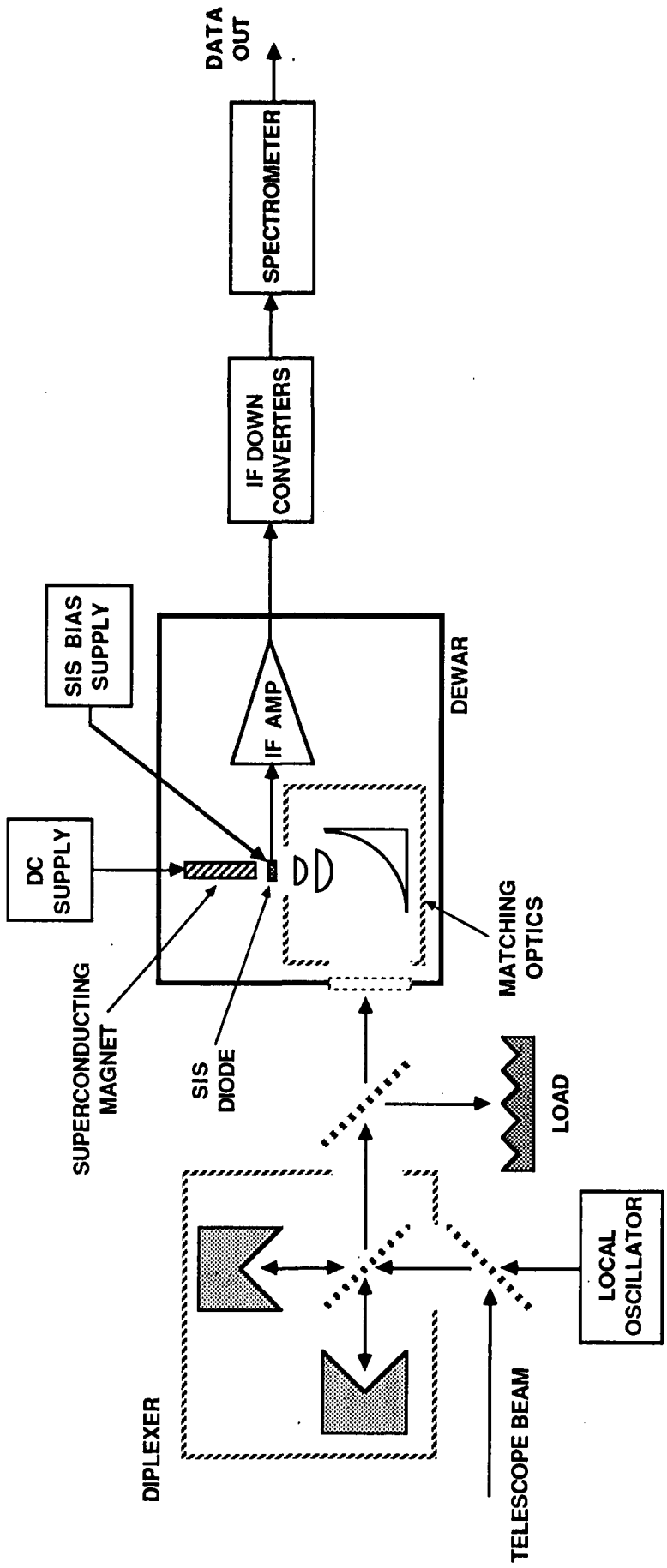

Figure 5.3-4 Block diagram of the University of Arizona Open Structure SIS Receiver. The signal from the telescope is combined, quasi-optically, with the local oscillator signal in the diplexer. The signal is then coupled, through focusing elements, to the SIS junction inside the cryostat at 4 K. A superconducting magnet is built into the block which holds the SIS junction so that magnetic fields can be employed at high frequencies of observation.

The receiver development efforts proposed here will benefit from other submillimeter heterodyne projects now being pursued at Steward Observatory and at SAO. In particular, our Steward Observatory collaborators are involved in the construction and instrumentation of the SMT, a 10-meter dedicated submillimeter telescope on Mt. Graham. Work on SIS heterodyne receivers of the type needed for the two-meter telescope has been going on for a few years now. SAO is developing heterodyne SIS receivers for a proposed submillimeter telescope array. Establishment of the SAO receiver lab is progressing at a rapid pace, and an operating base budget of $402,000 per year from the Smithsonian Institution ensures a state-of-the-art effort.

It should be emphasized that the development of a balloon-borne submillimeter heterodyne system will contribute in turn to the technology base for submillimeter ground-based instrumentation.

6.0 GROUND SUPPORT EQUIPMENT REQUIREMENTS

The Two-Meter Balloon-Borne Telescope gondola is a complex and versatile experiment and requires certain specialized equipment throughout the program to support assembly, development testing, subsystem testing and finally full flight level system testing including experiment testing and calibration. This section identifies, in general terms, the GSE required to support these assembly and test activities.

6.1 Optical GSE

Primary and secondary mirror handling, transport and alignment fixtures will be required. These will be supplied by the mirror contractor. Once assembled, the telescope will require the following specialized equipment for shipping and its alignment and installation into the gondola:

- o Shipping container
- o Telescope optical alignment fixture
- o Star tracker and aspect TV co-alignment fixtures
- o Alignment telescope with accessories
- o Laser alignment system
- o Miscellaneous optical accessories (mirrors, beamsplitters, corner cubes, etc.)
- o Automatic auto-collimator for stability testing

Experiment optical alignment and calibration with the telescope will require the following optical/mechanical GSE:

- o Light sources
- o IR sources
- o Experiment FOV beam mapping device
- o Experiment installation/handling fixture

NOTE: The telescope alignment fixtures can also serve to optically align experiments.

6.2 Mechanical GSE

Mechanical GSE is required for assembly, handling, and recovery of the gondola. Gondola assembly will employ several fixtures for handling such large components as the telescope, structural members, crash rings and experiments. Gondola assembly and test will also require portable staging for access to the telescope and both servo-driven gimbal axes.

Handling fixtures are required for positioning and/or transporting major assemblies to facilitate independent testing or repair. The gondola, for example, will require a large base frame with soft (balloon tires) wheels to maintain it in an upright position when not attached to the crane.

Recovery will require several shipping containers for critical items, such as: Experiments, star tracker, aspect TV's, secondary mirror assembly, servo components, etc. Also a standard, 36-foot flat-bed trailer with air suspension and crane is desirable. This will facilitate gondola disassembly and placement on the trailer for transport back to the NSBF.

6.3 Electrical GSE

The Two-Meter Balloon-Borne Telescope program will have an independent, self-contained telemetry ground station except for the use of the NSBF receiver, discriminators, and directional antennas. Being independent of the NSBF ground station as much as possible permits economical full-time use of the equipment for testing and flight preparation. A permanent facility that doesn't have to be moved in and out of the NSBF control room, or respond to the needs of other payloads, is needed to support the proposed schedule of flights. Only a coax connection is needed to receive the PCM data. The PCM data is patched out to several areas in the setup bay. The serial PCM data is decoded by a D-Pad 3 PCM decommutator and sent to a central minicomputer (e.g., a VAX 11/750) that will provide real-time output of the scientific data and housekeeping information, on strip charts, video consoles, and a printer. We assume NSBF will continue to be responsible for recording the data on digital and analog tapes. The minicomputer will also be used to send commands, and provide star field information for the graphics overlay system. The graphics controller mixes the incoming video signal with a graphics overlay generated by the computer and

displays the result on a monitor. This is very helpful in rapid identification of the desired area of the sky. Both the acquisition and focal-plane television information will be displayed and recorded on tape.

A block diagram of the ground support equipment and facilities is illustrated in Figure 6.3-1.

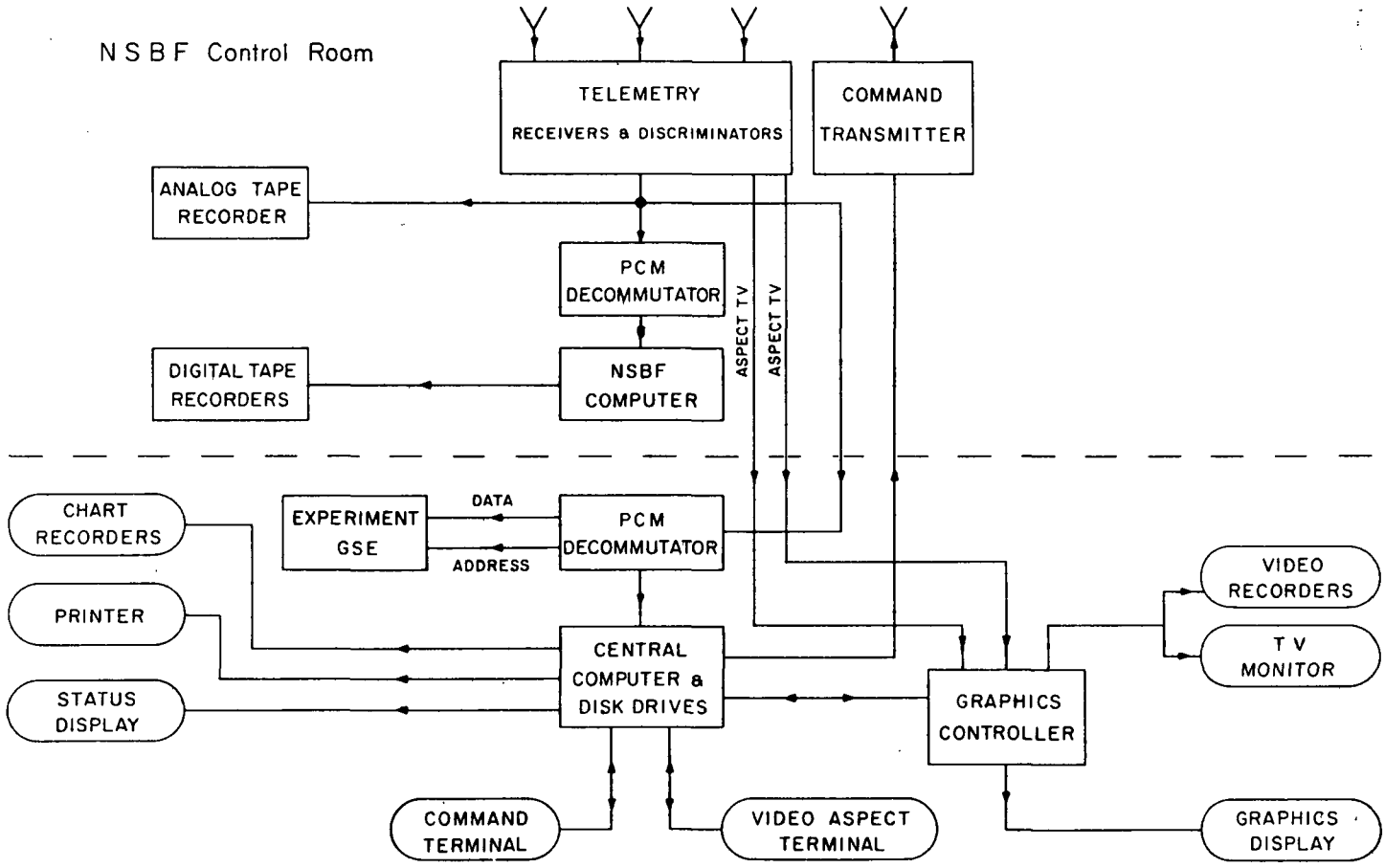

Figure 6.3-1. Gondola Electrical Ground Support Equipment

7.0 NSBF DESIGN DRIVERS AND PAYLOAD SUPPORT REQUIREMENTS

7.1 Payload Support Requirements

7.1.1 Staging

Figure 7.1-1 shows the gondola supported within the NSBF high bay experiment staging building.

The NSBF high bay experiment staging building is ideally suited for this program. It has a 3-ton traveling crane with a lift height of 30 ft. and experiment exit doors 27 ft. in height by 14.5 ft. in width. This combination allows gondola suspension for pointing and stabilization testing with access to evening skies and/or within the bay area. The bay's 24-ft. width is more than adequate and if about half the bay's length (30 ft.) is available then this floor area (720 sq. ft.) is adequate for this testing of all operations planned at NSBF. All other staging area facilities are adequate such as lights, power, heat, air conditioning, office space, and so forth.

The gondola is designed for convenient transport to sites away from Palestine, Texas, such as a winter launch site in New Mexico and transport from the recovery site. The former is particularly important because of the increasing emphasis of the NSBF on remote launches to overcome constraints of balloon ascents over areas of rapidly growing population in East Texas.

Space must also be provided within the high bay building for staging and use of the optical, mechanical and electrical GSE associated with these missions. GSE requirements are identified in Section 5.0.

7.1.2 Command and Telemetry Trailer

The gondola also has been designed to operate within the existing NSBF command and telemetry system limitations. This system is adequate for our projected needs at its present 81-kilobit data rate; however, the planned expansion to a 256-kilobit data rate is highly desirable to accommodate efficiently the high bit rates associated with the larger IR imaging arrays now under development.

The construction and outfitting of a complete command and telemetry ground station trailer in support of this program is highly desirable. Tracking antennas and an appropriate area for NSBF equipment and personnel would be included. This ground station trailer would greatly enhance the test phase by allowing testing to be conducted in a flight configuration thereby eliminating the NSBF interface and other specialized test equipment to support operational testing. It could also be moved to experimenter's facilities for the same purpose. Further, it removes conflicts normally associated with operating from the NSBF control room where priorities, set up time, and communications during testing are sometimes difficult.

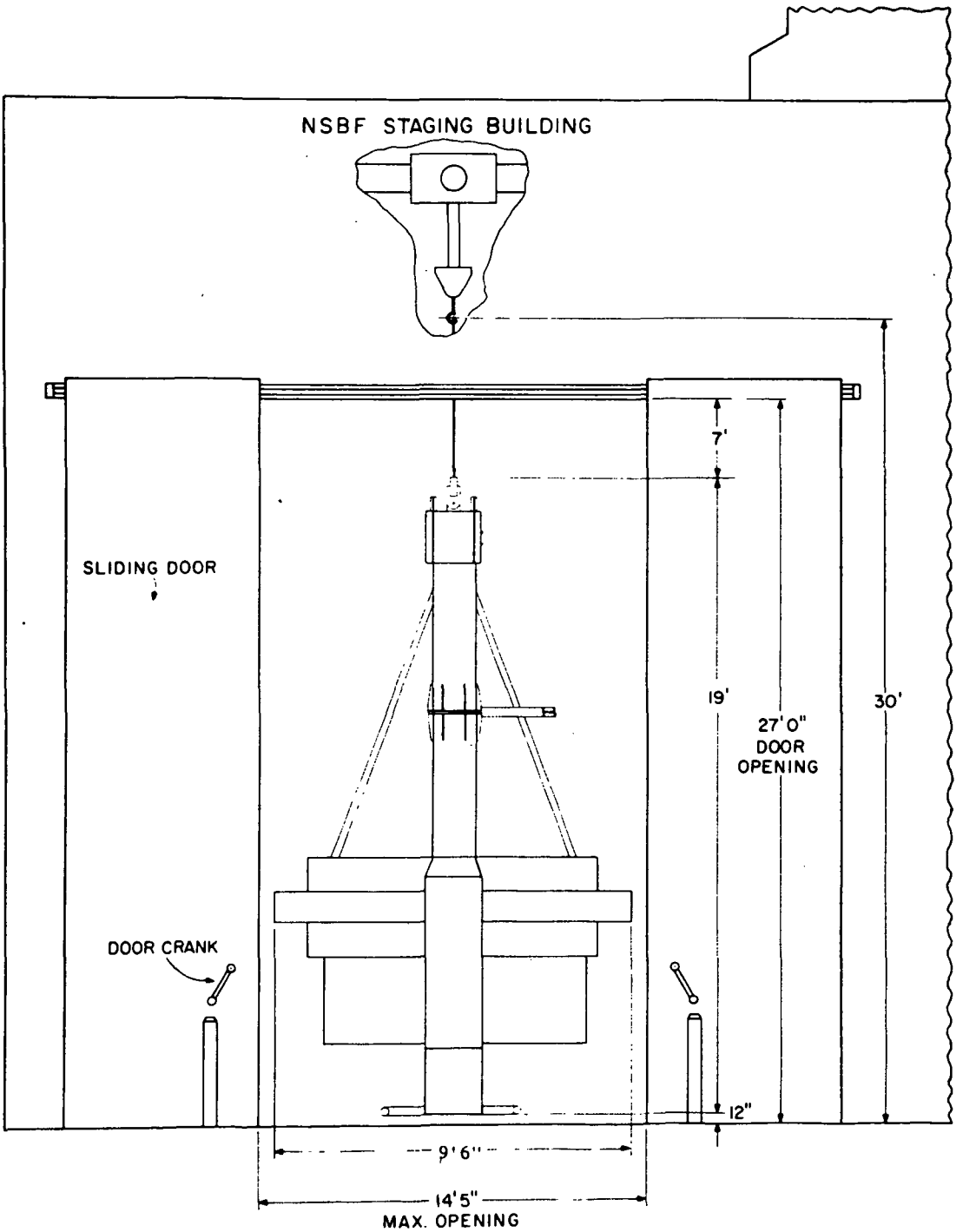

Figure 7.1-1. Gondola Supported Within the NSBF High Bay Experiment Staging Building.

The trailer would also be a valuable asset to support long duration flights, or for launch times when float winds are high. Also, launches from remote sites, such as Fort Sumner could be accomplished more easily.

7.2 Launch Requirements

This experiment requires no special and/or different launch requirements than presently employed by the NSBF. The experiment is shown suspended from the launch vehicle in Figure 7.2-1. It requires a suspension height of 29 ft. which is located 9 ft. ahead of the vehicle. This position is easily achievable because of our light weight. All launch vehicle radial clearances with the launch arms are as requested by the NSBF.

Launch requirements relative to science aspects will be similar to those associated with our present One-Meter Balloon Infrared Telescope program. These have been mentioned previously and are summarized below:

Flight Altitude:	28-30 km
Flight Duration:	6-10 hours at altitude
Launch Time:	Local sunset $\pm$ 1 hour
Termination Time:	After sunrise at altitude

The current NASA balloon flight policy concerning the Palestine, Texas launch site is:

- Experiments weighing less than 3500 pounds below balloon can fly any time throughout the year. This weight includes approximately 1050 pounds of NSBF equipment.

- Experiment weighting less than 5000 pounds, below balloon, can fly without a waiver, when the trajectory is in a westerly direction. This occurs approximately between May through September. The remainder of the year a waiver would be required.

The two-meter gondola weighs 3,809 pounds below the balloon. We believe this can be brought down below 3500 pounds by careful design and materials selection and expect to qualify the gondola for year round flights from Palestine.

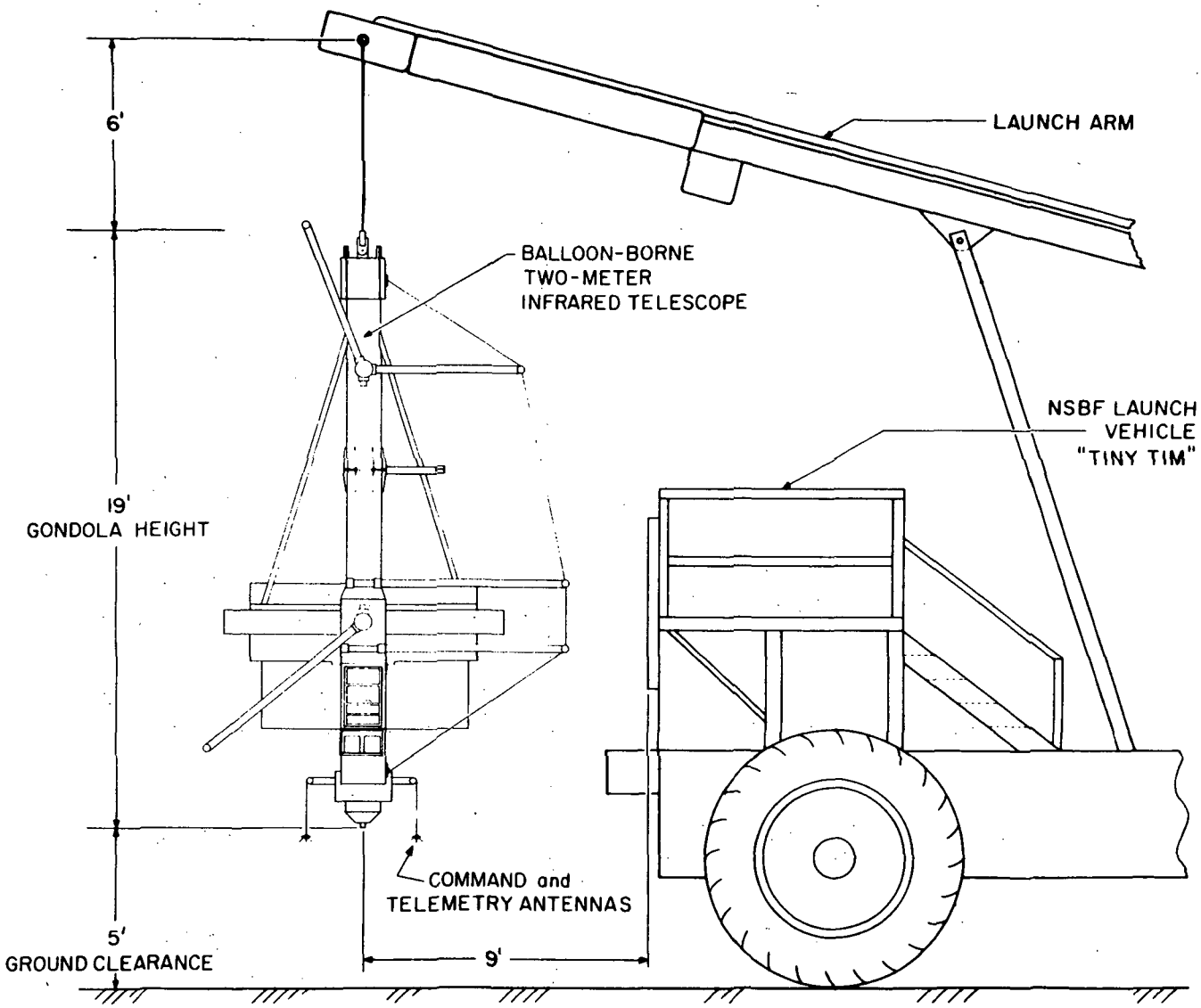

Figure 7.2-1. Gondola Suspended from Launch Vehicle

C-2

7.3 Ascent and Float Environment

The gondola will be subjected to a temperature change of 130°F between launch and float altitude with an expected float temperature minimum of -50°F. These environments are well understood and have been successfully managed in numerous balloon payloads including our own One-Meter Balloon Infrared Telescope.

Thermal design does not represent an area of technical concern or development, although stabilization of the mirror temperature is a new design area, which requires diagnostic measurements and testing.

The gondola must also operate in reduced atmospheric pressure (approximately 10 Torr). Operation of balloon payloads in this pressure range is also well understood and therefore is not an area of concern.

Present far-infrared balloon-borne telescopes operate at altitudes of approximately 30 ± 2 km. This altitude is high enough to be above most (>99%) of the water vapor in the earth's atmosphere, yet not so high that it taxes the size of the balloon required. This reduces cost, handling complexity and risk.

The balloon volume required is calculable once the altitude and the suspended weight are specified. For a suspended gondola weight of 3,809 lbs. and a flight altitude of 29-31 km, a 11.6 million cubic ft. (MCF) balloon is required. This is a "small" balloon by NSBF standards and, therefore, should have the highest probability for a flight success.

In the atmospheric region of interest wind velocity also increases with altitude, limiting the time in which the payload will remain within the telemetry range of the base station. Four months a year the wind velocity at 29-31 km is $\leq$ 30 knots. Telemetry range at this altitude is ~300 miles. Therefore, flights of 8-10 hours can be routinely conducted throughout this period. This takes advantage of the full night time period.

The gondola has been designed to operate without performance degradation at vibration levels in the 3-5 g rms range, which is well above the 1-2 g rms expected during ground testing, transportation to the launch pad, launch and ascent.

The number of flights that can occur per year depends primarily on the manpower and funds available. A typical time between flights for a recovered and refurbished payload of this complexity is about three weeks assuming adequate spare parts and minimal damage. During the first year we believe that one flight is a reasonable goal with the new gondola. During the operational phase as many as five flights could be accommodated each year.

During long duration flights, the increased flight time produces demands on the gondola and ground operations, including the additional weight of ballast, additional thermal problems resulting from both day and night operations, downrange telemetry stations, remote launch operations,

additional battery packs, etc. The initial flights are limited to the night, about eight to ten hours at the float altitude, and launching the balloon from the NSBF base site. The next step would be to increase the flight time to observing one night and daytime (approximately 23 hours), followed by eventual cross-country flights of two to three days. Such cross-country flights have already been performed by the NSBF.

7.4 Termination, Landing and Recovery

The task of recovering, loading and transporting gondolas back from remote areas is difficult at best. This size gondola requires that careful attention be paid to recovery operations to assure a safe and straightforward return of the gondola. The two-meter gondola can fit fully assembled into an enclosed air cushion truck for non-abusive transport back to the launch site without concern for special routing and/or the need for local road variances.

Modular design will minimize the damage usually associated with recovery and will keep recovery time to a minimum and allow critical components to be removed following landing for separate transportation back to the launch site.

The NSBF requires that a balloon experiment not experience a structural failure resulting in an article or payload free falling from the suspension train. The structural loads are specified as 10 g's (static) along the suspension axis or 5 g's at 45° about a 360° cone located at the attachment point to the NSBF equipment, whichever is limiting. The proposed Two-Meter Balloon-Borne Telescope design meets all these requirements.

8.0 IMPLEMENTATION PHASE SUMMARY DEVELOPMENT PLAN

8.1 Introduction

A plan for designing, building, and flying the Two-Meter Balloon-Borne IR Telescope has been developed based upon the assumption that the telescope subassembly and optics would be built by industry, the gondola would be built by the Smithsonian Astrophysical Observatory (SAO), the photometer built by the University of Chicago, and the Heterodyne receiver built by the University of Arizona. The resulting cost estimate therefore covers the development and initial flight of the entire payload.

8.2 Statement of Work

The Smithsonian Astrophysical Observatory and its team members -- the University of Arizona (UA) and the University of Chicago -- will design, build, and operate the Two-Meter Balloon-Borne Telescope in accordance with this program plan and NASA requirements. One flight is planned during the first year of field operations.

Specifically, the Smithsonian Astrophysical Observatory will:

1. Hold overall responsibility for systems design, fabrication, test and integration including integration of the mirrors, secondary mechanisms and primary mirror cover subassembly with the telescope.

2. Hold overall responsibility for program management.

3. Define instrument and telescope interfaces.

4. Be responsible for configuration management, reliability, and quality assurance.

5. Be responsible for field operations, with the support of the University of Arizona and the University of Chicago, including instrument and telescope integration and test.

6. Be responsible for data acquisition and reduction.

7. Perform scientific data analysis and publication of results.

8. Provide the secondary mechanisms and cover mechanisms to the University of Arizona for telescope integration.

The University of Arizona will:

1. Be responsible for optical design, mirror fabrication and test.

2. Provide the telescope assembly to SAO by means of a subcontract to industry.

3. Perform scientific data analysis and publication of results.

4. Provide the heterodyne receiver.

5. Support field operations and test.

The University of Chicago will:

1. Define instrument accommodation requirements.

2. Provide the IR photometer for the first mission.

3. Support field operations and test.

4. Perform scientific data analysis and publication of results.

8.3 Schedule

The Implementation Phase is planned as a four-year program with the six months devoted to field operations (see Figure 8.3-1). Completion of the gondola in forty months is an ambitious effort, but the schedule is realistic. It will require a heavy front-end loading of engineering personnel to allow the many design tasks to be carried out in parallel. The present SAO Central Engineering organization is ideally suited for working in this manner because it allows us to transfer people into and out of the program as required; only a core staff of engineers will be retained throughout the program for the purpose of providing continuity to the effort.

March 28, 1988

FIGURE 8.3-1
PROGRAM SCHEDULE

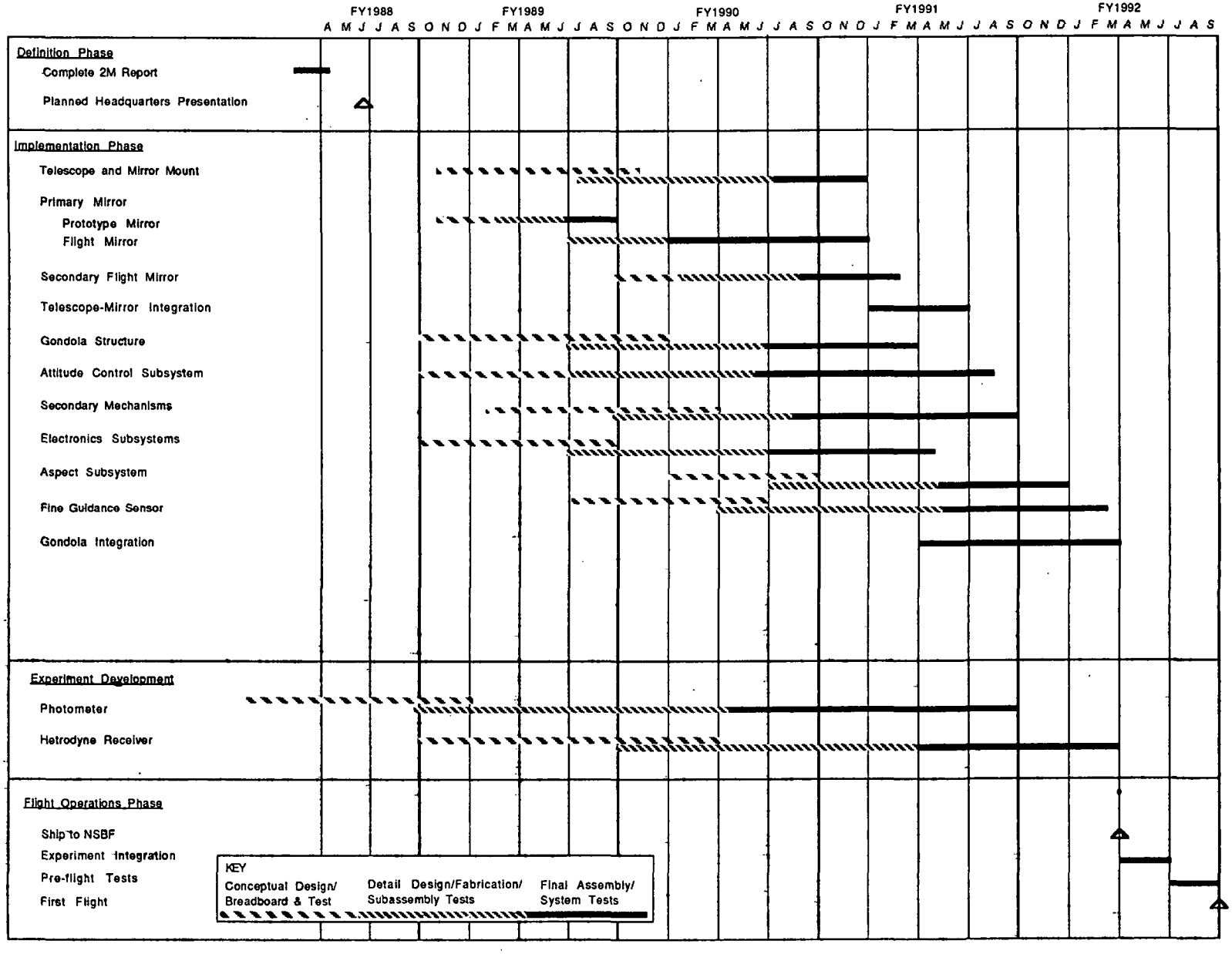

8.4.3 Cost Estimate Assumptions

The following assumptions were made as a basis for this estimate

- The gyro package is assumed to be provided as GFE.
- All shipments are by government bills of lading (GBL's).
- Gondola buildup and test will be done in a rented high bay area at Hanscom Air Force Base, Bedford, MA.
- "WAE" employee is servo system analyst.
- Travel is ROM estimate based on experience with similar programs.
- Engineering salaries are FY88 actuals with 5% average increase per year assumed, full-time employees listed at 88% productivity.
- No command and telemetry trailer costs are included.

9.0 COMPARISON OF THREE-METER AND TWO-METER GONDOLA CONCEPTS

In Table 9-1 the telescope and gondola specifications are given for both a two-meter and three-meter mirror in the telescope. The three-meter mirror offers the advantages of higher angular resolution and greater collection area, and as a result has greater sensitivity for detecting and resolving astronomical sources.

The three-meter system was our first choice and has been studied extensively. However, there are difficulties in constructing, testing, flying, and recovering such a system when compared to a two-meter system. Obviously the three-meter system is also more expensive. The first concern was the fabrication of a three-meter carbon-fiber epoxy mirror which would be diffraction limited at 30 microns. We have shown that such a mirror could be constructed, but with difficulty and it would be expensive. A two-meter mirror can more readily be constructed using presently existing facilities, and obviously would cost less. The two-meter system could probably be launched from NSBF, Palestine, TX where extensive support facilities exist, whereas the three-meter system would have to be launched from a remote site.

A smaller sized less expensive balloon would also be required for the two-meter gondola after flight and its recovery would be considerably easier, using standard trucking facilities.

It is not easy to relinquish scientific capability, but the two-meter system will still be a major step forward over our present capability, a one-meter system which is now 18 years old.

Table 9-1 Comparison of Two-meter and Three-meter Gondola Specifications

Optical Characteristics	2 Meter Design	3 Meter Design
Aperture	2 Meters	3 Meters
Spectral Range	Visible to millimeter	Visible to millimeter
Optics Design	Cassegrain	Cassegrain
Focal Ratio	f/13.5	f/13.5
Back Focus	93 cm from primary mirror vertex	140 cm from primary mirror vertex
Angular Resolution	Diffraction limited to 30μm (Raleigh Criterion 3.9")	Diffraction limited to 30μm (Raleigh Criterion 2.5")
Infrared Field of View	6' diameter unvignetted with ± 3' chop and diffraction spillover at 1 mm	5' diameter unvignetted with ± 2.5' chop and diffraction spillover at 1 mm
Optical Field of View	15' vignetted only by the primary	15' vignetted only by the primary
Pointing Stability		
Inertial Mode	1" rms	1" rms
Magnetometer Mode	± 10' azimuth, ± 5' elevation	± 10' azimuth, ± 5' elevation
Source Offset	± 1/2° (Magnetometer Mode)	± 1/2° (Magnetometer Mode)
Slew Rate	10'/S	10'/S
Thermal Stability		
Telescope	-40° ± 10° C	-40° ± 10° C
Mirror Stabilization Time	< 1 Hour	< 1 Hour
Command and Telemetry		
Number of IRIG User Channels	6	6
Useful Range	To limit of standard NSBF telemetry	To limit of standard NSBF telemetry
IRIG VCO Channels Available	1/3/5/7/8/9/10/11/12/B/E/H/HH	1/3/5/7/8/9/10/11/12/B/E/H/HH
PCM Bit Rate	81 KBpS; expandable to 256 KBpS	81 KBpS; expandable to 256 KBpS
Video Bandwidth	4.5 MHz	4.5 MHz
Gondola Characteristics		
Total Weight	1731 kg (3809 lbs.)	2,168 kg (4,780 lbs.)
Overall Height	5.8 Meters (19 Feet)	8.0 Meters (26 Feet 2 Inches)
Overall Width	2.9 Meters (9 Feet 6 Inches)	5.49 Meters (18 Feet)
Overall Depth	2.5 Meters (8 Feet 2 Inches)	4.0 Meters (13 Feet 3 Inches)
Experiment Accommodations		
Power	140 W typical; 425 W maximum	140 W typical; 425 W maximum
Weight	125 kg at focal plane	125 kg at focal plane

References

Allen, C.W. 1973, Astrophysical Quantities (Athlone, London).

Aumann, H.H. 1984, Bull. AAS, 16, 483.

Aumann, H.H., Gillett, F.C., Beichman, C.A., de Jong, T., Houck, J.R., Low, F.J., Neugebauer, G., Walker, R.G., and Wesselius, P.R. 1984, Ap. J. Lett. 278, L23.

Carleton, N.P., and Traub, W.A. 1972, Science, 177, p 988.

Chance, K.V., and Traub, W.A. 1987, J. Geophys. Res., 92, p. 3061.

Compton, C.C., McPhedron, R.C., Popovic, Z., Rebeiz, G.M., Tong, P.P., and Rutledge, D.B., 1987, IEEE Trans. Antennas Propagat., vol AP-35, p. 622.

Crawford, M.K., Genzel, R., Townes, C.H., and Watson, D.M. 1985, Ap.J., 291, p. 755.

D'Addario, L.R., 1985, Intl. J. of IR and Millimeter Waves, Vol. 5, pp. 1419-1442.

Ellison, B.N. and R.E. Miller, 1987, Intl. J. of IR and Millimeter Waves, Vol. 8, No. 6.

Farmer, C.B. 1974, Can. J. Chem., 52, p. 1544.

Farmer, C.B., et al. 1988, to appear in J. Atm. Chem.

Gascoigne, S.C.B., 1973, Applied Optics, 12, 1419.

Goody, R.M. 1964, Atmospheric Radiation (Clarendon, Oxford), Vol. 1.

Gundlach, K.H., Takada, S., Zahn, M. and Hartfuss, H.J., 1982, Appl. Phys. Lett. 41, 294.

Harper, D.A., Loewenstein, R.F., and Davidson, J.A. 1984, Ap.J., 285, 808.

Keene, J., Davidson, J.A., Harper, D. A., Hildebrand, R.H., Jaffe, D. T., Loewenstein, R.F., Low, F.J., and Pernic, R. 1983, Ap. J. Lett., 274, L43.

Lugten, J.B., Watson, D.M., Crawford, M.K., and Genzel, R. 1986, Ap.J., 311, L51.

Maddalena, R.J., and Thaddeus, P. 1985, Ap.J., 294, p. 231.

McGrath, W.R., Räisänen, A.V., Richards, P.L., Harris, R.E., and Lloyd, F.L., 1985, IEEE Trans. Magn. MAG-11, 212.

Melnick, G.J., Genzel, R., and Lugten, J.B. 1987, Ap.J., 321, p. 530.

Meyer, A. 1988, private communication.

Murcray, D.G., Goldman, A., Kosters, J., Zander, R., Evans, W., Louisnard, C., Alamichel, C., Bangham, M., Pollitt, S., Carli, B., Dinelli, B., Piccioli, S., Volboni, A., Traub, W.A., Chance, K. 1988, to appear in J. Atm. Chem.

Norris, C.H. 1960, Elementary Structural Analysis, (New York: McGraw-Hill), second edition.

Noxon, J., Traub, W.A., Carleton, N.P., and Connes, P. 1976, Ap.J., 207, p. 1025.

Pan, S.K., Feldman, M.J., Kerr, A.R., and Timby, P., 1983, Appl. Phys. Lett. 43, 786.

Pan, S.K., Kerr, A.R., Lamb, J.W., and Feldman, M.J., 1987, NRAO Electronics Division Internal Report No. 268.

Phillips, T.G., 1988, Astro. Lett. and Communications, Vol. 26, pp. 293-304.

Richards, P.L., Shen, T.M., Harris, R.E., and Lloyd, F.L., 1980, Appl. Phys. Lett. Vol. 36, p. 480.

Robbins, D., Waters, J., Zimmerman, P., Jarnot, R., Hardy, J., Pickett, H., Pollitt, S., Traub, W.A., Chance, K., Louisnard, N., Evans, W., and Kerr, J. 1988, to appear in J. Atm. Chem.

Rothman, L.S., Gamache, R.R., Barbe, A., Goldman, A., Gillis, J.R., Toth, R.A., Flaud, J.M., and Camy-Peyret, C. 1983, Appl. Opt.,22, p. 2247.

Rudner, S., and Claesan, T., 1979, Appl. Phys. Lett. 34, 711.

Shen, T.M., Richards, P.L., Harris, R.E., and Lloyd, F.L., 1980, Appl. Phys. Lett. Vol. 36, p. 777.

Smith, B.A., and Terrile, R.J. 1984, Science, **226**, 1421.

Solomon, S. 1986, private communication.

Sutton, E.C. 1983, IEEE Trans. Microwave Theory Tech., Vol. MIT-31, p. 589.

Tielens, A.G.G.M., and Hollenbach, D. 1985, Ap.J., 291, p. 722.

Traub, W.A., and Carleton, N.P., 1974, in Exploration of the Planetary System, Proc. IAU Symposium 65, A. Wosczcyk and C Iwaniszewska, Eds. (Reidel Dordrecht), p. 223.

Traub, W.A., Chance, K.V., Brasunas, J.C., Vrtilek, J.M., and Carleton, N.P. 1983, Proc. SPIE on "Instrumentation in Astronomy IV", 331, p. 208-218.

U.S. Standard Atmosphere, and Supplements, NASA, USAF, USWB (U.S. Printing

Office, Washington, D.C., 1962 and 1966).

Watson, D.M. 1985, Physica Scripta, T11, p. 33.

Wengler, M.J., Woody, D.P., Miller, R.E., and Phillips, T.G., 1985, Intl. J. of IR and Millimeter Waves, Vol. 6, No. 8.